Habilitationsschrift

zur

Erlangung der Venia legendi

für das Fach Physik

der

Ruprecht-Karls-Universität

Heidelberg

vorgelegt von

Carsten Müller

aus Gießen

2009

Laser-induced high-energy processes in atomic, nuclear, and particle physics

Contents

1 Introduction

1.1 High-intensity laser-matter interactions

After the invention of the laser almost 50 years ago, further technological breakthroughs have paved the way to the extremely short and powerful pulses of coherent electromagnetic radiation available today. By using optical or near-infrared laser pulses of femtosecond duration, peak intensities of the order of $I \sim 10^{18}$–$10^{22}\,\mathrm{W/cm^2}$ can nowadays be generated in the laboratory. The corresponding laser field strengths are by far larger than the electric field experienced by outer-shell electrons in atoms. Large photon densities of $n \sim 10^{30}\,\mathrm{cm^{-3}}$ allow for highly nonlinear multiphoton processes where many laser photons simultaneously interact with atomic electrons. Free electrons exposed to such a super-intense laser wave may acquire relativistic kinetic energies in the MeV or even GeV domain. Moreover, novel light sources of high-frequency are presently being developed, with the aim to provide coherent X-ray pulses of several keV photon energy. Thus, the energy scales of the most powerful present and near-future laser sources lie far beyond the typical energetic range of atomic physics but rather reach into nuclear and particle physics. This opens up prospects to extend the important role traditionally played by lasers in atomic physics or quantum optics also to these areas. Against this background, ultrafast processes in strong laser fields at the borderlines between atomic, nuclear, and particle physics are studied in this thesis by theoretical means. Well-established strong-field phenomena such as multiphoton ionization (being the nonlinear generalization of Einstein's photoelectric effect, where an atomic electron absorbs multiple photons at once to overcome the binding potential) or laser-driven recollisions will find their counterparts in other fields of physics.

A laser wave is mainly characterized by its peak electric field strength E and frequency ω. While the former may be considered representing the classical nature of the field, the latter is characteristic for its quantum aspect in terms of photons. Depending on how the typical time scale of a process compares with the laser cycle duration, one or the other aspect dominates: When the process is fast on the time scale of the field oscillation, the laser wave essentially appears as a static field; otherwise the photon nature becomes important. Let us suppose that a laser field interacts with a quantized matter system having a typical level spacing of $\Delta\varepsilon$. There are essentially two possibilities for the electromagnetic wave to have an appreciable influence on the system's quantum dynamics. On the one hand, even a rather weak laser field will certainly exert a substantial impact when the resonance condition

$$\hbar\omega \sim \Delta\varepsilon \tag{1}$$

holds, with $\hbar$ the reduced Planck constant. On the other hand, in a quasi-static nonresonant situation where $\hbar\omega \ll \Delta\varepsilon$, an efficient direct coupling of the particles to the coherent radiation field is guaranteed if the condition

$$\Delta\varepsilon \sim eE\Delta r \tag{2}$$

is fulfilled. Here, e is the electric charge of the particles, and Δr the characteristic length of the system along which the laser field may perform electric work. We consider a few examples, comprising the systems of interest in this thesis. For

outer electrons in atoms, $\Delta r \sim a_0 \sim 10^{-8}\,\mathrm{cm}$ is the Bohr radius; for tightly bound systems like highly charged ions or muonic hydrogen, the atomic dimension is reduced to $\Delta r \sim 10^{-10}\,\mathrm{cm}$; for nuclei, $\Delta r \sim R_n \sim 10^{-12}\,\mathrm{cm}$ is the nuclear size; and for the quantum electrodynamic (QED) vacuum, $\Delta r \sim \lambda\!\!\!^{-}_C \sim 10^{-10}\,\mathrm{cm}$ is the Compton wavelength of the electron. The respective transition energies are of the order of $\Delta\varepsilon \sim 1\,\mathrm{eV}$, $1\,\mathrm{keV}$, $100\,\mathrm{keV}$, and $1\,\mathrm{MeV}$. With optical and X-ray laser facilities, a resonant coupling to atoms and ions can therefore be achieved. In principle, the resonance condition (1) may also be met for certain nuclei and the QED vacuum when pre-accelerated particles are employed, this way exploiting the relativistic Doppler shift of the laser frequency. In the regime of nonresonant interaction, according to Eq. (2), an efficient direct coupling of the electromagnetic wave to ordinary or muonic atoms requires intensities of the order of $I \sim 10^{16}\,\mathrm{W/cm^2}$ or $10^{24}\,\mathrm{W/cm^2}$, respectively. For direct interactions with nuclei or the QED vacuum, intensities approaching the critical Schwinger value $I_c = 2.3 \times 10^{29}\,\mathrm{W/cm^2}$ are needed, which sets the natural scale for spontaneous vacuum breakdown into real electron-positron pairs. The corresponding laboratory-frame intensities can be reduced to about $I \gtrsim 10^{22}$–$10^{23}\,\mathrm{W/cm^2}$, when pre-accelerated particles of high energy are utilized in the initial state.

1.2 Experimental facilities

A comparison of the above numbers with the parameters of the most advanced laser sources is instructive (see Table 1). During the last two decades the development of the chirped-pulse amplification (CPA) technique [Str85] has boosted the level of accessible laser intensities from about $I \sim 10^{15}\,\mathrm{W/cm^2}$, which was available before by mode-locked laser systems, by several orders of magnitude. Based on the CPA, a record intensity of $I \approx 2 \times 10^{22}\,\mathrm{W/cm^2}$ has recently been produced by the HERCULES laser at the University of Michigan (Ann Arbor, USA) [Yan08]. Besides, several other petawatt-class laser systems exist around the globe such as the VULCAN laser at Rutherford Appleton Lab (Didcot, UK) [VUL] or the PHELIX laser at GSI (Darmstadt, Germany) [Hof05], reaching peak intensities of $I \sim 10^{21}\,\mathrm{W/cm^2}$. The next generation of high-power lasers in the near-optical frequency range ($\hbar\omega \sim 1\,\mathrm{eV}$) aims at an intensity level of $10^{23}\,\mathrm{W/cm^2}$ and beyond within the framework of the Extreme-Light Infrastructure (ELI) [Mou06, ELI].

At VUV frequencies ($\hbar\omega \sim 10$–$100\,\mathrm{eV}$), intensities of $\sim 10^{16}\,\mathrm{W/cm^2}$ are generated by the FLASH facility with a free-electron laser at DESY (Hamburg, Germany) [Sor07]. Similar frequencies are obtained from attosecond pulse trains (APTs) which are produced by high-harmonic generation from atoms in the gas

Facility	Frequency domain [eV]	Maximum intensity [W/cm^2]	Starting year
High-power CPA	1	10^{22}	operational
ELI	1	10^{26}	~ 2025
FLASH-FEL	10-100	10^{16}	operational
XFEL	10^3-10^4	10^{20}	2014
gas HHG (APT)	10-100	10^{14}	operational
surface HHG	10-1000	$> 10^{20}$	medium future

Table 1: Parameters of present and near-future intense laser sources.

phase [Ago04, Dre05, Scr06], or from solid surfaces [Tsa06] where higher conversion efficiencies can be exploited. For the near future, coherent photon sources with frequencies in the keV domain are envisaged. At DESY (as an upgrade of the FLASH beamline) and SLAC (Stanford, USA), X-ray free electron lasers (XFELs) are currently under development which aim at maximum frequencies of 10 keV at intensities close to $10^{20}\,\mathrm{W/cm^2}$ [Alt06, DiM07]. Apart from these large-scale XFEL facilities, efforts are made to build table-top XFEL devices at MPQ (Garching, Germany) [Grü07]. These might be able to reach comparable operation parameters due to very high quality of the laser-generated driving electron beam. Ultrashort keV pulses can also be produced via plasma surface harmonics when an intense laser pulse impinges on a solid target [Puk06, Dro09]. Based on the so-called *relativistic flying mirror* formed by oscillating electron sheets in the plasma, extremely high intensities might be attainable by this technique, possibly approaching the critical Schwinger value [Bul03].

With these sources of high-intensity and/or high-frequency laser radiation it will become possible for experimentalists to substantially influence the quantum dynamics of strongly bound systems like highly charged ions or muonic atoms, of bare nuclei, and of virtual electron-positron pairs in the QED vacuum, while real electrons and positrons are accelerated to highly relativistic energies where particle reactions can be triggered.

1.3 Theoretical methods

In certain regimes of laser-matter coupling, multiphoton processes can in principle be treated in higher orders of perturbation theory. This way, Goeppert-Mayer performed the first calculation of a quantum mechanical two-photon process already in 1931 [Goe31]. At high photon orders the evaluation of the corresponding perturbation theory becomes tedious, though. When the laser intensity grows too large, the perturbative approach even breaks down completely and nonperturbative methods are required. To this end, analytical as well as fully numerical methods have been developed. Moreover, very powerful laser fields are able to accelerate electrons to velocities close to the speed of light, so that a relativistic treatment of the electron motion is necessary. The borderline between the nonrelativistic and relativistic regimes is marked by the dimensionless parameter

$$\xi = \frac{e|\mathbf{A}|}{mc^2}\,. \tag{3}$$

Here, $-e$ and m are the electron charge and mass, respectively, $|\mathbf{A}|$ is the amplitude of the laser vector potential, and c is the velocity of light. For $\xi \ll 1$, the laser-induced dynamics stays nonrelativistic, while the relativistic domain is entered at $\xi \sim 1$, where the kinetic energy supply to a free electron by the laser field is on the order of its rest energy.

Analytical calculations mostly rely on the strong-field approximation (SFA) which was introduced by Keldysh [Kel64] to describe atomic ionization by intense laser fields and generalized by Reiss [Rei80, Rei92] to the relativistic domain. The relativistic SFA utilizes the fact that the time-dependent Dirac (as well as Klein-Gordon) equation of a free electron in a plane-wave laser field can be solved analytically. The wave does not need to be monochromatic, but characterized by a uniform propagation direction. The laser field is included as a classical

external potential via the minimal coupling scheme; the classical field description is justified by the large number of photons contained therein, so that depletion effects may be ignored. After their discoverer, these exact analytical solutions are named Volkov states [Vol35]. Similarly, in the nonrelativistic domain Volkov solutions to the Schrödinger equation exist when the laser field is treated as a purely time dependent electric field (dipole approximation). The main properties of the relativistic Volkov states can be inferred from the scalar Klein-Gordon case where the positive-energy wave function reads

$$\Psi_p^{(\mathrm{V})}(x) = N_p \, \mathrm{e}^{\frac{i}{\hbar} S(x)} \,, \tag{4}$$

with a normalization factor N_p and the phase

$$S(x) = \mathbf{p}\cdot\mathbf{r} - \varepsilon_p t - \frac{c}{\omega\varepsilon_p - c^2\mathbf{k}\cdot\mathbf{p}} \int^{\eta} \left[e\mathbf{p}\cdot\mathbf{A}(\tilde{\eta}) + \frac{e^2}{2c}\mathbf{A}^2(\tilde{\eta}) \right] d\tilde{\eta} \,, \tag{5}$$

which coincides with the classical action of the electron in the field. Here, $x^\mu = (ct, \mathbf{r})$ denotes the time-space four-vector, $\mathbf{p}$ is the particle momentum outside the field, $\varepsilon_p = \sqrt{p^2c^2 + m^2c^4}$ is the corresponding energy, $\mathbf{k}$ and ω are the wave vector and frequency of the plane-wave laser field, and $\eta = \omega t - \mathbf{k}\cdot\mathbf{r}$ is the laser phase. The immaterial lower bound of the $\tilde{\eta}$ integration has been omitted here, giving merely rise to a constant phase factor. For a vanishing field, $\mathbf{A} = 0$, the Volkov state reduces to a free solution. Due to the oscillating nature of the external field, a periodic part can be isolated from the Volkov state (4) and expanded into a Fourier series according to

$$\Psi_p^{(\mathrm{V})}(x) = N_p \, \mathrm{e}^{\frac{i}{\hbar}(\mathbf{q}\cdot\mathbf{r} - \varepsilon_q t)} \sum_{n=-\infty}^{\infty} J_n \, \mathrm{e}^{in(\mathbf{k}\cdot\mathbf{r} - \omega t)}. \tag{6}$$

As usual, the mode expansion introduces photons into the picture: each Fourier component describes the emission ($n < 0$) or absorption ($n > 0$) of a certain number of laser photons with momentum $\hbar\mathbf{k}$ and energy $\hbar\omega$. The Fourier coefficients J_n measure the probability amplitude for each multiphoton mode. The J_n are typically some kind of Bessel functions, with the concrete functional relation being determined by the polarization state of the laser field. In the nonperiodic part in Eq. (6), an averaged four-momentum $q^\mu = (\varepsilon_q/c, \mathbf{q})$ of the particle appears, which reads

$$q^\mu = p^\mu + \frac{e^2\overline{\mathbf{A}^2}}{2(\omega\varepsilon_p - c^2\mathbf{k}\cdot\mathbf{p})} k^\mu. \tag{7}$$

The average is taken over a full laser cycle. The additional energy of a particle in a laser field $U_p = \varepsilon_q - \varepsilon_p$ is called "ponderomotive" energy, from the Latin word "pondus" for weight. It represents the mean kinetic energy contained in the field-induced oscillatory motion of the particle. In the nonrelativistic limit, the ponderomotive energy becomes $U_p = \frac{1}{4}mc^2\xi^2$ for a linearly polarized wave. The quasi-momentum (7) corresponds to an effective particle mass of $m_* = \frac{1}{c}\sqrt{q_\mu q^\mu} = m\sqrt{1 + \frac{1}{2}\xi^2} \approx m + \frac{1}{c^2}U_p$, assuming $\xi \ll 1$ in the last step. The particle is said to be *dressed* by the field. The decomposition of a Volkov wave function into periodic and nonperiodic parts in the space-time dependence is

analogous to the quantum mechanical Floquet picture in the time domain and the Bloch theorem in the spatial domain. From the latter case, the appearance of an effective electron mass due to the motion in the periodic potential of a crystal is known, as well. The properties of the Klein-Gordon-Volkov states (4) are shared by the corresponding solutions to the Dirac equation, which correctly account for the electron spin; they are slightly more complicated due to the spinor character of the wave function. In relativistic problems where the electron spin plays a minor role only, the Klein-Gordon-Volkov state may be utilized instead. For example, spin effects are inconsequential for the laser-driven electron dynamics as long as the laser field strength is far below critical, $E \ll E_c$ [Wal02].

With the Volkov states at hand, the basic idea of the SFA is to divide the interaction space into suitable regions and to account in each region for the strongest field only while disregarding any other. For the example of an ionization process in the presence of a laser field this means that bound atomic electrons are described by Coulomb wave functions, whereas ionized electrons are treated as Volkov states. Although appearing simple and rather approximate at first sight, this method nevertheless has proven to be a very useful and reliable tool by showing an overall good agreement with elaborate numerical computations and experimental data. Application of the SFA in a field-theoretic framework results in the theory of laser-dressed QED [Mit75, Nik85, Rit85]. The Volkov states are used here as basis states in a perturbative treatment of the interaction with the quantum vacuum, representing a special realization of the Furry picture. The rules familiar from field-free QED thus carry over to laser-dressed QED when the free-particle states are replaced by Volkov states in the corresponding Feynman graphs.

In field configurations which deviate substantially from a plane wave, analytical approaches are in general very difficult to pursue. Typical examples are tightly focused laser beams, or fields consisting of several waves travelling in different directions. Under such circumstances, numerical ab-initio solutions of the corresponding wave equation represent a more feasible approach which is flexible with respect to the field structure. For relativistic problems, numerical computations are very demanding, though, since the appearance of the electron rest mass in the Dirac Hamiltonian calls for a very fine time resolution [Moc08]: for instance, the temporal step size has to be smaller than an optical laser period by more than six orders of magnitude (since $mc^2 \sim 1\,\mathrm{MeV}$, while $\hbar\omega \sim 1\,\mathrm{eV}$). Numerical treatments therefore often assume laser frequencies high above the optical range and very short pulse durations.

The theoretical investigations of laser-matter interactions during the last decade have rendered increasingly clear that main features of strong-field processes can often be described in terms of the classical electron motion. The basic reason is that the Volkov states, though representing exact wave functions, exhibit the quasi-classical form $\Psi \sim \exp\left(\frac{i}{\hbar}S\right)$ which is familiar from the WKB approximation. Atomic recollision phenomena such as high-harmonic generation allow for an intuitive explanation by so-called simple-man's models which rely on the classical electron trajectory in the laser field between the ionization and recollision instants of time [Bec02]. The quantum mechanical nature of these processes can partially be accounted for by means of Monte-Carlo simulations, where the quantum wavefunction is mimicked by a statistical ensemble of point particles moving along their classical trajectories. This way, certain quantum effects like wave-packet spreading can be described.

In this thesis, essentially all theoretical methods outlined above are applied. Most of the problems are treated within the relativistic SFA, which allows to advance by analytical means to an appreciable extent. In two studies, results of ab-initio numerical computations of the time-dependent Schrödinger and Dirac equations are presented, respectively. We point out that these simulations have been performed in cooperation with two Ph.D. students and a postdoc, rather than by the present author himself.

1.4 Structure of this thesis

In the following, we consider highly energetic, mostly relativistic collision processes in strong laser fields, which belong to the areas of atomic, nuclear, and particle physics. The scattering particles involve electrons, positrons, muons, protons, and heavy ions. Being concerned with the interaction of simple quantum systems such as single atoms with intense laser radiation, we refrain from the investigation of collective many-particle phenomena occurring in laser-induced plasmas (see, e.g., [Mar06]). The laser intensities assumed range from $I \sim 10^{17}\,\mathrm{W/cm^2}$ to $10^{28}\,\mathrm{W/cm^2}$ in the laboratory frame, with frequencies from the near-infrared to the X-ray regime. The various processes under consideration are discussed in ascending order of their energy scale, ranging from the keV to the 100 MeV domain.

Section 2 treats the photoemission of atoms and electrons in weakly relativistic laser fields. The preliminary Section 2.1 illustrates the quantum dynamics of a free-electron wave packet evolving in a strong laser field. It is demonstrated in particular that the magnetic component of the laser field leads to a drift motion of the electron into the wave propagation direction at high intensities. Section 2.2 shows a way how to partially compensate for the electron drift by assisting the driving infrared laser field with a weak attosecond pulse train. In this way, coherent hard X-ray pulses can be produced via the atomic ionization-recollision mechanism. A fundamental problem of quantum mechanics is addressed in Section 2.3, namely the radiation pattern emitted by a strongly laser-driven single-electron wave packet. It represents an example where the often trustworthy semiclassical approach indeed fails.

Section 3 is devoted to laser-driven muonic atoms and their application in nuclear physics. Because of the small Bohr radius of these exotic atoms, the harmonic response to an applied laser field is sensitive to nuclear structure features, as shown in Section 3.1. Moreover, high-harmonic cutoff energies in the hard X-ray and even γ-ray domain can be obtained. Apart from being a dynamic nuclear probe, the laser-driven muon can also lead to nuclear excitation through the periodically time-dependent Coulomb interaction between the nucleus and the oscillating muonic charge cloud. Corresponding probabilities of nuclear electric multipole transitions in suitable light muonic ions are presented in Section 3.2.

Decay of the QED vacuum into electron-positron (e^+e^-) pairs in the presence of very strong electromagnetic fields is considered in Section 4. Nonlinear pair production in the superposition of a laser wave with a nuclear Coulomb field is treated in Section 4.1. In addition to the standard SFA approach to this problem, an alternative field-theoretic treatment based on the laser-dressed polarization operator is introduced (Section 4.1.1). A detailed discussion follows of e^+e^- pair creation in the multiphoton (Section 4.1.2) and tunneling (Section 4.1.3) regimes of interaction, which by analogy are known from strong-field photoionization. Promising

prospects for an experimental observation of this process are revealed. Bound-free pair production with capture of the electron into a low-lying atomic shell of the nucleus is also analyzed (Section 4.1.4). In Section 4.2, pair creation in two counterpropagating laser pulses of high frequency is studied, with a focus on the impact of the laser magnetic-field component. Interestingly, this QED process exhibits characteristic similarities with quantum optical few-level systems in external laser fields.

Section 5 represents a first step towards laser-particle physics. The combination of ultrastrong laser fields with positronium atoms offers particularly promising prospects in this regard, as elaborated in Section 5.1. First, the fundamental high-energy process $e^+e^- \to \mu^+\mu^-$ driven by a superintense laser wave is considered within the framework of laser-dressed QED (Section 5.1.1). In order to obtain not only high collision energies but also high luminosities, the electron and positron are assumed to form a bound state initially, which allows for microscopically small impact parameters. A semiclassical simple-man's model for this QED process can be given which demonstrates that reaction rates in laser fields can be obtained from field-free cross sections combined with the particles' wave packet size at the moment of collision. More suitable field configurations such as two counterpropagating laser waves impinging on the positronium target are discussed, leading to laser-driven e^+e^- collider schemes (Section 5.1.2). An alternative setup for laser-induced muon pair creation is presented in Section 5.2, which is based on collisions of ultrarelativistic nuclei with XFEL radiation pulses. The laser intensities assumed in this section are on the order of $I \gtrsim 10^{22}\,\mathrm{W/cm^2}$.

We finish with a short conclusion and outlook in Section 6.

The following notational conventions are used: $\hbar$ denotes Planck's constant divided by 2π, c is the speed of light, e is the (positive) elementary charge, ϵ_0 denotes the vacuum permittivity, $\alpha = e^2/(4\pi\epsilon_0\hbar c) \approx 1/137$ is the QED fine-structure constant, m is the electron mass, m_μ is the muon mass, $\rho = m/m_\mu$ is the electron-to-muon mass ratio; ω denotes the laser frequency and $\mathbf{k}$ the laser wave vector, $\mathbf{A}$ is the laser vector potential, with the corresponding electric and magnetic field strengths $\mathbf{E}$ and $\mathbf{B}$, and I stands for laser intensity. Particle energies are denoted by ε (in order not to confuse them with electric field strengths) and momenta by $\mathbf{p}$ or $\mathbf{q}$; nuclear charge numbers are denoted by Z.

2 Photoemission by electrons and atoms in weakly relativistic laser fields

The emission of photons by electrons in external fields represents one of the most fundamental processes in physics. While photoemission or absorption by a free electron is kinematically forbidden, atomic electrons can radiate, of course, due to the presence of the nucleus which is capable of absorbing recoil momentum. Also electrons subject to external laser fields can emit non-laser photons. This process may be viewed as (multiphoton) Thomson scattering of one (or several) laser photons into a single outgoing photon; it is addressed in Section 2.3. Similarly, atoms exposed to a laser field show a nonlinear radiative response, emitting harmonics of the fundamental laser frequency (Section 2.2). The basic properties of the underlying frequency upconversion mechanism can be explained by the laser-driven dynamics of ionized electrons, which are reviewed in Section 2.1.

2.1 Quantum dynamics of an electron wave packet in a strong laser field

First, we consider the classical nonrelativistic motion of a free electron in an external laser field $\mathbf{E} = E(t) = E_0 \sin(\omega t + \eta_0)\mathbf{e}_x$ which is treated in the dipole approximation. The corresponding Newton equation of motion reads

$$m\ddot{x}(t) = -eE_0 \sin(\omega t + \eta_0)\,. \tag{8}$$

The y and z directions remain unaffected by the external force and are omitted here. Assuming the initial conditions $x(0) = 0$ and $\dot{x}(0) = 0$, the electron velocity and trajectory read

$$\dot{x}(t) = \frac{eE_0}{m\omega}[\cos(\omega t + \eta_0) - \cos\eta_0]\,, \tag{9}$$

$$x(t) = \frac{eE_0}{m\omega^2}[\sin(\omega t + \eta_0) - \omega t\cos\eta_0 - \sin\eta_0]\,. \tag{10}$$

A weak laser field of linear polarization thus leads to a one-dimensional electron motion along the electric-field axis. The magnitude of the electron velocity is $\dot{x} \sim c\xi$ and its kinetic energy amounts to $\varepsilon_{\rm kin} \sim U_p$. When the value of ξ approaches unity, a relativistic treatment is therefore required [see Eq. (3)].

In the relativistic case, the electron motion becomes more involved. Explicit expressions for the classical electron trajectory can be found, for example, in [Itz80]. The main differences as compared to Eqs. (8)–(10) can be seen as follows. First, the spatial dependence of the laser field must be taken into account since, during a field cycle, the electron covers a distance which is comparable with the laser wavelength. Moreover, the magnetic field component of the laser wave becomes important for electron velocities close to the speed of light. The full Lorentz force $\mathbf{F} = -e[\mathbf{E}(\mathbf{r},t) + \frac{\dot{\mathbf{r}}}{c} \times \mathbf{B}(\mathbf{r},t)]$ is thus responsible for the dynamics. The magnetic field induces a drift motion of the electron in the wave propagation direction. Hence, a relativistically strong laser field of linear polarization leads to a two-dimensional electron motion in the $\mathbf{E},\mathbf{k}$ plane, resembling the form of a numeral eight ("figure-8 motion"). During each laser cycle, the electron moves distances of $\Delta x_{\rm pol} = 2eE_0/(m\omega^2)$ and $\Delta x_{\rm prop} = \pi e^2 E_0^2/(2m^2 c\omega^3)$ in laser polarization and propagation direction, respectively, which are of similar size at $\xi \sim 1$.

In principle, we have already met this dynamical behavior when we introduced the Volkov states in Eq. (4). The phase $S(x)$ contained therein coincides with the classical action of the electron in a plane laser wave. By taking the gradient, we obtain the classical canonical electron momentum in the field, so that its kinetic momentum reads

$$\begin{aligned}\mathbf{p}_{\rm kin}(\eta) &= \nabla S(x) + \frac{e}{c}\mathbf{A}(\eta) \\ &= \mathbf{p} + \frac{e}{c}\mathbf{A}(\eta) + \left[\frac{e}{c}\,\mathbf{p}\cdot\mathbf{A}(\eta) + \frac{e^2}{2c^2}\mathbf{A}^2(\eta)\right]\frac{c^2\mathbf{k}}{\omega\varepsilon_p - c^2\mathbf{k}\cdot\mathbf{p}}\,.\end{aligned} \tag{11}$$

As before, $\mathbf{p}$ is the asymptotic electron momentum outside the field. In accordance with the above, Eq. (11) exhibits an oscillatory motion along the laser polarization direction plus a forward-drift component along the laser wave vector. It is important to note that the longitudinal component into forward direction

$p_{\rm prop} \sim mc\xi^2$ predominates over the transversal component $p_{\rm pol} \sim mc\xi$ in super-intense laser fields with $\xi \gg 1$. Phase averaging of Eq. (11) gives the laser-dressed quasi-momentum of Eq. (7) since $\overline{\mathbf{A}} = 0$.

In addition to the signatures of the classical motion, typical quantum features become apparent when the time evolution of a quantum mechanical electron wave packet is considered. This is illustrated in Fig. 1 for an initially spherical-symmetric Gaussian wave packet in a strong plane-wave laser pulse of linear polarization. Figure 1 is the result of a numerical propagation of the initial wave packet on a 2+1 dimensional space-time grid employing an advanced computer code [Moc08]. For computational reasons, a high laser frequency and short pulse length have been chosen. In accordance with the classical equations of motion, the electron oscillates by a distance $\Delta x_{\rm pol}$ along the laser polarization direction and is continuously pushed into the forward direction by the amount $\Delta x_{\rm prop}$ each cycle. By virtue of Ehrenfest's theorem, the center of the wave packet follows exactly the classical trajectory. Moreover, the wave packet substantially spreads as time goes by due to quantum mechanical dispersion. During its evolution, the wave packet is periodically tilted and twisted by the laser field.

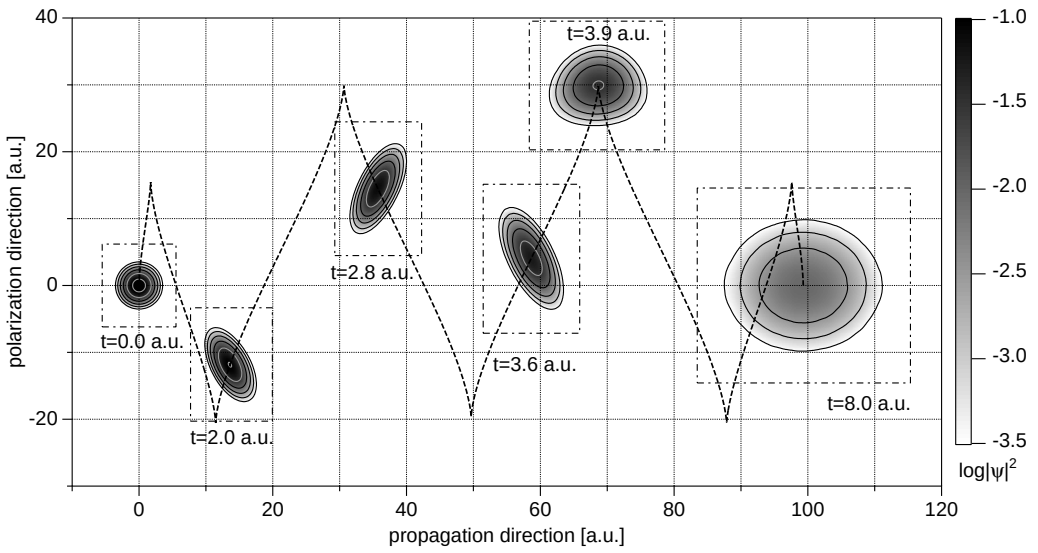

Figure 1: Characteristic time evolution of an electron wave packet in a relativistically strong plane-wave laser pulse of linear polarization ($\xi = 1$). The electron probability distribution is shown at six different times as indicated. Note that the atomic units (a.u.) of length and time are 5.29×10^{-9} cm and 2.42×10^{-17} s, respectively. The laser pulse has a peak intensity of 2×10^{22} W/cm^2 and a photon energy of 150 eV. The laser electric field comprises a total of five cosine-oscillations with sin^2-shaped turn-on and turn-off phases of two cycles each. The dashed trajectory indicates the motion of the wave packet center. (from [22])

For longer propagation times, more complicated wave-packet features arise. They are displayed in Fig. 2 which has been calculated analytically via a wave packet $\psi_i(x) = \int d^3p\, a(\mathbf{p})\psi^{(V)}_{\mathbf{p}}(x)$ formed of Klein-Gordon-Volkov solutions [see Eq. (4)], with a Gaussian distribution of momenta $a(\mathbf{p})$. It is an advantage of analytical approaches to be able to deal with long laser pulses of low-frequency in

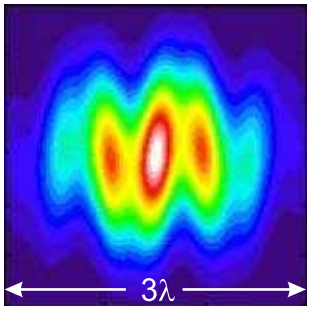

Figure 2: An electron wave packet after natural spreading from an initially Gaussian-shaped size of 1Å. The spreading takes places during 190 cycles in a plane wave of intensity $2 \times 10^{18}\,\mathrm{W/cm^2}$ and wavelength $\lambda = 800\,\mathrm{nm}$. (from [20])

full spatial dimensionality. The wave packet has an initial spatial size on the scale of an atom. Under certain approximations, a closed-form analytical expression can be derived for its time evolution in the field [20]. The figure shows that a wave packet in a long laser pulse can grow to a size on the scale of a wavelength, leading to so-called wave-packet shearing and the formation of multiple peaks [Rom00].

The laser-driven electron dynamics is crucial for the understanding of recollision phenomena which we will discuss repeatedly in different physical contexts.

2.2 Laser-driven recollisions and coherent hard X-rays from high-harmonic generation

In the nonrelativistic domain of laser-atom interaction, the oscillatory motion of a free electron along the field direction [see Eq. (10)] gives rise to manifold nonlinear phenomena via *laser-driven recollisions*. The recollision concept can be understood within an intuitive semiclassical picture which is called the "simple-man's three-step model" [Kuc87, Cor93, Kul93]. (1) An atom subject to a strong laser field can be ionized via tunneling ionization so that the electron enters the continuum with zero velocity, $\dot{x}(0) = 0$. (2) After having been set free, the electron is first driven away from the atomic core by the laser field but when the laser electric field has changed its direction after a while, the electron will be driven back to its parent ion located at $x = 0$. (3) The electron recollides with the ion. As can be seen from Eq. (10), electron-ion recollisions occur for certain ionization phases only, otherwise the electron is driven away. We further note that recollisions require the laser field to be linearly polarized since otherwise an electron set free at any time during the optical cycle with velocity zero will never return to the point where it was released. The maximum recollison energy available is proportional to the laser intensity and given by $3.17U_p$. It is reached for the ionization phase $\eta \approx 1.9\,\mathrm{rad}$ which occurs shortly after the electric field has attained its peak value. During the electron-ion collision, several secondary processes can occur. The electron can be scattered, thereby gaining additional energy; this leads to the plateau in *above-threshold ionization* (ATI) spectra. Or it may set free another electron causing *nonsequential double ionization*, or radiatively recombine with the atomic core. The last process is called *high-harmonic generation* (HHG) since the emitted photon frequency ω_n is an (odd) multiple of the driving field frequency, $\omega_n = n\omega$. The spectrum of harmonics is characterized by an extended plateau

region of approximately constant spectral intensity, which terminates at a rather sharp cutoff. The latter is located at the photon energy $\hbar\omega_n^{\max} = \varepsilon_b + 3.17U_p$, with the atomic binding energy ε_b which naturally arises in the recombination step, together with the maximum kinetic energy of the returning electron. Moreover, superposition of selected harmonics near the cutoff allows for the production of ultrashort VUV pulses below 1 fs duration. This has opened the field of attosecond science, involving perspectives for time-resolved spectroscopy of atomic electron transitions [Ago04, Dre05, Scr06]. In the nonrelativistic regime, the various nonlinear processes based on electron recollisions have intensively been studied, both in theory and experiment [Fed97, Bec02, Mil06]. Especially HHG is also of practical interest, for instance to material science and structural biology, where coherent high-frequency light pulses can be utilized for imaging purposes [Kap07].

For certain applications it is of particular interest to reach high recollison energies. For example, time-resolved studies in nuclear physics would require photon energies in the MeV regime. Those, however, are difficult to produce since the HHG mechanism is suppressed at high laser intensities. Due to the relativistic drift motion, the center of the electron wave packet is considerably displaced from its initial position each cycle (see Fig. 1). If the wave packet was created by tunneling ionization of an atom, then the returning electron would miss the ionic core when the drift distance exceeds the wave packet size, i.e., when $\sqrt{2m\varepsilon_b}(\xi^3/16)(c/\hbar\omega) > 1$ [Sal06]. As a consequence, the highest recollision energy achieved so far is limited to about 1 keV. It has been attained from helium atoms under a driving laser field of $I \sim 10^{16}\,\mathrm{W/cm^2}$ [Ser05]. Various methods for counteracting the relativistic drift have been proposed. To this end, either the properties of the atomic system or of the driving field can be modified. For example, highly charged ions [Kei02] which move relativistically against the laser propagation direction [Chi04], or antisymmetric molecular orbitals [Fis06] could be used. In the first case, the drift of the ionized electron is reduced by the increase of the laser frequency in the comoving frame; in the second, the drift is partially compensated for by the initial momentum of the tunneling electron from the antisymmetric state. With regard to modification of the field, the theoretical proposals comprise the application of tightly focused laser pulses [Lin06], specially tailored pulse shapes [Kla06], two counter-propagating laser beams of equal intensity [Tar00, Mil04, Ver07] or time-delayed crossed beams of different intensity [Chi02] instead of a single laser wave. An additional electromagnetic force appears in these cases which counteracts the drift. In spite of the many suggestions concerning the relativistic drift problem, no universal solution has been found. Some of the proposed setups have a limited scope of applicability, whereas others are challenging to realize.

Exploiting the recent availability of attosecond pulse trains (APTs), we have introduced a novel scheme which enables HHG in the weakly relativistic regime [24]. The process is driven by a strong infrared laser field which is crossed with an APT of XUV radiation. The setup is shown in Fig. 3(a). The impact of the APT, being parallel to the propagation direction of the laser field, is fewfold. First and most importantly, it ionizes the atom upon photoabsorption and induces an initial electron momentum which can compensate the subsequent relativistic drift in the infrared laser field when the central frequency ω^a of the APT is sufficiently large as compared to the atomic binding potential, i.e., $\hbar\omega^a - \varepsilon_b \approx p_{\mathrm{prop}}^2/(2m)$. For a hydrogen-like ion in an s-state, ionization by a large XUV photon takes place predominantly in the XUV field direction. Therefore, the electron emission

probability in the direction along or opposite the laser propagation is the largest here and, in the second case, the compensation of the relativistic drift is most efficient. Hence, in contrast to the earlier proposals, the supplementary field does not exert an additional force during the electron propagation but it changes the initial electron velocity. Another effect of the APT arises from its ultrashort duration as compared to the infrared field, which leads to a practically fixed ionization time allowing to optimize a certain range of harmonics [Sch04]. At very high XUV intensities, the APT may also enhance the ionization probability as compared to tunneling.

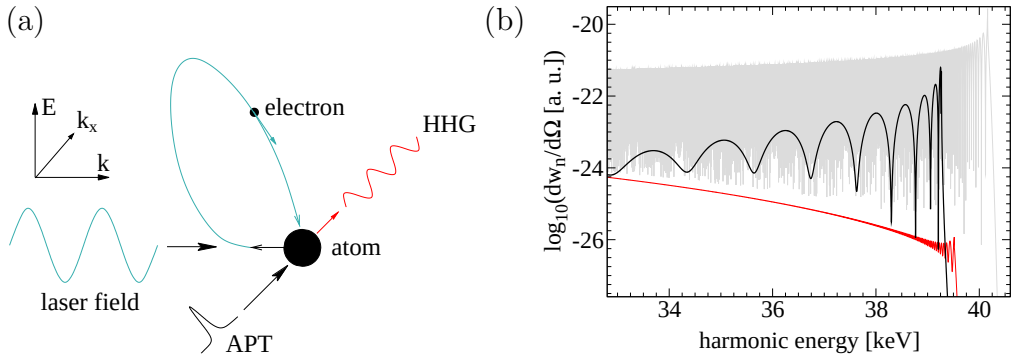

Figure 3: (a) Scheme of the HHG process in the relativistic regime driven by crossed beams of an infrared laser field and an APT; $\mathbf{E}$, $\mathbf{k}$ and $\mathbf{k}^a$ are the laser polarization, laser propagation, and APT propagation directions. (b) HHG spectra in an infrared laser field with intensity $I = 1.5 \times 10^{17}\,\mathrm{W/cm^2}$ and frequency $\hbar\omega = 1.4\,\mathrm{eV}$ for $\varepsilon_b = 144\,\mathrm{eV}$ (Ar^{7+} ions). Shown are results in the dipole approximation, neglecting the drift (gray curve); employing the Klein-Gordon equation (red curve); and additionally assisted by an APT with $I^a = 1.4 \times 10^{13}\,\mathrm{W/cm^2}$, $\hbar\omega^a = 230\,\mathrm{eV}$, pulse length $\tau = 100\,\mathrm{as}$, and a phase delay of -1.2 rad with respect to the laser wave (black curve). (from [24])

The HHG amplitude in our setup is given, within the SFA, by

$$M_n = -i \int d^4x' \int d^4x'' \Phi(x')^* V_H(x') G_L^{(V)}(x', x'')\, \mathbf{x}'' \cdot \mathbf{E}^a(x'') \Phi(x''). \qquad (12)$$

Starting from the atomic ground state $\Phi(x'')$, the electron is ionized by the APT field $\mathbf{E}^a$ and propagates in the continuum until it recombines again into the ground state $\Phi(x')$ by emission of the harmonic photon; $V_H(x')$ describes the corresponding interaction between the electron and the quantized harmonic field. Taking into account the shortness of the pulses in the APT ($\tau = 100\,\mathrm{as}$), we assume that the dynamics of the electron wave-packet after the ionization is governed by the laser field only. Therefore, in the spirit of the SFA, the full Klein-Gordon Green function in the total field has been replaced by the Volkov-Klein-Gordon Green function $G_L^{(V)}(x', x'')$ in the laser field. Equation (12) determines the differential HHG rate for emission of the n^{th} harmonic by virtue of $dw_n/d\Omega = n\omega^3/(2\pi c)^3 |M_n|^2$, where Ω is the solid angle of emission. Figure 3(b) demonstrates that the superposition of an APT can largely increase the HHG yield as compared to the conventional case of a driving laser field only, shown by the red curve. For comparison, the gray

curve displays the result within the nonrelativistic dipole approximation which ignores the relativistic drift motion; it serves as an indicator for ideal HHG via the tunneling-recombination mechanism. The APT assistance enhances the HHG yield in the cutoff region almost to the optimum level. Efficient HHG in the moderately relativistic regime ($\xi \approx 0.3$) is rendered feasible this way with maximum photon energies of about 40 keV. Furthermore, by superposing suitable parts of the spectrum, ultra-short pulses with durations of ~ 10 as can be generated in this energy range [24, 28].

2.3 Thomson scattering off a single-electron wave-packet

As we have seen in the previous section, the coherent photoemission of electrons and atoms in intense laser fields enables manifold applications such as high-harmonic generation and the production of attosecond laser pulses. However, also fundamental questions of quantum mechanics are connected with this process. For example, how does a single-electron wave-packet in a strong laser field radiate? Under which circumstances is quantum interference present in the emission pattern? Theoretical attempts to answer these questions have been undertaken recently [27].

A free-electron wave packet with an initial spatial size on the scale of an atom undergoes natural quantum spreading, which eventually reaches the scale of an optical wavelength [20], as illustrated in Fig. 2. Besides, when born through field ionization, the wave packet is pulled from its parent atom at a finite rate, emerging over multiple laser cycles. This, combined with the Lorentz drift and sharp ponderomotive gradients in a relativistic laser focus, can cause a single-electron wave packet to be dispersed throughout a volume several laser wavelengths across. It is not obvious how the electron radiates when it undergoes such highly non-dipole dynamics, where different parts of the electron wave packet experience entirely different phases of a stimulating laser field. It is tempting to treat the problem within an intuitively appealing model where the quantum probability current is multiplied by the electron charge to produce an extended current distribution used as a source in Maxwell's equations. The intensity computed classically from the extended current distribution is then associated with the probability of measuring a photon. Due to interference, this semiclassical approach leads to large suppression of radiation for many directions [Kre02, Cho05].

A proper description of the process within the framework of quantum electrodynamics leads to a different picture, though. In order to demonstrate the main point let us consider a simple example: an initial electron wave packet $\psi_i(x) = \int d^3p\, a(\mathbf{p})\psi_{\mathbf{p}}(x)$ in a plane-wave driving laser field of uniform wave vector $\mathbf{k}$. Here, $\psi_{\mathbf{p}}$ are the Volkov states and $a(\mathbf{p})$ describes the momentum distribution in the wave packet. In the low-intensity case (i.e., one-photon Thomson scattering), one can easily show that the emitted intensity adopts the structure

$$\frac{d\varepsilon_{\mathbf{k}'}}{d\Omega' d\omega'} = \int d^3p\, |a(\mathbf{p})|^2 \frac{d\varepsilon_{\mathbf{k}'}(\mathbf{p})}{d\Omega' d\omega'}\,. \tag{13}$$

The photon is scattered with wave vector $\mathbf{k}'$ and frequency ω' into the solid angle $d\Omega'$, and $d\varepsilon_{\mathbf{k}'}(\mathbf{p})$ denotes the contribution emitted from a specific initial $\mathbf{p}$ state. Equation (13) represents an *incoherent* sum over the wave-packet distribution, and thus no interference occurs. The underlying reason is that, for given final

electron and photon momenta $\mathbf{p}'$ and $\mathbf{k}'$, a particular initial electron momentum $\mathbf{p} = \mathbf{p}' + \hbar(\mathbf{k}' - \mathbf{k})$ is required by energy-momentum conservation (i.e., there is a unique quantum path). Hence, independent of wave-packet size and shape, individual electrons radiate with the strength of point emitters. This argument also holds in the case of multiphoton Thomson scattering in a plane-wave field.

The situation is more complicated in a focused laser beam when the driving field contains a distribution of initial photon momenta $\mathbf{k}$. In this case, interference in the emitted radiation in principle is possible. If, for example, the initial electron is in a superposition of two momentum states $|\mathbf{p}_1\rangle$ and $|\mathbf{p}_2\rangle$, then the final electron state $|\mathbf{p}'\rangle$ with emission of a photon of certain momentum $\mathbf{k}'$ can be reached by two indistinguishable paths: either from the state $|\mathbf{p}_1\rangle$ or from $|\mathbf{p}_2\rangle$ by absorption of different photons $\mathbf{k}_{1,2} = \mathbf{k}' + (\mathbf{p}' - \mathbf{p}_{1,2})/\hbar$ from the external field, giving rise to quantum interference. It is important to note, though, that the latter is qualitatively distinct from the classical interference in the coherent radiation of an extended charge distribution, which was mentioned above.

Equation (13) can be generalized with the help of the Wigner function of the electron wave packet $\rho_{\mathrm{w}}(\mathbf{r}, \mathbf{p}) = \int d^3q\, a(\mathbf{p} + \mathbf{q}/2)\, a^*(\mathbf{p} - \mathbf{q}/2) \mathrm{e}^{\frac{i}{\hbar}\mathbf{qr}}$. This way a relation between the quantum formulation and its classical counterpart can be established. When the Wigner function is non-negative (e.g., for a Gaussian wave packet), it may be interpreted as the initial electron distribution in phase space and the total photoemission probability becomes again an *incoherent* sum over the contributions of each local phase-space element of the electron distribution, which can be modelled by a classical ensemble of point emitters, taken individually. A different situation arises when the Wigner function is negative in some phase-space region, indicating intrinsic quantum behavior. This happens, for instance, when the initial electron is in a superposition of two momentum states, leading to interference in the emitted radiation. Here it might be possible to reconstruct the electron wave-packet structure by analyzing the radiation pattern emitted.

Our predictions can be tested by modern experimental methods combining high-field science with sensitive single-photon detection techniques known from quantum optics. A corresponding collaboration with Prof. Justin Peatross from the Brigham-Young University (Provo, USA) has been established.

3 Nuclear physics with muonic atoms in superintense laser fields

At the borderline between atomic and nuclear physics, muonic systems play a prominent role. Because of the small Bohr radius of the bound muon, there is an appreciable influence of the nuclear structure on the atomic states and vice versa. Muonic atoms therefore have represented powerful tools for nuclear spectroscopy for more than 50 years. Precision measurements of muonic transitions to deeply bound states reveal nuclear structure information such as finite size, deformation, surface thickness, and polarization. The first X-ray spectroscopy of muonic atoms was performed in 1953 using a 4-m cyclotron [Fit53]. Today, large-scale facilities like TRIUMF (Vancouver, Canada) or PSI (Villingen, Switzerland) exist which are specialized in the efficient generation of muons and muonic atoms [Mul06]. New developments aim at the production of radioactive muonic atoms for conducting spectroscopic studies on unstable nuclear species [Nil04]. Furthermore, muonic

atoms play a prominent role as potential catalysts for nuclear fusion [Bre89].

On a different front, the field of laser-nuclear physics is emerging. While lasers have always represented important tools for nuclear spectroscopy, in recent years their role is changing qualitatively and growing because of the tremendous progress in high-power laser technology. Pioneering experiments on intense laser-plasma interactions have observed incoherent nuclear reactions through laser-generated electrons and bremsstrahlung, such as laser-induced nuclear fusion, photofission, and neutron production [Led03, Sch06a]. High-precision experiments have moreover been able to monitor ultrafast vibrations of the nuclei in diatomic molecules via pump-probe spectroscopy [Erg06] or a comparative HHG study [Bak06]. Advanced laser sources might also pave the way to coherent nuclear excitation and nuclear quantum optics [Bür06].

In light of this, the combination of muonic atoms with intense laser fields opens promising perspectives. Contrary to the traditional spectroscopy of muon transitions between stationary bound states, the exposure of a muonic atom to a strong laser field renders the problem explicitly time-dependent and the muon, thus, a *dynamic* nuclear probe. In this setup, the muon is coherently driven across the nucleus, which may give rise to the emission of radiation, for example, and allow for time-resolved studies on a femtosecond scale. The information on the nucleus gained by laser-assistance can in principle complement the knowledge obtained from the usual field-free spectroscopy of muonic atoms. Superintense laser beams can influence the dynamics of bound muons because they are comparable in strength with the Coulomb fields in light muonic atoms. In the ground state of muonic hydrogen the muon is bound by 2.5 keV at a Bohr radius of 280 fm and experiences an electric field intensity of $4.2 \times 10^{25}\,\mathrm{W/cm^2}$, which raises like Z^6 with atomic number. It is important to note that light muonic atoms are practically stable on the ultrashort time scales of strong laser pulses ($\tau \sim$ fs$-$ns) since the free muon life time amounts to $2.2\,\mu$s. In heavy muonic atoms, muon absorption by the nucleus reduces the lifetime of deeply bound states significantly.

Against this background, we have considered the HHG process from strongly laser-driven muonic hydrogen and deuterium atoms [21]. In the corresponding radiation spectra, characteristic nuclear signatures arise (Section 3.1). The oscillating muonic charge cloud may also excite the nucleus via the time-dependent Coulomb interaction [36], which is analyzed in Section 3.2. We restrict ourselves to nuclear charges $Z \lesssim 10$ since otherwise the required laser intensities become unrealistically large. An advantage of these systems as compared to heavier ones is that the relative differences among isotopes in mass and size are larger for low-Z atoms in the nuclear chart. It is worth mentioning that the combination of muonic deuterium molecules with superintense laser fields represents another interesting example, where field-induced modifications of muon-catalyzed fusion have been investigated recently [Che04].

3.1 Dynamic nuclear probing via high-harmonic generation

We consider the interaction of hydrogen-like muonic atoms with superstrong laser fields of intensity $I \gtrsim 10^{22}\,\mathrm{W/cm^2}$. Despite these ultrahigh laser intensities, the muon motion stays nonrelativistical because of the large muon mass and can be described by the time-dependent Schrödinger equation. For the same reason, the magnetic-field induced drift is suppressed. As usual for muonic atoms, the

nucleus cannot be considered as infinitely heavy, so that the motion of both binding partners must be taken into account. The calculation is facilitated by the fact that the two-body problem separates into relative and center-of-mass coordinates when the laser field is treated in dipole approximation. The higher harmonics are generated by the relative motion which is nonlinear and governed by

$$i\hbar\frac{\partial}{\partial t}\psi(\mathbf{r},t) = \left[\frac{\hat{\mathbf{p}}^2}{2m_r} - e\mathbf{r}\cdot\mathbf{E}(t) + V(\mathbf{r})\right]\psi(\mathbf{r},t) \tag{14}$$

in the case of muonic hydrogen with $Z = 1$. Here, $\mathbf{E}(t) = E_0\sin(\omega t)\mathbf{e}_x$ is the laser field, $V(\mathbf{r})$ the nuclear Coulomb potential, $\hat{\mathbf{p}} = -i\hbar\partial/\partial\mathbf{r}$ the relative momentum, and $m_r = m_\mu m_n/(m_\mu + m_n)$ the reduced mass, with the nuclear mass m_n. We point out that for higher Z values the muon would couple to the laser field via an effective charge $q_{\text{eff}} = m_r(Z/m_n + 1/m_\mu)e$ [38] (see also [Rei79]). In the special case $Z = 1$ considered here, the effective charge reduces to $q_{\text{eff}} = e$.

By applying a standard scaling transformation: $t = \rho t'$ and $x = \rho x'$, with the mass ratio $\rho = m/m_\mu$, one can recast Eq. (14) into a form that essentially describes an ordinary hydrogen atom in a laser field of the scaled parameters $\omega' = \rho\omega$, $E_0' = \rho^2 E_0$. This means that a muonic hydrogen atom in a laser field with parameters E_0 and ω behaves like an electronic hydrogen atom in a field with E_0' and ω', provided that the binding potential $V(\mathbf{r})$ arises from a pointlike nucleus. To give an example, the typical parameters of an intense Ti:Sapphire laser $\hbar\omega' = 1.5\,\text{eV}$, $E_0' = 2.7\times10^8\,\text{V/cm}$ ($I' = 10^{14}\,\text{W/cm}^2$) translate to muonic hydrogen as $\hbar\omega = 280\,\text{eV}$, $E_0 = 9.3\times10^{12}\,\text{V/cm}$ ($I = 1.2\times10^{23}\,\text{W/cm}^2$). We emphasize, though, that the scaling procedure does not account for nuclear parameters like the finite nuclear size or the nuclear shape. Evidently, when the transition from a muonic hydrogen atom to a normal hydrogen atom is performed, the proton radius is not to be length-scaled but remains fixed. As a consequence, for atomic systems where nuclear properties play a role, not all physical information can be obtained via scaling.

The main influence of the nuclear mass on the spectrum can be inferred directly from Eq. (14). The harmonic cutoff position is determined by the formula $\hbar\omega^{\text{max}} = \varepsilon_b + 3.17U_p$, with the binding potential ε_b and the ponderomotive energy U_p (see Section 1.3). In the present case, the latter amounts to

$$U_p = \frac{e^2E_0^2}{4\omega^2 m_r} = \frac{e^2E_0^2}{4\omega^2}\left(\frac{1}{m_\mu} + \frac{1}{m_n}\right) \tag{15}$$

and is, thus, the larger the smaller the reduced mass is. Consequently, in an intense laser field with $U_p \gg \varepsilon_b$, muonic hydrogen (H) gives rise to a larger cutoff energy than muonic deuterium (D); the relative difference is about 5% according to $\omega_{\text{max}}^{(\text{H})}/\omega_{\text{max}}^{(\text{D})} \approx m_r^{(\text{D})}/m_r^{(\text{H})} \approx 1.05$. The nuclear mass effect can also be explained by the separate motion of the atomic binding partners. The muon and nucleus are driven by the laser field into opposite directions along the polarization axis. Upon recombination their kinetic energies sum up as indicated on the right-hand side of Eq. (15). Within this picture, the larger cutoff energy for muonic hydrogen results from the fact that, due to its smaller mass, the proton is more strongly accelerated by the laser field than the deuteron.

In order to reveal the effects arising from the finite nuclear size, the Schrödinger equation (14) has been solved numerically for a suitably chosen nuclear potential.

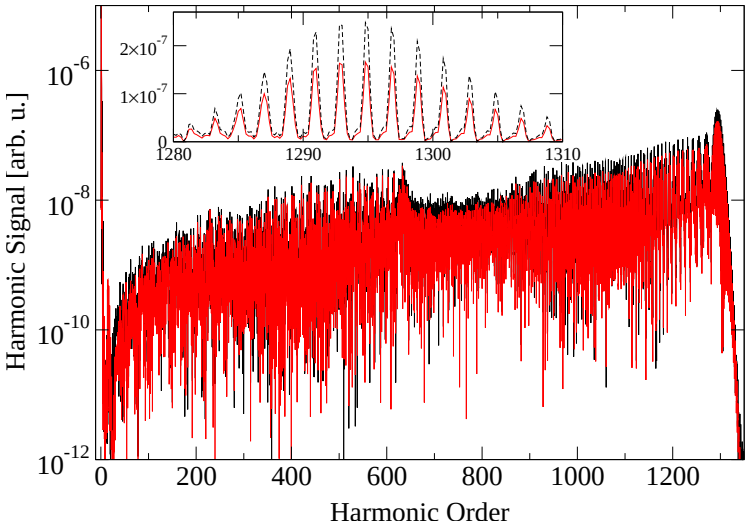

Figure 4: Finite nuclear size effects in the high-harmonic response from different muonic hydrogen isotopes. The black line shows the spectrum for muonic hydrogen at the laser parameters $I^{(\mathrm{H})} = 8.5 \times 10^{22}\,\mathrm{W/cm^2}$ and $\hbar\omega^{(\mathrm{H})} = 59\,\mathrm{eV}$. The red line gives the spectrum for muonic deuterium at the scaled laser parameters $I^{(\mathrm{D})} = 1.05 \times 10^{23}\,\mathrm{W/cm^2}$ and $\hbar\omega^{(\mathrm{D})} = 62\,\mathrm{eV}$ (see text for explanation). The inset shows an enlargement of the cutoff region on a linear scale. (from [21])

From the numerical solution the dipole acceleration can be obtained, which yields the harmonic spectrum via a Fourier transformation. We employ the nuclear drop model and consider the nucleus as a sphere of uniform charge density within the nuclear radius R. The corresponding potential reads

$$V(x) = \begin{cases} -\frac{e^2}{4\pi\epsilon_0 R}\left(\frac{3}{2} - \frac{x^2}{2R^2}\right) & \text{for } |x| \leq R, \\ -\frac{e^2}{4\pi\epsilon_0 |x|} & \text{for } |x| > R \end{cases} \tag{16}$$

where we restrict the consideration to the dimension along the laser polarization direction. The proton and deuteron charge radii amount to $R_p \approx 0.875\,\mathrm{fm}$ and $R_d \approx 2.139\,\mathrm{fm}$, respectively. Figure 4 shows the resulting harmonic spectra for muonic hydrogen versus muonic deuterium. The nuclear mass effect mentioned above was compensated for by applying properly scaled frequencies and intensities with $\omega \propto m_r$ and $E_0 \propto m_r^2$, so that the cutoff positions $N_{\max} = \omega_{\max}/\omega$ of both spectra coincide. We see that the harmonic signal from muonic hydrogen is larger (by about 50 % in the cutoff region) than that from muonic deuterium. The reason is that a smaller nuclear radius steepens the potential near the origin, which leads to more violent acceleration and enhanced harmonic emission. The finite nuclear size has therefore an impact on the plateau height of high-harmonic spectra from muonic atoms.

Finite nuclear size effects are also visible in high-precision spectroscopy of electron transitions in (ordinary) highly charged ions (see, e.g., [Bru07, Bra08] for recent experiments). In the harmonic response from such systems when exposed to a superintense laser field [Cas02], nuclear signatures can also be present. We compare the expected effects in the HHG spectra between highly charged ions and muonic atoms via a simple analysis. We assume a hydrogenlike system of

nuclear charge number Z and employ the mass scaling parameter ρ, with $\rho \approx 1/200$ for a muonic atom and $\rho = 1$ for an electronic ion. The K-shell Bohr radius, binding energy, and electric field strength amount to $a_K(Z,\rho) = a_H\rho/Z$, $\varepsilon_b(Z,\rho) = \varepsilon_H Z^2/\rho$, and $E_K(Z,\rho) = E_H Z^3/\rho^2$, respectively, where a_H, ε_H and E_H denote the corresponding quantities for electronic hydrogen. The nuclear radius can be approximated as $R(Z) = 1.2A^{1/3}\,\mathrm{fm} \approx 1.2(2Z)^{1/3}\,\mathrm{fm}$. Similar finite nuclear size effects in the HHG spectra may be expected when the ratio $R(Z)/a_K(Z,\rho) \propto Z^{4/3}/\rho$ has a similar value for two atomic systems that are compared. This is the case, e.g., for electronic U^{91+} (where $Z = 92, \rho = 1$) and muonic He^+ (where $Z = 2, \rho \approx 1/200$). The above relations imply, however, that the binding energy and electric field strength in the electronic ion are substantially larger than in the muonic atom when both have the same ratio of $Z^{4/3}/\rho = \mathrm{const}$. As a consequence, the laser frequency and intensity that must be applied to the electronic highly charged ion in order to reveal finite nuclear size effects in the harmonic response, need to be larger than in the muonic atom case. From this point of view, muonic atoms are more favorable systems than ordinary heavy ions to study the influence of the nuclear size on the HHG process.

Finally, we comment on the maximum harmonic cutoff energies which can be achieved with muonic atoms. Since the conversion efficiency into high harmonics from gas targets is rather low ($\sim 10^{-6}$), it is generally desirable to maximize the radiative signal strength. In our situation, the optimization is of particular importance as the density of muonic atom samples is low. A sizeable HHG signal requires efficient ionization on the one hand, as well as efficient recombination on the other hand. The former is guaranteed if the laser peak field strength lies just below the border of over-barrier ionization (OBI) where the Coulomb barrier is suppressed all the way to the bound energy level by the laser field [Sal06]. From the generalized version of Eq. (14) for $Z \geq 1$, we obtain

$$E_0 \lesssim E^{\mathrm{OBI}} = \frac{m_r^2 c^3}{q_e \hbar}\,\frac{(\alpha Z)^3}{16}. \tag{17}$$

Efficient recollision is guaranteed if the magnetic drift along the laser propagation direction can be neglected, which limits the relativistic parameter to (see Section 2.2)

$$\xi = \frac{q_e E_0}{m_r c \omega} < \left(\frac{16\hbar\omega}{\sqrt{2 m_r c^2 \varepsilon_b}}\right)^{1/3}. \tag{18}$$

The latter condition also confirms the applicability of the dipole approximation in Eq. (14). The Eqs. (17) and (18) define a maximum laser intensity and a minimum laser frequency which are still in accordance with the conditions imposed. At these laser parameters, the maximum harmonic cutoff energies are attained and an efficient ionization-recollision process is taking place. For muonic hydrogen the corresponding lowest frequency lies in the VUV range ($\hbar\omega \approx 27\,\mathrm{eV}$), and the maximum field intensity amounts to $1.6 \times 10^{23}\,\mathrm{W/cm^2}$. At these values, the harmonic spectrum extends to a maximum energy of $\hbar\omega^{\mathrm{max}} \approx 0.55$ MeV. For light muonic atoms with nuclear charge number $Z > 1$, the achievable cutoff energies are even higher, reaching several MeVs. A summary is given in Table 2.

Our results demonstrate that muonic atoms in high-intensity, high-frequency laser fields can in principle be utilized to dynamically gain structure information on nuclear ground states via their high-harmonic response. Maximum cutoff energies

Z	$\hbar\omega_{\min}$	$\xi_{\min}$	$\xi_{\max}$	$\hbar\omega^{\max}$
1	27 eV	0.007	0.085	0.55 MeV
2	170 eV	0.015	0.12	1.1 MeV
4	960 eV	0.03	0.17	2.2 MeV
10	9.5 keV	0.07	0.27	5.7 MeV

Table 2: Maximum HHG cutoff energies $\hbar\omega^{\max}$ achievable with hydrogenlike muonic atoms of nuclear charge number Z. The applied laser frequency $\omega_{\min}$ and intensity parameter $\xi_{\max}$ are chosen in accordance with Eqs. (17) and (18) to allow for an efficient ionization-recollision process. $\xi_{\min}$ denotes the minimum intensity parameter leading to tunneling ionization. (from [38])

in the MeV domain can be achieved, rendering muonic atoms promising candidates for the generation of (weak) ultrashort coherent γ-ray pulses which might be employed to trigger photo-nuclear reactions. The considered setup moreover offers prospects for pump-probe experiments on excited nuclear levels: the periodically driven muon may first excite the nucleus and subsequently probe the excited state and its deexcitation mechanism. This nuclear excitation process is investigated in the following.

3.2 Laser-induced nuclear excitation in muonic atoms

When a muonic atom is exposed to a very strong laser field, the periodically oscillating muonic charge density can also lead to nuclear excitation. The process may be called nuclear excitation by coherent muon motion, NECμM, and is shown schematically in Fig. 5. It belongs to a class of excitation mechanisms which rely on the coupling of the nucleus with atomic states. For example, when the energetic difference between two atomic states matches a low-lying nuclear transition energy ($\hbar\omega_N \lesssim 100\,\mathrm{keV}$), the energy released during the atomic deexcitation can be transferred resonantly to the nucleus leading to its excitation (nuclear excitation by electron transition, NEET [Mor73]). Similar mechanisms proceed via electron capture or scattering [Gol76, Pal08]. While NEET has been measured for the first time in the mid 1970s [Oto78], with conclusive evidence even only recently [Kis00], in muonic atoms the equivalent process was already observed in 1960 [Bal60]. Despite their rather small probabilities, these kind of processes are of both fundamental and practical interest since potential applications comprise the efficient triggering of isomeric nuclear states [Car04, Pal07] and especially the development of a nuclear γ-ray laser [Bal97].

We have studied electric multipole transitions in nuclei via the NECμM process in light muonic atoms, focusing on a regime where the laser-driven muon is not ionized but rather remains bound [36]. Nuclear excitation by rescattering of ionized electrons in laser fields has been discussed elsewhere [Mil04, Moc04, Kor07]. In contrast to NEET, the NECμM effect does not rely on a resonance condition. The corresponding process in electronic atoms has been studied before [Sol88, Ber91], with a focus on the transition to the very low-lying isomeric level in ^{235}U at 76 eV. The predicted excitation probabilities are small, though, and could not yet be verified in experiment [Bou92, Cla04]. From the experimental data an upper bound for the excitation probability of $\sim 10^{-5}$ was extracted. We point out that contrary to laser-generated plasma experiments [Sch06a], the nucleus is excited solely by

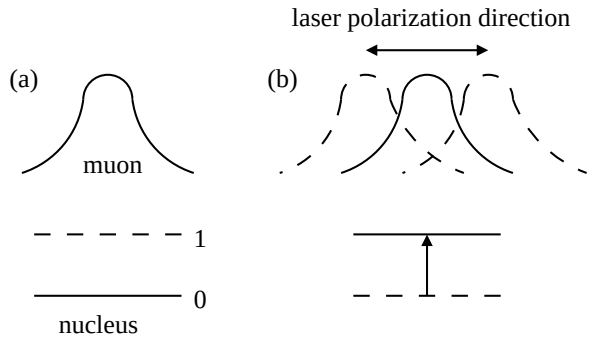

Figure 5: Schematic diagram of the NECμM process. (a) Initially, in the absence of an external field, the muon and nucleus of the hydrogenlike muonic atom are in their respective ground states. (b) When exposed to a strong laser field, the muonic charge cloud is driven into oscillation which leads to nuclear excitation $|0\rangle \to |1\rangle$ via the resulting time-dependent Coulomb interaction. (from [36])

its own electron or muon.[1] Muonic atoms are in principle favorable candidates to observe the effect as the muon produces a much higher charge density within the nuclear volume. Below we will show that the excitation probabilities nevertheless are very small, because the driving laser frequency is far off resonance with the nuclear level spacing. Observation of NECμM therefore represents a challenging task, but it might come into experimental reach by powerful XFEL facilities in the near future.

The combined influence of the nuclear Coulomb field and the laser field on the muon produces a time-dependent charge density $\rho(\mathbf{r},t) = e|\psi(\mathbf{r},t)|^2$, with the muon wave function ψ, which may cause nuclear excitation. The Hamiltonian for the interaction between the muonic and nuclear charge densities is given by

$$H_{\rm int}(t) = \int d^3r \int d^3r_N \frac{\rho(\mathbf{r},t)\rho_N(\mathbf{r}_N)}{4\pi\epsilon_0|\mathbf{r}-\mathbf{r}_N|}\,, \tag{19}$$

within the nuclear long-wavelength limit [Eis76]. Being interested in electric multipole transitions here, we neglect the current-current part which would give rise to magnetic transitions. After a multipole expansion of the Coulomb interaction in Eq. (19), the probability for an electric $E\ell$-transition between the nuclear states $|0\rangle$ and $|1\rangle$ becomes within the first order of perturbation theory

$$P_{0\to1}(E\ell) = \left(\frac{e}{\epsilon_0\hbar}\right)^2 \frac{B(E\ell)}{(2\ell+1)^3} \left| \int_0^T dt\ \mathrm{e}^{i\omega_N t} \int d^3r \frac{\rho(\mathbf{r},t)}{r^{\ell+1}} Y_\ell^0(\Omega) \right|^2 \tag{20}$$

with the duration $T = 2\pi N/\omega$ of an N-cycle laser pulse, the nuclear transition energy $\hbar\omega_N$, and the multipolarity ℓ. Cylindrical symmetry along the laser field $\mathbf{E}(t) = E_0 \sin(\omega t)\mathbf{e}_z$ is employed. The reduced transition probability $B(E\ell)$ in Eq. (20) results from the integral of the nuclear transition density ρ_N over nuclear coordinates in the usual way.

In order to proceed analytically, we apply a simplified model for the muon dynamics. This allows us to derive an order-of-magnitude estimate for the nuclear

[1] The analogous, purely atomic effect of inner-shell excitation by coherent motion of outer-shell electrons in a strong driving laser field has been proposed in [Boy85].

transition probability in closed form. Since the nuclear Coulomb and laser field strengths experienced by the muon are of similar magnitude, an SFA approach based on Volkov states is not applicable here. Instead, the muon interaction with both fields must be accounted for in a nonperturbative manner. This is achieved by modelling the atomic binding of the muon to the nucleus by an harmonic oscillator potential of frequency ω_b; the oscillator length $\sqrt{\hbar/m_\mu\omega_b}$ is chosen to coincide with the atomic Bohr radius. The corresponding Schrödinger equation for the muon motion in the combined fields can be solved analytically. While the model appears rather crude, it carries the main features of the muonic time evolution in a qualitative fashion. Moreover, we consider only the nonresonant case where ω_b is significantly different from ω_N. In this situation the correct atomic level structure is of minor importance. (Note that for $\omega_b \approx \omega_N$ the NEET process may occur anyway.) Within the model, the muon wave function reads [Ber91]

$$\psi(\mathbf{r},t) = \phi(\mathbf{r} - \mathbf{u}(t)) \tag{21}$$

where $\phi(r)$ is the ground-state wave function in the harmonic oscillator potential and $\mathbf{u}(t)$ is the periodic displacement caused by the laser field. In the limit $\omega \ll \omega_b$ of interest here, $\mathbf{u}(t) \approx u_0 \sin(\omega t)\mathbf{e}_z$ looks similar to the classical trajectory of a free muon in the laser field [see Eq. (10) in Section 2.1], but the excursion amplitude $u_0 \approx eE_0/(m\omega_b^2)$ is reduced by a factor $(\omega/\omega_b)^2$ due to the harmonic binding force. Equation (21) has an intuitive interpretation of the muon time evolution: the wave packet keeps its shape but is periodically shifted across the nucleus by the driving laser field. With the corresponding charge density $\rho(\mathbf{r} - \mathbf{u}(t))$, the space-time integrals in Eq. (20) can be solved analytically. Per cycle, we obtain the NECμM probability

$$P_{0\to1}(E\ell) \sim \alpha^2 \frac{B(E\ell)}{e^2 a_0^{2\ell}} \frac{\lambda\!\!\!^{-2}_N}{a_0^2} \left(\frac{u_0\omega}{a_0\omega_N}\right)^{2\ell}, \tag{22}$$

with $\lambda\!\!\!^{-}_N = c/\omega_N$. The nuclear excitation probability in Eq. (22) essentially scales like $P_{0\to1}(E\ell) \propto a_0^{-2(\ell+1)}$ with the Bohr radius a_0, which clearly demonstrates the expected result that compact atomic states are advantageous. Apart from this scaling, the atomic size enters through the factor $(u_0/a_0)^{2\ell}$ which depends on the applied laser intensity. The appearance of the ratio u_0/a_0 is intuitive since the larger its value the closer the muon comes to the nucleus, this way increasing the mutual Coulomb interaction. By choosing appropriately large laser fields with $E_0 \lesssim E_{\mathrm{OBI}}$, the ratio u_0/a_0 can be optimized to values of several percent. Via the displacement u_0, the excitation probability depends like $P_{0\to1}(E\ell) \propto E_0^{2\ell}$ on the laser field strength. This behavior is reminiscent of multiphoton processes in atoms or molecules, which scale as E_0^{2n} when n laser photons are involved and perturbation theory applies [Sal06]. The photon order n formally corresponds to the multipolarity ℓ of the transition here. Within this analogy, the excitation mechanism might be interpreted as "multiphonon" absorption from the periodically oscillating muon charge density. The main factor, however, determining the absolute value of the probability is the frequency ratio $(\omega/\omega_N)^{2\ell}$. In optical or infrared laser fields, the large frequency mismatch suppresses the nonresonant process by many orders of magnitude since the lowest transition energies in light nuclei are $\hbar\omega_N \sim 100\,\mathrm{keV}$ so that $\omega/\omega_N \sim 10^{-5}$. High laser frequencies are therefore desirable in order to reduce this detrimental mismatch. We note that for the

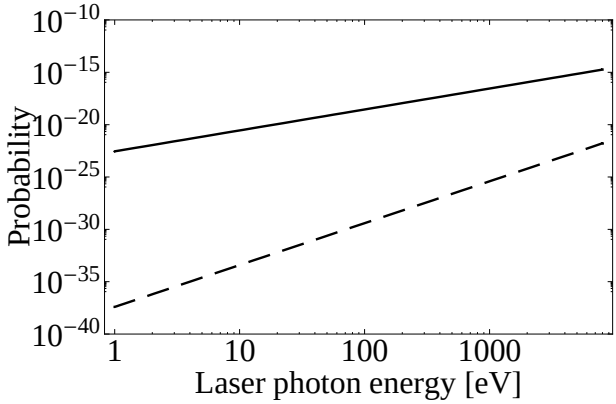

Figure 6: NECμM probabilities in laser-driven muonic ^{19}F (solid curve) and ^{16}N (dashed curve), as function of the laser frequency. The curves refer to a single atom, initially in the $1s$ ground-state. The laser intensity is $10^{26}\,\mathrm{W/cm^2}$. (from [36])

case of magnetic $M\ell$ transitions, Eq. (22) is modified approximately by a factor of $(\alpha Z)^2(\hbar/m_p c R_N)^2 \ll 1$, with the proton mass m_p, which results from the gradient operators in the current-current interaction.

We illustrate Eq. (22) by the examples of the NECμM probability in hydrogenlike muonic ^{19}F and ^{16}N. These nuclei possess the lowest-energy electric transitions among isotopes with $Z \lesssim 10$. There is an $E1$ transition at $\hbar\omega_N \approx 110\,\mathrm{keV}$ in ^{19}F, and an $E2$ transition at $\hbar\omega_N \approx 120\,\mathrm{keV}$ in ^{16}N. Figure 6 shows the dependence of the corresponding NECμM probabilities as a function of laser frequency from the infrared to the envisaged XFEL domain [Alt06]. The laser intensity amounts to $10^{26}\,\mathrm{W/cm^2}$. With increasing laser frequency the excitation probability is substantially enhanced, in particular for the non-dipole transition in ^{16}N. The absolute values of the nuclear excitation probability are always very small, though. The maximum probability of about 10^{-14} is obtained from the $E1$ transition in ^{19}F when 10 keV XFEL radiation is applied.[2]

Despite the very small nuclear transition probabilities shown in Fig. 6, the muon still leads to a substantial enhancement of the laser-nucleus interaction. This is clearly demonstrated by a comparison with the corresponding probability for direct nuclear excitation by the laser field. When the intensity is extremely high, nuclei can be excited directly by an off-resonant laser field [Mat98]. In the present situation, however, this direct excitation channel is still of negligible importance. Applying n-th order perturbation theory, the latter can be estimated as $P \sim \Gamma^{2n}$, with $\Gamma \approx eE_0R_N/\hbar\omega_N$ and $n \approx \omega_N/\omega$. For the light muonic isotopes at the laser

[2] An alternative way of obtaining high laser frequencies is to employ (instead of fixed target nuclei) an ion beam which counterpropagates the laser pulse at relativistic speed. The laser frequency appears Doppler-blueshifted in the nuclear rest frame. In this geometry, even a resonant laser-nucleus coupling [Bür06] could be achieved when a bare ^{235}U beam collides at a Lorentz factor $\gamma \approx 30$ with a near-infrared laser beam ($\hbar\omega \approx 1.2\,\mathrm{eV}$). The Doppler-shifted laser frequency $\omega' \approx 2\gamma\omega$ can be tuned into resonance with the nuclear transition frequency of 76 eV. In fact, such an experiment would be tailormade for the future GSI facility where a beam of hydrogenlike or fully stripped U ions of the required energy will be available, along with the intense PHELIX laser [Hof05].

parameters $I = 10^{26}$ W/cm^2 and $\hbar\omega = 10\,\mathrm{keV}$ (where the maximum NECμM probabilities are reached), we obtain $\Gamma \sim 10^{-2}$ and $n \approx 10$, so that $P \sim 10^{-40}$.

Regarding the experimental measurability of the NECμM process, we note that the probability in Eq. (22) refers to a single atom. When more than one atom interacts with the laser field, the total yield could be increased proportionally. However, intense laser pulses possess a small focal volume only ($V_f \sim 10^{-10}\,\mathrm{cm}^3$, to give a typical number), while on the other side it is difficult to produce exotic atoms at very high densities. An achievable number density of trapped muonic atoms is $n \sim 10^{10}\,\mathrm{cm}^{-3}$ which is comparable with the densities available for other exotic species such as positronium (where $n \sim 10^{15}\,\mathrm{cm}^{-3}$ [Cas05]) or antihydrogen (where $n \sim 10^{6}\,\mathrm{cm}^{-3}$ [Amo02]). According to these numbers, only a few muonic atoms are contained in the interaction volume, which prevents a substantial yield enhancement, unfortunately. Instead of using a fixed target of muonic atoms in a trap, it might therefore be more promising to employ a nonrelativistic beam of muonic atoms. Such beam experiments are in principle feasible [Mul06], based on the availability of beams of 10^5 muons per second. The atomic beam could be synchronized with a bunch of laser pulses: at the upcoming XFEL facilities, pulse repetition rates of $40\,\mathrm{kHz} \sim 10^5\,\mathrm{s}^{-1}$ are envisaged [Alt06]. In this setup, one muonic atom would interact with one laser pulse at a time. By assuming the highest nuclear excitation probability of about 10^{-14} shown in Fig. 6, we obtain a total yield estimate of roughly one excitation event per week. This clearly indicates that an experimental observation of the NECμM process is not completely impossible, but certainly an extremely challenging task. The signature for exciting a nucleus would be its delayed γ-emission. It could be discriminated from the photon background of atomic high-harmonic generation (see Section 3.1) by its characteristic energy and angular distribution.

4 Laser-induced electron-positron pair creation

The creation of electron-positron (e^+e^-) pairs in intense laser fields is encountering a growing interest in recent years. It has been stimulated by a pioneering experiment in the late 1990s at SLAC (Stanford, USA) where e^+e^- pair creation via multiphoton absorption was observed for the first time [Bur97]. According to Eqs. (1) and (2), pair creation by laser radiation requires $\hbar\omega \sim mc^2$ or $E \sim E_c$. The critical field strength $E_c = m^2c^3/e\hbar$ (also called Schwinger field [Sch51]) was introduced already in 1931 by Sauter who studied the Klein paradox in a linearly increasing potential, corresponding to a constant field [Sau31, Itz80, Kre04]. A constant electric field with strength E_c supplies an energy of mc^2 to an electron along a Compton wave length $\lambda\!\!\!^{-}_C = \hbar/mc$. A virtual electron can therefore be extracted from the vacuum, leaving behind – in the Dirac-sea picture – a positively charged hole state: an e^+e^- pair has been created. A plane-wave laser field cannot produce pairs, though, no matter how strong it is. In fact, because of the Lorentz invariant shape of a plane wave, one can always perform a transformation to a frame of reference where $E \ll E_c$ and $\hbar\omega \ll mc^2$ and pair creation is excluded. The production probability is a function of the field invariants $F^{\mu\nu}F_{\mu\nu} = \mathbf{E}^2 - \mathbf{B}^2$ and $F^{\mu\nu}\tilde{F}_{\mu\nu} = \mathbf{E}\cdot\mathbf{B}$, with the field strength tensor $F^{\mu\nu}$ and its dual $\tilde{F}_{\mu\nu}$, which vanish identically for a plane wave. Therefore an additional perturbation is required for pair creation in a laser field. Possible candidates are the Coulomb field

of a charged particle [Yak65, Rit72], an additional non-laser photon [Rei62], or a second laser beam with different propagation direction [Bre70, Pop71].

The conversion of high-energy photons with $\hbar\omega > mc^2$ into e^+e^- pairs is a well-known phenomenon. For example, in the Breit-Wheeler process

$$\gamma_1 + \gamma_2 \to e^+e^- \tag{23}$$

two colliding high-energy photons combine their energies to produce the particles [Bre34]. In accordance with Eq. (1), the energy of each photon in the center-of-mass frame needs to exceed the electron rest mass mc^2. In the Bethe-Heitler process a pair is generated by γ-photon absorption in the Coulomb field of an atomic nucleus [Bet34]. Here, $\hbar\omega_\gamma \geq 2mc^2$ is required, since a Coulomb field cannot exchange energy but only momentum. The Bethe-Heitler process is similar to the Breit-Wheeler process (23), but with the second photon being virtual:

$$\gamma + \gamma^* \to e^+e^- \,. \tag{24}$$

It was first observed 60 years ago by employing synchrotron radiation or nuclear γ-rays (see, e.g., [Ada48]). In the Bethe-Heitler process, due to the presence of the nucleus, the electron can also be created in a bound atomic state [Agg97].

The Breit-Wheeler and Bethe-Heitler mechanisms of pair production allow for nonlinear generalizations when the photon source is an intense laser beam. Then, multiphoton processes are possible where more than one photon of the same sort (i.e., with the same four-momentum and polarization) participate in the pair production. Different regimes of laser-induced pair creation can be distinguished with the help of the invariant adiabaticity parameter $\xi = eE_0/m\omega c$ [cf. Eq. (3)]. For $\xi \ll 1$, pair creation occurs via multiphoton absorption and the probability follows a perturbative power law: $W \sim \xi^{2n_0}$, where n_0 is the minimal number of laser photons to be absorbed, as required by energy conservation. Significant production probabilities in the multiphoton regime are reached for $\hbar\omega \sim mc^2$. For $\xi \gg 1$, the process evolves quasi-statical and its probability shows a tunneling behavior similar to $W \sim \exp(-\pi E_c/E)$. In this case, the adiabaticity parameter has an intuitive interpretation via the tunneling time τ_{tun} as $\xi = \omega\tau_{\text{tun}}$. Efficient pair creation in the tunneling regime requires $E \sim E_c$ in agreement with Eq. (2). A close analogy exists with the strong-field ionization of atoms where the tunneling and multiphoton regimes are well known and distinguished by the value of the Keldysh parameter [Kel64, Rei92, Fed97]. The formal similarity between ionization and pair creation processes is illustrated in Fig. 7. Recently, the analogy has been extended to include also the recollision mechanism [Kuc07]. In the SLAC experiment mentioned above, the nonlinear Breit-Wheeler effect

$$\gamma + n\omega \to e^+e^- \tag{25}$$

was observed in the multiphoton regime ($\xi \approx 0.3$), with a high-energy Compton photon of $\hbar\omega_\gamma \approx 30\,\text{GeV}$ and $n = 5$ optical laser photons of $\hbar\omega \approx 2\,\text{eV}$. The high-energy photon was first produced by Compton backscattering of the same laser beam off a 46 GeV electron beam. In the center-of-mass frame this implies $\hbar\omega'_\gamma = 5\hbar\omega' \approx mc^2$. Recently, an all-optical setup for realization of the nonlinear Breit-Wheeler process through laser-accelerated electrons has been proposed theoretically [Bel08]. In contrast, nonlinear Bethe-Heitler pair creation

$$\gamma^* + n\omega \to e^+e^- \tag{26}$$

has not been observed in experiment yet.[3] It is important to note that the energy-conservation condition for this process reads $n\hbar\omega \geq 2m_*c^2$, with the laser-dressed mass $m_* = m\sqrt{1+\frac{1}{2}\xi^2}$. The latter appears since the leptons are to be created not in free space, but rather *inside* the field where their mass is effectively enhanced due to the ponderomotive energy.

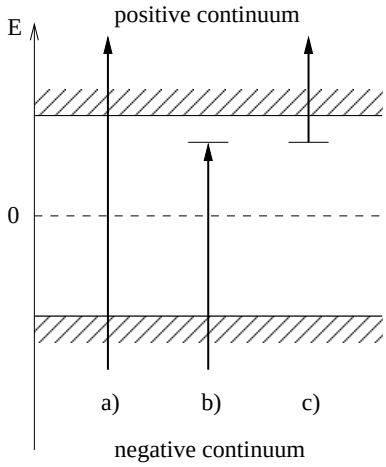

Figure 7: Schematic sketch of the processes of (a) free-free pair creation, (b) bound-free pair creation, and (c) ionization.

In this section we discuss various nonlinear schemes of pair production in intense laser fields. The focus lies on pair creation in combined laser and nuclear Coulomb fields via the nonlinear Bethe-Heitler process (26) which is elaborated in detail in Section 4.1. Both free and bound-free pair creation are treated and different interaction regimes considered. In Section 4.2, pair creation in two counterpropagating laser beams of equal intensity and frequency is briefly discussed. In this situation the pair is created by "doubly nonlinear" variants

$$n_1\omega_1 + n_2\omega_2 \to e^+e^- \tag{27}$$

of the Breit-Wheeler reaction (23), where n_1 photons are absorbed from the first beam and n_2 photons from the second.

It is noteworthy that in laser-ion and laser-laser collisions also other nonlinear QED processes than pair creation can occur. Recent theoretical studies have considered elastic photon-photon scattering and harmonic generation from vacuum, photon-splitting, photon-fusion, changes in the refractive index, and Delbrück scattering (see [Mar06, DiP08a, DiP08b], and references therein). These processes arise from the nonlinear response of the quantum vacuum due to virtual e^+e^- pairs which are polarized by the external laser field and mediate the interac-

[3] In recent studies on relativistic laser-plasma interactions, e^+e^- pair production via the ordinary Bethe-Heitler effect has been observed [Gah00, Che09]. In these experiments, a solid target is irradiated by an intense laser pulse which creates a hot plasma and accelerates electrons to high energies. The fast electrons emit bremsstrahlung which is converted into e^+e^- pairs in the field of the ions through the linear reaction (24). The laser field plays an indirect role only in the pair production here, by serving as a particle accelerator. In contrast to that, the Bethe-Heitler processes discussed in this section proceed nonlinearly via multiphoton absorption, with direct participation of the laser field in the pair creation step (26).

tion between electromagnetic fields. Also laser-induced quantum vacuum effects beyond QED and even the standard model are being considered [Gie08].

4.1 Pair creation in combined laser and Coulomb fields

The nonlinear Bethe-Heitler process (26) was first studied by Yakovlev [Yak65] and Mittleman [Mit87]. Both assumed a laser wave impinging on a nucleus at rest. Because of the large discrepancy between the laser peak field strengths available at that time and the critical field, the predicted production probabilities were very small. In his article, Mittleman even made the statement:

> *The cross section for this process at optical frequencies or below is so small at any laser intensity as to make it completely negligible. It may be the smallest (nonzero) cross section on record.*

Later on, however, enormous technological progress has been made, and the SLAC experiment has shown a way how to effectively extent the available laser parameters into the required domain. In a head-on collision geometry, the laboratory values of both the laser field strength E_L and frequency ω_L are enhanced by a factor $(1+\beta)\gamma$ in the projectile frame due to the relativistic Doppler shift, leading to $E \approx 2\gamma E_L$ and $\omega \approx 2\gamma\omega_L$ in this frame. Here, γ denotes the projectile Lorentz factor and β its reduced velocity. The most powerful ion accelerator is the Large Hadron Collider (LHC) at CERN (Geneva, Switzerland) which is currently starting operation [Yao06]. It will reach ion energies up to 7 TeV/nucleon corresponding to proton beams with a Lorentz factor of $\gamma \approx 7000$ and Pb nuclei with $\gamma \approx 3300$. When brought into collision with either an intense XUV beam of $\hbar\omega_L \sim 100\,\mathrm{eV}$ or a superstrong optical laser pulse of $I_L \sim 10^{22}\,\mathrm{W/cm^2}$, the pair creation conditions (1) and (2) can be met, respectively. Against this background we present in the following results on pair creation by relativistic ion impact on laser radiation in the multiphoton (Sections 4.1.2 and 4.1.4) and tunneling regimes (Section 4.1.3). To begin with, we describe two alternative theoretical approaches to the problem. All formulas refer to the projectile frame, unless explicitly stated otherwise.

4.1.1 Volkov-state versus polarization-operator approach

When considering pair creation in a laser-nucleus collision, one has to treat the lepton motion in the combined electromagnetic fields of the nucleus and the laser wave. The corresponding Hamiltonian reads

$$H = -i\hbar c\,\hat{\boldsymbol{\alpha}}\cdot\boldsymbol{\nabla} + \hat{\beta}mc^2 - eV_{\mathrm{ion}} + e\hat{\boldsymbol{\alpha}}\cdot\boldsymbol{A}\,. \tag{28}$$

Here, $\hat{\boldsymbol{\alpha}}$ and $\hat{\beta}$ denote Dirac matrices, $V_{\mathrm{ion}} = Ze/(4\pi\epsilon_0|\boldsymbol{r}|)$ is the ionic Coulomb potential in the rest frame of the nucleus, and $\boldsymbol{A}$ the laser vector-potential taken in the radiation gauge. In general, the transition amplitude for a quantum mechanical process can be expressed in two equivalent ways, either in the post form (see, e.g., [Rei92])

$$(S-1)_{fi} = -\frac{i}{\hbar c}\int \left[(H - i\hbar\partial_t)\,\Phi_f\right]^\dagger \Psi_i\, d^4x \tag{29}$$

or in the prior form

$$(S-1)_{fi} = -\frac{i}{\hbar c}\int \Psi_f^\dagger \,(H - i\hbar\partial_t)\,\Phi_i \,d^4x, \tag{30}$$

where Ψ_i (Ψ_f) is an eigenstate of the full Hamiltonian H, while Φ_f (Φ_i) is an exact asymptotic final (initial) state lacking only the potential which causes the transition. For the fully interacting states $\Psi_{i,f}$ no analytical expressions are known. In order to advance analytically, suitable approximations are therefore required.

The standard approach to pair creation in combined laser and Coulomb fields applies the SFA [Yak65, Mit87] (see also [9, 12, 33]). It is based on the fact that very high laser field strengths $E \sim E_c$ are necessary to extract pairs from vacuum, which exceed the typical Coulomb field (taken at a distance of $\lambda\!\!\!^{-}_C$) by orders of magnitude. Moreover, if the electron velocity v_- with respect to the nucleus is not too small (i.e., if $\alpha Zc/v_- \ll 1$) then the influence of the laser field on the electron should be dominant in comparison with the nuclear Coulomb field. In light of this, it is a reasonable approximation to describe the final-state particle in Eq. (30) by a Volkov state, this way taking its interaction with the laser field fully into account. The remaining interaction with the nucleus is considered as the perturbation which is treated in lowest order. It causes the transition from an electron in the negative continuum $\Phi_i = \Psi^{(+)}_{p_+,s_+}$ to a positive-energy state $\Psi_f \approx \Psi^{(-)}_{p_-,s_-}$. Within the SFA, the amplitude for free-free (ff) pair creation thus reads

$$S_{\rm ff}^{\rm SFA} = \frac{ie}{\hbar c}\int [\Psi^{(-)}_{p_-,s_-}]^\dagger V_{\rm ion}\, \Psi^{(+)}_{p_+,s_+}\, d^4x\,. \tag{31}$$

The labels "$(\pm)$" refer to the sign of charge of the created particles, $p_\pm$ are their momenta, and $s_\pm$ their spin states. We would have found the same expression, if we had started from the post-form amplitude (29) instead.

With the help of Eq. (31), all regimes of laser-induced pair creation can be described. It allows, in particular, to derive the fully differential process rate from which energy and angular particle spectra and, by integration over all final momenta, the total pair production rate can be obtained. Due to its complexity, the latter is usually performed numerically. In the case of small $\xi \ll 1$, the transition amplitude can be expanded into a perturbation series in powers of ξ by decomposing the product of Volkov states as in Eq. (6), where $J_n \sim \xi^n$ and n denotes the photon order. In this regime of laser-matter coupling, the leading-order rate for nonlinear Bethe-Heitler pair creation by absorption of n laser photons scales like $R^{(n)} \sim \xi^{2n}$. Accordingly, the SLAC experiment found a reaction rate $\sim \xi^{10}$, which agrees with the absorption of five laser photons as mentioned earlier. We note that in multiphoton physics total probabilities are preferably given as reaction rates since the cross section for a multiphoton process $\sigma^{(n)} = R^{(n)}/j$, with the photon flux $j = \omega\xi^2/(8\pi\alpha\lambda\!\!\!^{-2}_C)$, still involves powers of ξ^2 and thus depends on the incoming photon intensity, which is an undesirable feature for a cross section in the usual sense. (The notion of a *nonlinear* process is, in fact, motivated by its nonlinear dependence on the photon field intensity, $R^{(n)} \sim I^n$.) Higher-order corrections to the leading term stem from additional photon exchange which goes beyond the minimum photon number required from energy conservation. For example, when pair creation is energetically possible by two-photon absorption, there will be small additional contributions where more

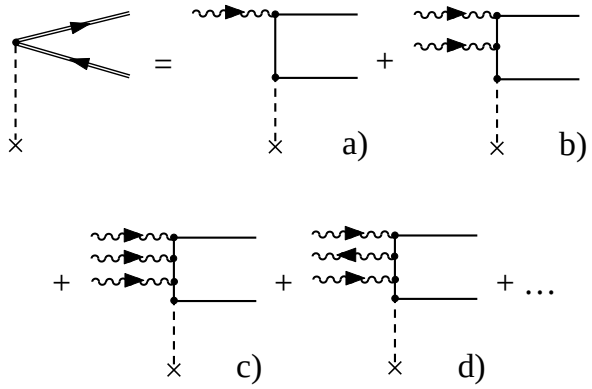

Figure 8: Graphical equation in terms of Feynman diagrams describing free e^+e^- pair production in combined laser and Coulomb fields. The interaction of the leptons with the latter is treated within the first order of perturbation theory here and indicated by the dashed lines. The interaction with the laser wave is accounted for to all orders within the framework of laser-dressed QED, as expressed by the first Feynman graph where the double lines represent the exact lepton wave-functions in the laser field (Volkov states). Expanding the Volkov states with respect to the lepton-laser coupling results in a perturbation series, some typical low-order terms of which are shown by diagrams a)-d). The laser photons are symbolized by the wavy lines and the arrows indicate whether the respective laser photon is emitted or absorbed during the process. (from [33])

than two photons have been absorbed. These corrections are suppressed by an additional ξ^2 factor. The perturbation series is visualized in terms of Feynman diagrams in Fig. 8. For larger values $\xi \gtrsim 1$, the nonperturbative domain of pair creation is entered.

For calculations of total pair production rates, an alternative approach based on the optical theorem may be used. It has been developed in [16] and employs the explicit form of the polarization operator of a photon in a laser field [Bai75, Bec75]. Similarly to the SFA approach, the interaction of the leptons with the laser field is taken into account to all orders, while the effect of the Coulomb field is treated in first order. The main advantage of this method is that the asymptotic behavior of the total process probability can be evaluated by analytical means for various limits of interest.

The polarization operator $\Pi^{\mu\nu}(\kappa)$ generally describes the propagation of a photon of four-momentum κ^μ in a background field (e.g., the QED vacuum), including self-energy corrections. It is related to the corresponding exact photon propagator $\mathcal{D}^{\mu\nu}(\kappa)$ via Dyson's equation [Ber71]

$$\mathcal{D}_{\mu\nu}(\kappa) = D_{\mu\nu}(\kappa) + D_{\mu\sigma}(\kappa)\frac{\Pi^{\sigma\lambda}(\kappa)}{4\pi}\mathcal{D}_{\lambda\nu}(\kappa) \tag{32}$$

where $D^{\mu\nu}(\kappa)$ denotes the free photon propagator. Apart from its theoretical significance, the knowledge of the polarization operator allows for a number of applications. For example, the total probability for e^+e^- pair production by a photon of momentum κ^μ in an external field (e.g., a plane laser wave) is related

to the imaginary part of the corresponding polarization operator via [Ber71]

$$W = \frac{\epsilon_\mu \epsilon_\nu^*}{\kappa^0} \mathrm{Im}\Pi^{\mu\nu}(\kappa) \tag{33}$$

where ϵ_μ denotes the photon's polarization four-vector. Equation (33) follows from an application of the optical theorem to the elastic forward scattering amplitude of the photon through an intermediate laser-dressed e^+e^- state, including a sum over all these states.

The calculation of the polarization operator in Ref. [Bai75] was performed for an arbitrary photon momentum κ^μ, including the case $\kappa^2 \neq 0$, and therefore not only applies to the combination "photon + laser wave". Instead, the photon may be replaced by any additional external field $A_\mu^{(\mathrm{ext})}(\kappa)$ such as a nuclear Coulomb field. Since a Coulomb field can transfer momentum but not energy, here one has $\kappa^\mu = (0, \mathbf{q})$ and needs to replace the photon wave-function $A_\mu^{(\mathrm{ph})}(\kappa) = \sqrt{4\pi/2\kappa^0}\epsilon_\mu$ in Eq. (33) by the Fourier transform of the Coulomb field $A_\mu^{(\mathrm{ion})}(\mathbf{q}) = (4\pi Ze/\mathbf{q}^2)\delta_{\mu 0}$. The total production rate then is found by integration over all possible momenta:

$$R = \dot{W} = \frac{(4\pi Ze)^2}{4\pi} \int \frac{d^3q}{(2\pi\hbar)^3} \frac{\mathrm{Im}\,\Pi^{00}}{q^4}. \tag{34}$$

By inserting the explicit form of the polarization operator into Eq. (34), it is possible to derive, independent of the laser's polarization state, in an analytical manner compact formulas for the total production rate which only involve low-dimensional integrals and no additional summations. Based on these representations one can rather easily find all different kinds of asymptotics, which will be presented in Sections 4.1.2 and 4.1.3. Since Π^{00} already contains a summation over the electron and positron momenta, it is however not possible to obtain differential rates in this way. From this point of view, the SFA and polarization operator approaches complement each other.

4.1.2 Multiphoton pair production in XUV and X-ray laser fields

In relativistic collisions of protons or heavy ions with high-frequency laser beams nonlinear Bethe-Heitler pair creation in the multiphoton regime can be realized. The highest laser frequencies presently available amount to $\hbar\omega_L \sim 100\,\mathrm{eV}$ and are produced by attosecond pulse trains (APTs) from gas harmonics or the DESY-FLASH facility. Near-future XFEL facilities will even provide coherent radiation of $\hbar\omega_L \sim 10\,\mathrm{keV}$. When such an X-ray pulse collides with a relativistic ion beam of $\gamma \sim 50$, the photon energy in the ion frame approaches the MeV range and pair creation becomes feasible. This would require, however, the combination of two large-scale XFEL and ion accelerator facilities.[4] Similarly, the condition $\hbar\omega \sim mc^2$ can be met when an XUV pulse of 100 eV photon energy collides with an ultrarelativistic ion beam of $\gamma \sim 5000$. Such nuclear Lorentz factors lie in the range of the LHC at CERN . While the main physics objectives of this new machine are the search for the Higgs boson and for physics beyond the

[4] Relativistic protons with $\gamma \approx 50$ might also be attainable through laser wakefield acceleration in the so-called piston regime [Esi04]. So far, laser-based acceleration devices have been able to generate ion energies in the MeV range, which still lies in the nonrelativistic regime ($\gamma \sim 1$) [Heg06, Sch06a, Ton06].

standard model [Yao06], the research domain of nonlinear QED processes might become interesting for the LHC once its major tasks have been accomplished. For realization of multiphoton Bethe-Heitler pair creation the combination of LHC with a source of attosecond pulses appears most practical, in fact, since these are generated by table-top devices which are conceivable to install at CERN-LHC [33].

In view of the experimental prospects, it is interesting to consider laser-induced pair creation at low intensities ($\xi \ll 1$) in a situation where the required energy can only be supplied by the simultaneous absorption of (at least) two photons instead of a single one [see Fig. 8(b)]. Two-photon absorption represents a nonlinear process of lowest order. The corresponding production rate has been derived in Ref. [16]. Close to the energetic threshold, it reads

$$R^{(2)} = \frac{(\alpha Z)^2}{64}\xi^4\omega\left(\frac{\hbar\omega}{mc^2} - 1\right)^2 \tag{35}$$

in the nuclear rest frame, assuming a linearly polarized laser wave. The corresponding rate in the laboratory frame is reduced by a factor γ^{-1} due to time dilation. It is interesting that the frequency scaling changes for circular laser polarization to

$$R^{(2)}_{\mathrm{circ}} = \frac{(\alpha Z)^2}{4}\xi^4\omega\left(\frac{\hbar\omega}{mc^2} - 1\right)^4 . \tag{36}$$

Polarization dependence of total probabilities is a characteristic feature of nonlinear processes, in general. One can compare Eqs. (35) and (36) with the well-known Bethe-Heitler formula for pair creation by a single photon of energy $\hbar\omega > 2mc^2$ [see Fig. 8(a)]. In the nonrelativistic limit close to the energetic threshold ($\hbar\omega - 2mc^2 \ll mc^2$), the latter possesses a rather similar structure [Ber71]

$$R^{(1)} = \frac{(\alpha Z)^2}{96}\xi^2\omega\left(\frac{\hbar\omega}{mc^2} - 2\right)^3 . \tag{37}$$

In the opposite high-energy limit, $\hbar\omega \gg 2mc^2$, the linear Bethe-Heitler rate can be written in closed form as

$$R^{(1)} = \frac{7}{18\pi}(\alpha Z)^2\xi^2\omega\left[\ln\left(\frac{2\hbar\omega}{mc^2}\right) - \frac{109}{42}\right] . \tag{38}$$

The next-to-leading order correction term to Eq. (38) is found to be [16]

$$\Delta R = -\frac{13}{90\pi}(\alpha Z)^2\xi^4\omega\left[\ln\left(\frac{2\hbar\omega}{mc^2}\right) - \frac{22}{13}\ln 2 - \frac{124}{195}\right] . \tag{39}$$

It contains the process of two-photon pair production as well as ξ^2-corrections to one-photon pair creation [arising, e.g., from the interference between the diagrams in Fig. 8(a) and 8(d)]. The correction (39) would have an appreciable effect in stronger laser fields with $\xi \gtrsim 0.1$ where it reaches the percent level. Corresponding XUV intensities are likely to be attainable from plasma harmonics (see Section 1.2). Signatures of the additional photon involved would also arise in the energy spectra of the created particles.

Let us consider the collision of an intense, linearly polarized APT ($\hbar\omega_L = 100\,\mathrm{eV}$, $\xi = 1.4 \times 10^{-4}$) with the LHC ion beams. For proton impact with

$\gamma = 7000$, an e^+e^- pair is produced by one-photon absorption since $\hbar\omega = 1.4\,\mathrm{MeV}$. Numerically evaluating Eq. (31), we obtain a corresponding lab-frame rate of $R^{(1)}_{\mathrm{lab}} \approx 5.79 \times 10^2\,\mathrm{s}^{-1}$, which is in reasonable agreement with the appropriately Lorentz-transformed threshold formula (37). The latter slightly overestimates the rate by a factor of 2 since the frequency value lies above its range of applicability. When Pb projectiles with $\gamma = 3300$ are used instead, two photons are needed to overcome the energy barrier. The higher-order in ξ^2 leads to a smaller total rate of $R^{(2)}_{\mathrm{lab}} \approx 2.53 \times 10^{-2}\,\mathrm{s}^{-1}$. Coulomb corrections to the first-order treatment of the nuclear field in Eq. (31) could slightly modify this value ($\alpha Z \approx 0.6$). For comparison we note that a proton at the same speed leads to a rate of $R^{(2)}_{\mathrm{lab}} \approx 3.76 \times 10^{-6}\,\mathrm{s}^{-1}$. These numbers agree with Eq. (35), again within a factor of 2. The rates can be transformed into total yields by taking the laser pulse length and repetition rate as well as the projectile beam density into account. We assume that in the experiment a single LHC ion bunch containing $N_{\mathrm{ion}} \approx 10^{11}$ particles is used. It has a transverse radius of about $\varrho_{\mathrm{ion}} \approx 16\,\mu\mathrm{m}$ and circulates with a revolution frequency of $f_{\mathrm{ion}} \approx 11\,\mathrm{kHz}$ [Yao06]. An APT of 30 fs total duration is supposed, consisting of 25 single attosecond pulses with a duration of 300 as each. The effective time when the field is present in the APT thus amounts to $\tau = 7.5\,\mathrm{fs}$. Note here that the individual attosecond bursts are separated by half a period of the driving optical laser. The train repetition rate can be synchronized with the circulating ion beam, i.e., $f_{\mathrm{APT}} = f_{\mathrm{ion}}$. The typical diameter of an APT is on the order of $10\,\mu\mathrm{m}$ so that we may assume perfect overlap with the ion beam. The number of pair creation events per unit of time is determined by $\dot{N}_{\mathrm{ev}} = R_{\mathrm{lab}} N_{\mathrm{ion}} f_{\mathrm{ion}} \tau/2$, with the factor of $1/2$ arising from the relative beam velocity. We obtain 0.1 nonlinear Bethe-Heitler pair creation events per second via two-photon absorption from the APT colliding with the LHC Pb beam. This event rate seems to render experimental observation feasible. For comparison, we note that about 2400 e^+e^- pairs per second are produced through the ordinary Bethe-Heitler process (24) when the 7 TeV proton beam is used instead.

When the value of the intensity parameter ξ approaches unity, the perturbative multiphoton character of pair creation is changing. At $\xi \sim 1$ not only the smallest possible photon number n_0, but several photon orders make significant contributions to the total rate. This behavior is generally called an above-threshold phenomenon since the excess photons absorbed lead to particle energies substantially above the energetic threshold of the process. The transition from the multiphoton to the above-threshold regime is illustrated in Fig. 9, where the collision of a relativistic proton ($\gamma = 50$) with an intense XFEL beam ($\hbar\omega_L = 9\,\mathrm{keV}$) is considered. The contributions of different photon orders $n \geq n_0 = 2$ are shown for various laser intensities. While for the smallest intensity the pairs are produced exclusively by two-photon absorption, higher photon orders become non-negligible when the intensity is raised and eventually exceed the leading-order contribution. At even higher laser intensities (not shown in Fig. 9), a channel-closing effect appears: Since the laser-dressed electron mass m_* grows with increasing field intensity, the energy gap for pair creation is growing and, at a certain point, cannot be overcome by only two photons anymore.

Analogous phenomena are known from extensive theoretical and experimental studies of the above-threshold ionization (ATI) of atoms in strong laser fields [Fed97, Bec02]. Similarly as for the ATI, the above-threshold pair creation at $\xi \gtrsim 1$

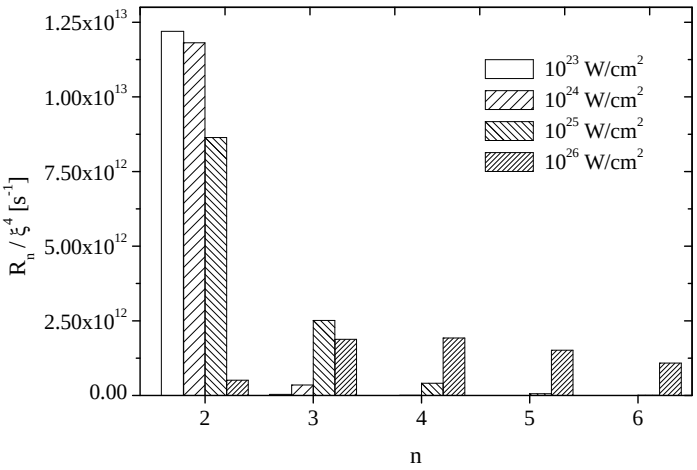

Figure 9: Above-threshold pair production in relativistic XFEL-proton collisions ($\gamma = 50$, $\hbar\omega_L = 9\,\mathrm{keV}$, circular polarization), for various values of the laser intensity. Shown are the contributions of different photon orders to the process. When $\xi \approx 1$ is reached at $I_L \sim 10^{26}\,\mathrm{W/cm^2}$, photon numbers beyond the leading order become appreciable and eventually dominant. (from [12])

forms a bridge between the multiphoton pair creation ($\xi \ll 1$) and the tunneling pair creation ($\xi \gg 1$) considered in the next section. Since above-threshold pair production represents an intermediate regime, it is difficult to derive closed-form expressions for the total pair creation rate by analytical means here. We have therefore performed numerical SFA calculations for $\xi = 1$ and fitted an analytical curve to our data. This way, we obtain the approximate scaling relation

$$R^{(\mathrm{AT})} \sim \exp\left(-3.49\frac{mc^2}{\hbar\omega}\right) \tag{40}$$

for the total rate of above-threshold pair production. The exponential behavior closely resembles the pair production rate in the tunneling regime which scales as $\sim \exp\left(2\sqrt{3}E_c/E\right)$ [see Eqs. (41) and (42) below]; note that $E_c/E = mc^2/\hbar\omega\xi$. Above-threshold pair production at low laser frequencies $\hbar\omega \ll mc^2$ is therefore heavily suppressed.

4.1.3 Tunneling pair production in low-frequency laser fields

When CERN-LHC is combined with a superintense Petawatt-class laser system, e^+e^- pair creation could be realized in the tunneling regime [7, 9]. The most powerful present lasers reach field amplitudes on the order of $E_L \sim 10^{12}\,\mathrm{V/cm}$ in the infrared range ($\xi \sim 100$) so that the field strength in the ion frame $E \approx 2\gamma E_L$ would approach the critical value $E_c = 1.3 \times 10^{16}\,\mathrm{V/cm}$. Corresponding devices are large-scale facilities, though, such as HERCULES [Yan08], VULCAN [VUL] or PHELIX [Hof05], rendering their conjunction with LHC a rather hypothetical scenario. However, there are also efforts to develop a table-top Petawatt laser system [MPQ], which is going to be commissioned this year. Such a device, when combined with LHC, would render the first observation of tunneling pair creation feasible.

Pair creation occurs via tunneling when $\xi \gg 1$ and $\eta \ll 1$, where $\eta \equiv E/E_c$. The corresponding total rate in a circularly polarized laser wave reads [16]

$$R_{\mathrm{circ}}^{(\mathrm{tun})} = \frac{(\alpha Z)^2}{2\sqrt{\pi}} \frac{mc^2}{\hbar} \left(\frac{\eta}{2\sqrt{3}}\right)^{5/2} \exp\left(-\frac{2\sqrt{3}}{\eta}\right) , \tag{41}$$

referring to the rest frame of the projectile nucleus. The exponential dependence is characteristic for a quantum tunneling process. Equation (41) agrees with the corresponding results for a constant homogeneous or a constant crossed field [Rit72], indicating the quasi-static nature of the process. In comparison with the result for circular polarization, the production rate in a linearly polarized laser wave

$$R_{\mathrm{lin}}^{(\mathrm{tun})} = \frac{(\alpha Z)^2}{\sqrt{2}\pi} \frac{mc^2}{\hbar} \left(\frac{\eta}{2\sqrt{3}}\right)^{3} \exp\left(-\frac{2\sqrt{3}}{\eta}\right) \tag{42}$$

is suppressed by an additional factor of $\sqrt{\eta} \ll 1$. The reason for the suppression is that the modulus of the field strength has a constant value in a circularly polarized wave, whereas it is truly oscillating in a linearly polarized field. We also give a formula in the overcritical-field domain ($\xi \gg 1$, $\eta \gg 1$) which corresponds to the over-barrier regime of ionization. Here the exponential increase of the tunneling rates goes over into a logarithmic dependence on the field, and we obtain for circular polarization

$$R_{\mathrm{circ}}^{(\mathrm{OB})} = \frac{13}{6\sqrt{3}\pi} (\alpha Z)^2 \frac{mc^2}{\hbar} \eta \left[\ln\left(\frac{\eta}{2\sqrt{3}}\right) - C - \frac{58}{39}\right] , \tag{43}$$

with the Euler constant $C \approx 0.577$. In this regime, the laser polarization is of minor importance so that a very similar rate expression results for the linear polarization case.

While Eqs. (41)-(43) have been derived by the polarization operator approach, in the intermediate regime with $\xi \gg 1$ and $\eta \sim 1$ it is difficult to obtain analytical rate expressions. It is, however, exactly this intermediate regime which is most interesting from an experimental point of view, as it corresponds to the parameters outlined above. We have therefore performed SFA calculations in this regime, yielding information on the total pair production probability and the particle spectra [7, 9]. Figure 10 shows energy distributions of one of the created leptons in the laboratory frame. Since Eq. (31) treats the nuclear field in first order, the spectra of the electron and positron are identical within our approach. The particles possess highly relativistic energies in the GeV range. On the one hand, this is due to the high Lorentz factors γ which mediate the transformation between the nuclear rest frame (where the pairs are produced) and the laboratory system. On the other hand, the leptons are characterized by high energies also in the ion frame because the typical number of absorbed photons $n \sim \xi n_0 \sim 10^6$ lies far above the energy threshold. By energy-momentum conservation, the absorption of such a large number of laser photons, each with the same four-momentum, leads to "photon-like" kinematical features of the leptons: They are not only highly relativistic, so that their dispersion relation $\varepsilon_{p_\pm} \approx |\mathbf{p}_\pm| c$ resembles massless particles, but also emitted under small angles along the wave propagation direction. We note that the Lorentz transformation leads to a reversed emission direction in the laboratory system. A consideration of the linear-polarization case can be found in [Kam06].

Based on our numerical data, we performed again a fitting procedure and found for the total process rate the approximate relation

$$R \sim \exp\left\{-\mu\left(\frac{E_c}{E}\right)^{\kappa}\right\}, \tag{44}$$

with $\mu \approx 5.918$ and $\kappa \approx 0.8825$. For proton impact at $\gamma = 3500$, our calculated production rate amounts to 6×10^9 s^{-1} in the laboratory frame. Assuming a laser pulse duration in the picosecond range, an effective production rate of about 3×10^{-3} pairs per collision results. This amount seems to be accessible to experimental observation. The corresponding rate for a proton moving at the maximum LHC Lorentz factor of $\gamma = 7000$ is 8×10^{10} s^{-1}. The Z^2 scaling of the production rate implies, however, that an ion of charge $Z \geq 4$ moving at $\gamma = 3500$ is more efficient for pair creation than such a 7 TeV proton.

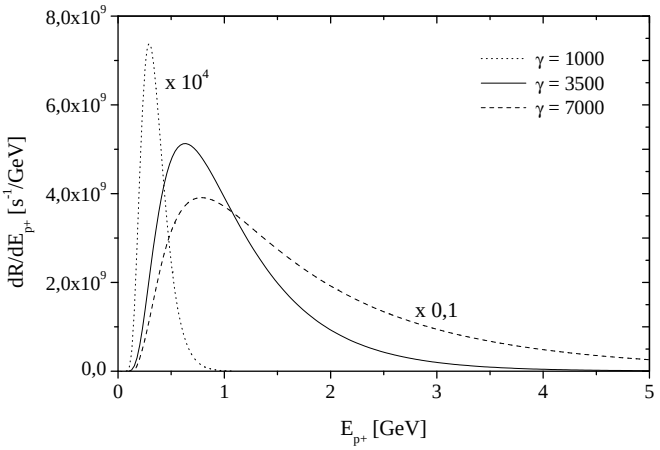

Figure 10: Laboratory-frame rates for pair production by an ultrarelativistic proton colliding with a powerful near-infrared laser beam ($I_L = 10^{22}\,\mathrm{W/cm^2}$, $\hbar\omega_L = 1.5\,\mathrm{eV}$, $\xi = 50$) of circular polarization, differential in the energy of one of the created leptons. The dashed, solid, and dotted lines assume a proton Lorentz factor of $\gamma = 7000$, 3500, and 1000, respectively. (from [9])

4.1.4 Multiphoton bound-free pair creation

In collisions of relativistic ion beams with intense laser pulses also bound-free pair production may occur. Here the electron is created in a bound atomic state of the projectile while the positron is free (see Fig. 7). The corresponding process is known from relativistic heavy-ion collisions and has been observed at CERN and Fermilab in the energy range $\sim$ 1–100 GeV/nucleon [Bau07]. For small nuclear charge numbers Z, bound-free pair creation is suppressed, but it becomes competitive with the free-free channel at intermediate and high Z values.

Bound-free pair creation by a single high-energy photon in a nuclear field was, in principle, already calculated in the early 1930s by Sauter (see [Ber71]), whose results on photoionization can be transformed into bound-free pair creation rates by the usual crossing symmetry. The multiphoton generalization can be obtained

within the SFA in a way similar to Eq. (31). We point out that the polarization operator approach of Section 4.1.1 cannot be applied here, since the electron is produced in a discrete state. The SFA amplitude for nonlinear bound-free (bf) pair creation can be written in the post-form as [10]

$$S_{\mathrm{bf}}^{\mathrm{SFA}} = -\frac{ie}{\hbar c} \int d^4x \; \Phi^\dagger \; (\boldsymbol{\alpha}\cdot\boldsymbol{A}) \, \Psi_{p_+}^{(\mathrm{V})} \; . \tag{45}$$

The bound-state electron wave function Φ is assumed to be free from the interaction for $t \to \infty$ while the free (i.e. unbound) positron wave function Ψ_{p_+} feels both the laser and the Coulomb field. The laser vector-potential $\mathbf{A}$ is considered as the interaction and assumed to be turned off asymptotically at $t \to \infty$. Within the SFA, the exact positron state Ψ_{p_+} is approximated by a Volkov state $\Psi_{p_+}^{(\mathrm{V})}$. The SFA can be applied, when the laser field is sufficiently strong and the influence of the Coulomb potential on the positron negligible. On the other hand, the laser field strength must not be too strong, so that the existence of bound states is assured. This sets limits on the nuclear charge number Z which should be of intermediate value to give reasonable results. Bound-free pair creation is particularly similar to strong-field ionization [Bec02] from a theoretical point of view. In ionization, an electron is lifted from a bound state to a state in the positive-energy continuum via the absorption of photons. Similarly, in pair production an electron in the negative-energy continuum is lifted into a bound state. Hence, initial and final states are essentially interchanged. While for pair production we describe the process in the post form, in ionization it is more appropriate to use the prior form [Rei92]. Due to the presence of a bound state in Eq. (45), the evaluation of the pair production rate can be carried out by analytical means to a large extent. The calculation was first performed for circular laser polarization [10] with electron capture to the K-shell, and recently generalized to a linearly polarized beam, including electron capture to excited states in the L-shell [32]. Bound-free pair creation in the combined fields of a nucleus and an ultrashort, single-cycle laser pulse has been treated within the sudden approximation in [Mat05].

We have considered bound-free pair creation at high laser frequencies in the multiphoton regime. In principle, also the tunneling and above-threshold regimes exist, but then the laser field strength considerably exceeds the atomic binding field, so that the notion of a "bound state" becomes questionable. Rather, we imagine the collision of a highly relativistic nucleus with an XUV or X-ray laser beam, where the energy gap for bound-free pair creation, $\Delta\varepsilon = 2m_*c^2 - \varepsilon_b$, can be overcome by few-photon absorption. The collision parameters coincide with those assumed in Section 4.1.2. When bound-free pair creation occurs by two-photon absorption and the electron is born in the K-shell, the total process rate in the ion frame scales approximately like

$$R_{\mathrm{bf}}^{(2)} \sim Z^5 \xi^4 \, (\omega - \omega_{\mathrm{min}})^\kappa \, . \tag{46}$$

Here, ω_{min} denotes the minimal frequency required to bridge the energy gap, i.e., $2\hbar\omega_{\mathrm{min}} = \Delta\varepsilon$. Equation (46) shows the typical Z^5 dependence of an atomic capture process. It originates from the fact that the spatial integral in Eq. (45) resembles a Fourier transformation of the bound state; the Fourier transform $\tilde{\Phi}(\mathbf{p})$ of an s-state scales like $Z^{5/2}$ for large momentum values. The exponent of the frequency scaling depends on the laser polarization and amounts to $\kappa \approx$

1/2 for linear polarization and $\kappa \approx 1$ for circular polarization. We have met a similar polarization dependence of free pair creation in Eqs. (35) and (36) where the exponent for circular polarization also was twice as large as for linear polarization. The different frequency scalings of the free versus the bound-free channel can be attributed to the different phase spaces which are occupied by the particles. We point out that both the laser and the nuclear field enter into Eq. (46) beyond first order. For the collision of a relativistic Sn nucleus ($Z = 50$, $\gamma = 50$) with an intense XFEL beam ($\hbar\omega_L = 9\,\mathrm{keV}$, $I_L = 8 \times 10^{19}\,\mathrm{W/cm^2}$), we obtain total rates in the laboratory frame of $R_{\mathrm{bf}}^{\mathrm{lin}} = 8.5 \times 10^3\,\mathrm{s}^{-1}$ and $R_{\mathrm{bf}}^{\mathrm{circ}} = 6.5 \times 10^3\,\mathrm{s}^{-1}$ for linear and circular laser polarization, respectively. At a given laser intensity, linear polarization leads to slightly larger production rates since the peak electric field is by a factor of $\sqrt{2}$ larger than for an equally intense circular-polarized wave. (Note that the opposite holds true, $R_{\mathrm{bf}}^{\mathrm{lin}} < R_{\mathrm{bf}}^{\mathrm{circ}}$, when equal peak field strengths are assumed instead so that the circularly polarized beam would be more intense.) The corresponding rates for free pair creation are $R_{\mathrm{ff}}^{\mathrm{lin}} = 1.2 \times 10^4\,\mathrm{s}^{-1}$ and $R_{\mathrm{ff}}^{\mathrm{circ}} = 9.6 \times 10^3\,\mathrm{s}^{-1}$. We see that the bound-free channel is comparable in size at high nuclear charge states, due to the much steeper increase with Z^5 which arises from the bound s-state involved. The free pair creation rate grows with Z^2 only, hence the portion of bound-free pair creation becomes increasingly important for higher Z values. The bound-free channel is also favored by the smaller energy gap which is reduced by the atomic binding energy. In the multiphoton regime, however, this difference is not as crucial as it would be in the tunneling regime.

In an experiment, the competing channels of free and bound-free pair production can be distinguished by positron detection solely [10]. This is important because the bound electron state can decay via photoionization in the laser field. Figure 11 shows the polar angle distributions of the positrons from the free and bound-free channel, respectively. The laboratory-frame spectra exhibit characteristic differences: While the positrons from free pair creation smoothly cover a narrow angular range between, say, 177.5° and 179.8°, practically all positrons from bound-free pair creation are emitted into the angle 177.25°, thereby forming an almost discrete spectrum located slightly below the continuous free spectrum. The (integrable) singularity is of kinematical origin and arises from the Lorentz transformation into the laboratory frame, because the positron velocity v_+ in the nucleus frame has a fixed value which is smaller than the relative velocity between the two frames of reference. Under such circumstances, a singularity appears at the polar angle given by

$$\sin\theta_{\mathrm{min}} = \frac{\gamma_+\beta_+}{\gamma\beta}\,, \tag{47}$$

with $\beta_+ = v_+/c$ and $\gamma_+ = (1-\beta_+^2)^{-1/2}$. To the positrons from the free pair production channel this argument does not apply since their energy in the nuclear rest frame is not fixed but varies over a broad range. The angular positron spectra are therefore a sensitive observable to discriminate bound-free from free pair creation in these collisions.

The contribution to the bound-free pair production rate from the L-shell is rather small, since the K-shell has a larger width in momentum space [32]. Capture processes occur preferentially into s-states which obey a Z^5 scaling law, in accordance with Eq. (46). For the $2s:1s$ ratio we find an approximately constant value of 1/8. This is in agreement with a general rule which is known, for example,

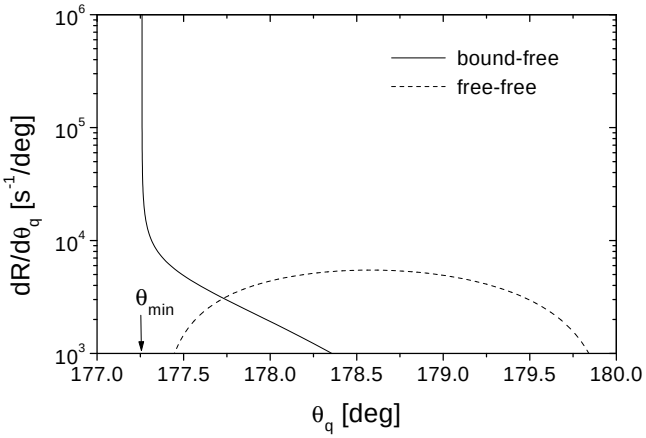

Figure 11: Lab-frame rates for free-free and bound-free pair creation by two-photon absorption from an intense XFEL ($\hbar\omega_L = 9\,\mathrm{keV}$, $I_L = 8 \times 10^{19}\,\mathrm{W/cm^2}$) colliding with a relativistic heavy nucleus ($Z = 50$, $\gamma = 50$). The rate is differential in the polar emission angle θ_q of the positron which is measured with respect to the laser propagation direction. (from [10])

from one-photon pair production in the high-energy limit [Agg97]: the contribution from the s-state with principal quantum number n_p is reduced by the factor n_p^{-3} as compared to the $1s$ contribution. For $Z = 50$ and linear laser polarization, the rate amounts to $R_{2s} = 1.1 \times 10^3\,\mathrm{s}^{-1}$. The $2p_{1/2}$ state contributes by three orders of magnitude less than the $2s$ state at low projectile charges. At high Z values, however, its contribution becomes appreciable as the scaling with Z^7 is steeper here. The reason is that the lower components of the bound Coulomb-Dirac state exhibit s-wave character and become comparable in size with the upper components for high nuclear charges. Accordingly, the total contribution from the L-shell to nonlinear bound-free pair creation amounts to about 15–20%.

It might be interesting to note that antihydrogen atoms could be produced through the bound-free pair creation channel in collisions of high-frequency laser pulses with antiprotons. The corresponding process in relativistic antiproton-ion collisions was realized a decade ago at the CERN-LEAR facility (see [Bau07]) and more recently with slow antiprotons at CERN-AD [Amo02].

4.2 Pair creation in counterpropagating laser beams

Purely light-induced pair production can occur when two laser waves are superimposed. The most simple field configuration consists of two counterpropagating laser pulses of equal frequency and intensity; the resulting field is a standing wave which is inhomogeneous both in space and time. While in the laser-ion collisions considered in Section 4.1 the Doppler boost of the laser parameters due to a highly relativistic Lorentz factor could be exploited, in laser-laser collisions this is not possible so that high laser field strengths E or frequencies ω are required to exist in the laboratory frame. In view of the envisaged progress in laser technology [ELI, Alt06] an experimental observation of pair creation in pure laser fields still seems to be coming into reach in the foreseeable future [Alk01, Rin01, Bul06]. Pair

production in a standing wave has been considered by many theoreticians (for a comprehensive list of references, see Sec. 7.1.3 in [Sal06]), starting with the seminal work of Brezin and Itzykson [Bre70] and Popov [Pop71]. All theoretical investigations so far have approximated the standing laser wave by a spatially homogeneous electric field oscillating in time, which allows for an analytical treatment of the problem. This dipole approximation is expected to be justified at low laser frequencies $\hbar\omega \ll mc^2$, since the spatial scale of the field variation $\sim \lambda = 2\pi c/\omega$ is much larger than the pair formation length, which is proportional to the Compton wave length $\lambda\!\!\!^{-}_C$ and amounts to $\ell = \lambda\!\!\!^{-}_C E_c/E$ in the tunneling regime. The relation $\lambda \gg \ell$ corresponds to $\xi \gg 1$ in terms of the relativistic laser parameter.

Nowadays the experimental realization of laser-induced pair production is also extensively discussed in connection with upcoming XFEL facilities [Alk01, Rin01]. In this case, however, the laser frequency is high, and $\xi \lesssim 1$. The XFEL prospect necessitates calculations involving the spatial field dependence and, thus, the laser magnetic field. A corresponding calculation is very difficult to perform by analytical means since the SFA is not applicable: Volkov states can only describe the interaction with one of the waves, but the other wave cannot be considered a perturbation. Rather, both laser waves have to be treated on the same footing because they are equally strong. Analytical wave functions in the combined field are not known, though. Problems in external fields with spatiotemporal dependence, in general, represent a challenge for nonperturbative quantum field theory [Gie05]. We have therefore calculated pair creation in counterpropagating high-frequency laser pulses by ab-initio numerical methods [34], employing the computer code which has been introduced in Section 2.1. We consider the above-threshold regime with $\xi = 1$ for both beams taken together. An initially free wave packet of zero momentum and negative energy, representing an electron in the Dirac sea, is propagated numerically in the presence of the fields and the pair creation amplitude is determined by projection onto positive-energy free states $\Phi^{(+)}_{\mathbf{p}'}$ after the external fields have been turned off. The computational procedure is equivalent to the field-theoretical approach to pair creation in external fields with unstable vacuum, which is based on a Bogoliubov transformation [Fra91]. The numerical ansatz allows us to reveal the influence of the spatial field dependence and the laser magnetic field component on the pair production dynamics.

First, we summarize the main results which have been found within the dipole approximation. Neglecting the spatial field variation by considering the standing laser wave as purely time dependent implies that momentum is conserved, in accordance with Noether's theorem. The problem is therefore effectively reduced to a two-level system since the field couples negative and positive-energy states of same momentum only (i.e., the total momentum of the electron and positron is zero). The production process exhibits a resonant nature when the energy gap is an integral multiple of the laser frequency. The laser frequencies where the resonances occur, are located at

$$\omega_n = \frac{2q_0(\mathbf{p})}{n\hbar}. \tag{48}$$

Here, n denotes the number of absorbed photons and the quasi-energy of the field-dressed state is given by $q_0(\mathbf{p}) = (c/T)\int_0^T \mathrm{d}t \sqrt{\left(\mathbf{p} + \frac{e}{c}\mathbf{A}(t)\right)^2 + m^2c^2}$, with the vector potential $\mathbf{A}(t)$, the pulse duration T, and the canonical momentum $\mathbf{p}$. For $\mathbf{p} = 0$ and $\xi = 1$, the value of the quasi-energy is $q_0(0) = 1.21mc^2$.

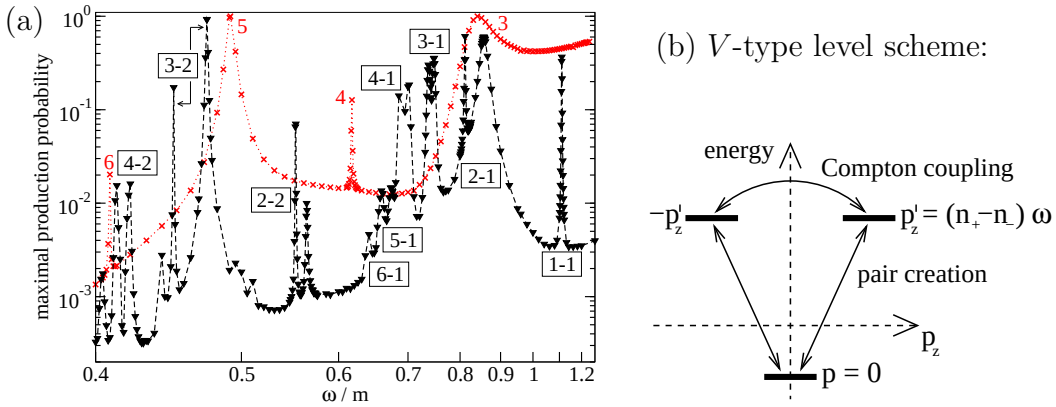

Figure 12: (a) Resonant probability spectrum of above-threshold pair production in two counterpropagating laser pulses, with the laser magnetic field included (black triangles) and excluded (red crosses). In the first case, the labeling $(n_+–n_-)$ signifies the number of absorbed photons from the right-left propagating waves; in the second case, the peak labels (n) denote the total photon number. A vanishing initial momentum (i.e. positron momentum) $\mathbf{p} = 0$ and a laser parameter of $\xi = 1$ have been assumed. (b) Level diagram in the nondipole case. (from [34])

On resonance, a characteristic Rabi flopping between the negative-energy and the positive-energy Dirac continua takes place. This dynamics is analogous to the oscillating population of an atomic two-level system coupled resonantly to an external field [Scu97]. The positions of the resonance frequencies are shown by the red line in Fig. 12(a), which displays the value of the pair production probability at the maximum of the Rabi oscillation.

Inclusion of the magnetic field strongly modifies the pair production process at the high laser frequencies under consideration [see the black line in Fig. 12(a)]: The height of the probability spectrum is reduced by approximately one order of magnitude, the resonances are shifted, several new resonances occur, and the resonance lines are split. The underlying reason for these effects is that, in contrast to a space-independent oscillating field, the photons in the counterpropagating laser pulses carry momentum along the beam axis, which is transferred to the electron wave-packet upon absorption. The energy-momentum conservation is given by [5]

$$\begin{aligned} q_+^0 + q_-^0 &= (n_+ + n_-)\hbar\omega\,, \\ \mathbf{q}_+ + \mathbf{q}_- &= (n_+ - n_-)\hbar\mathbf{k} \end{aligned} \tag{49}$$

where $q_\pm^\mu = (q_\pm^0, \mathbf{q}_\pm)$ are the laser-dressed momentum four-vectors of the created particles. The integers n_+ and n_- denote the number of photons absorbed from the right and left travelling laser pulse, respectively. According to Eq. (49), the

[5] We note that the situation is different for pair creation in combined laser and Coulomb fields, as considered in Section 4.1. There, the nuclear field introduces a spatial dependence and is able to absorb recoil momentum. As a consequence, the electron and positron momenta vary continuously and do not satisfy a quantization condition like in Eq. (49). The energy conservation law reads $q_+^0 + q_-^0 = n\hbar\omega$. No resonances occur in this process.

resonance condition in Eq. (48) is modified to

$$\omega_{n_+,n_-} = \frac{m_* c^2}{2\hbar} \frac{n_+ + n_-}{n_+ n_-} \,, \tag{50}$$

for the present case of a vanishing initial momentum of the negative-energy state. The value of the laser-dressed mass (satisfying $q_\mu q^\mu = m_*^2 c^2$) was numerically determined as $m_* = 1.11m$. The resonance peaks in Fig. 12(a) are labelled by the tupel (n_+, n_-) of laser photons absorbed. For a certain multiphoton order there exist multiple resonance frequencies now, e.g., for an $n = n_+ + n_- = 5$ photon transition there are two different resonance frequencies $\omega_{3,2}$ and $\omega_{4,1}$. The number of resonance lines is enhanced correspondingly. One might expect that the resonance frequency ω_{n_+,n_-} in Eq. (50) coincides for $n_+ = n_-$ with the frequency $\omega_{n=2n_+}$ in Eq. (48) since no momentum is transferred in this case. However, in the purely time-dependent field only odd-n resonances occur for $\mathbf{p} = 0$ because of a charge conjugation-related selection rule; the even-n peaks in Fig. 12(a), arising from the finite wave-packet width, thus are strongly suppressed. The figure demonstrates moreover that the resonance peaks for $n_+ \neq n_-$ are split into doublets, leading to a further enhancement of the resonance lines. This effect is not covered by Eq. (50) which rather predicts the center of the split lines. The splitting finds its natural explanation by the Autler-Townes effect known from atomic physics [Aut55]. Due to the non-zero photon momentum, the former two-level scheme is broken into a V-type three-level scheme: the initial negative-energy level and two positive-energy levels, having the same energy but opposite momenta [see Fig. 12(b)]. The upper two states are coupled via Compton scattering, which leads to a splitting of these levels and thus to a splitting of the resonant transition frequency.

In conclusion, the QED process of electron-positron pair creation from vacuum by counterpropagating laser beams exhibits manifold similarities with quantum optical systems under weak driving forces. In view of phenomena such as Rabi oscillations between the positive and negative Dirac continua, Autler-Townes level splitting, and also electron-positron entanglement [Fed06, Che08] one might speak of "vacuum quantum optics". Upcoming X-ray laser sources [Rin01, Alt06, Tsa06] offer prospects to enter the parameter regime of interest for above-threshold pair production in counterpropagating laser pulses. The anticipated XFEL bandwidth [Alt06] would be sufficient to resolve the increased number of resonance lines resulting from the influence of the laser magnetic-field component.

5 Towards laser-particle physics

In the previous section we have seen that the creation of an e^+e^- pair from vacuum in a laser field of low-frequency requires enormous intensities on the order of $I \sim 10^{29}\,\mathrm{W/cm^2}$. The reason is that the field has to supply the necessary rest energy to a virtual electron along its path of existence given by the Compton wavelength. Since the critical field strength scales with the square of the particle mass, the creation of even heavier particles such as muon-antimuon ($\mu^+\mu^-$) pairs by laser fields seems rather hopeless at first sight. The critical intensity for muon pair creation from vacuum in the tunneling regime is of the order of $I \sim 10^{38}\,\mathrm{W/cm^2}$.

However, the situation is very different when real particles exist already in the initial state. They can gain substantial kinetic energies during acceleration along

the laser wavelength which is larger than the Compton wavelength by orders of magnitude in an optical field. Therefore, in accordance with Eq. (2), an electron is accelerated to $\varepsilon_{\rm kin} = mc^2$ already at near-infrared field intensities on the order of $I \sim 10^{18}\,{\rm W/cm^2}$, where the relativistic parameter $\xi \sim 1$ is of order unity. With the energy gain being proportional to the field intensity, electrons (and positrons) can acquire ponderomotive energies in the GeV range inside the most powerful laser fields of intensity $I \sim 10^{22}\,{\rm W/cm^2}$ available today. The GeV energy domain has also been demonstrated accessible via laser-wakefield acceleration of electrons in plasmas [Lee06]. In principle, such high energies can be exploited to induce elementary particle reactions in laser-accelerated e^+e^- collisions [McD99, Nak04]. Apart from the high energies achievable, lasers can be utilized to generate well-controlled particle collisions at microscopically small impact parameters via the ionization-recollision mechanism (see Section 2.2), which can lead to high luminosities. Protons and ions can also be accelerated by lasers [Sch06a], which may be used for triggering hadronic processes, such as pion production [Kar99]. Consequently, intense laser fields offer alternative and supplementary ways towards high-energy physics [Kur99, Mar06, Mou06, Sal06]. Similar efforts to merge laser physics with nuclear physics are being undertaken successfully (see Section 3).

In Section 5.1 we discuss particle reactions arising from e^+e^- collisions which are driven by superintense near-infrared laser fields. Our focus lies on the process $e^+e^- \to \mu^+\mu^-$ which represents one of the most elementary reactions in particle physics (Section 5.1.1). Apart from a QED calculation, a semi-classical model is presented which allows to interpret the typical muon momenta and the total process probability in a simple and intuitive manner. The experimental feasibility of laser-induced muon production is discussed in Section 5.1.2. It is shown that an observation of the process will be rendered possible in a crossed-beam setup, employing high-power laser sources of the next generation combined with anticipated high-density positronium samples. An alternative way for laser-induced muon creation in high-frequency fields is briefly described in Section 5.2.

5.1 Particle physics with a laser-driven positronium atom

Motivated by the sustained progress in laser technology and the remarkable developments in preparing cold positron samples [Cas05, Jør05], we have addressed the question whether particle reactions such as $e^+e^- \to \mu^+\mu^-$ are feasible with low-energy electrons and positrons in the presence of an intense laser field [17, 23, 31]. The electrons and positrons are assumed to form initially a nonrelativistic e^+e^- plasma or a gas of positronium (Ps) atoms. Since the initial energy of the particles is far below $2m_\mu c^2 \approx 200\,{\rm MeV}$, their annihilation into a muon pair cannot occur without the influence of the external field.

Positronium atoms in the initial state are particularly interesting since they allows for *coherent* e^+e^- collisions which are characterized by microscopically small impact parameters $\varrho_{\rm coh}$, leading to high particle current densities. In conventional colliders such as the Large Electron-Positron (LEP) Collider at CERN, bunches of electrons and positrons collide head-on-head, with the particles in the bunch being randomly distributed. Each single e^+e^- collision therefore is not head-on-head but has a mean impact parameter $\varrho_{\rm incoh} \sim r_b$ determined by the macroscopic beam radius $r_b \sim 10^{-2}\,{\rm cm}$, characterizing the collision as *incoherent*. In contrast to that, in the case of laser-driven positronium atoms, e^+e^- collisions

at microscopically small impact parameters of the order of the atomic Bohr radius, $\varrho_{\rm coh} \sim a_0 \sim 10^{-8}\,$cm, can be generated. This is due to the fact that the electron and positron are initially confined to the atomic size of the bound Ps state. After instantaneous field ionization, they are coherently accelerated by the strong laser field which drives the particles into opposite directions along the laser electric-field component [see Fig. 13(a)]. This leads to periodic e^+e^- (re)collisions whose luminosity contains a coherent component [18]:

$$\mathcal{L} = \left[\frac{N(N-1)}{\pi\varrho_{\rm incoh}^2} + \frac{N}{\varrho_{\rm coh}^2}\right] f_{\rm rep}\,, \tag{51}$$

with the number of Ps atoms N and the repetition frequency of the collisions $f_{\rm rep}$. While the usual incoherent component of the luminosity [Pov06] increases with the square of the particle number, the coherent component is proportional to N. The latter can still lead to a luminosity enhancement when the corresponding impact parameter is very small: $\varrho_{\rm coh} \lesssim \varrho_{\rm incoh}/\sqrt{N}$. The combination of Ps atoms with intense laser fields might therefore be considered as an "e^+e^- micro-collider" (see Section 5.1.2). We emphasize that the magnetic field-induced ponderomotive drift motion into the forward direction is identical for the electron and positron due to the equal magnitude of their charge-to-mass ratios. In this respect the Ps system is distinguished from ordinary atoms where the heavy nucleus (or ionic core) stays behind, so that laser-driven collisions are suppressed at high field intensity (see Section 2.2). This rather unique dynamical response of Ps renders it also interesting as a HHG source [Hen04]. Similarly as the muonic atoms of Section 3, a free Ps atom may be considered stable on the typical time scale of strong laser pulses ($\tau \sim$ fs$-$ps), since its lifetime is $\sim 10^{-7}\,$s (ortho-Ps) or $\sim 10^{-10}\,$s (para-Ps), respectively. In a statistical mixture of Ps atoms, the longer-lived ortho-triplet has a relative abundance of 75%.

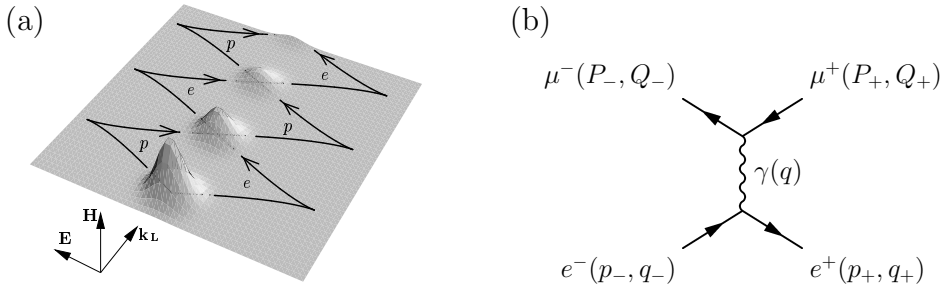

Figure 13: (a) Dynamics of a positronium atom in a strong laser field. After ionization, the electron and positron oscillate in opposite directions along the laser electric field and experience an identical magnetic drift motion, which leads to periodic e^+e^- collisions (from [Hen04]). (b) Feynman diagram for the process $e^+e^- \to \mu^+\mu^-$ in a background laser field. Driven into recollision by the laser field, the electron and positron annihilate into a virtual photon γ which afterwards decays into a muon-antimuon pair. The arrows representing Volkov states are labelled by the particle's free momenta $(p_\pm, P_\pm)$ outside and the dressed momenta $(q_\pm, Q_\pm)$ inside the laser field.

In the setup described, the e^+e^- collision energy is basically determined by the kinetic energy $\sim mc^2\xi$ contained in the transversal motion of the particles, which is considerably smaller than the ponderomotive energy $\sim mc^2\xi^2$ mentioned above [see Eq. (11)]. For the highest intensities attainable at present, ξ is of the order of 10^2. In this regard, the underlying laser acceleration of the particles is considerably different from the usual laser acceleration techniques, since the latter try to extract the ponderomotive energy gain along the laser propagation direction. As an advantage, the principal difficulties of laser acceleration in vacuum implied by the Lawson-Woodward theorem (see, e.g., Ref. [Esa95]) are completely absent here since the electron and positron collide *inside* the laser wave. The threshold laser intensity to render muon production with significant probability[6] from Ps or a low-energy e^+e^- plasma corresponds to

$$\xi_{\min} = \frac{m_\mu}{m} \approx 200. \tag{52}$$

For a near-infrared laser wavelength of $\lambda = 1\,\mu$m, the threshold intensity amounts to $I = 5.5 \times 10^{22}\,\mathrm{W/cm^2}$, which is almost reached by the most powerful present laser systems. The e^+e^- collision energy in their center-of-mass frame amounts to $2m_\mu c^2$ then. For later use we point out that this frame moves with a Lorentz factor of $\gamma_{\mathrm{cm}} \sim \xi$ into the laser propagation direction, because of the large longitudinal electron and positron momenta.

It is noteworthy that the process $e^+e^- \to \mu^+\mu^-$ in a laser field can in principle also occur via a two-step mechanism, when first an e^+e^- pair is created in the collision of a laser pulse with a relativistic ion beam (see Section 4.1), while the muons are subsequently produced in a laser-driven e^+e^- collision inside the field [Kuc07]. This way, the well-established analogy between atomic ionization and e^+e^- pair creation in strong laser fields has been extended to include also the recollision step. In a broader sense, the investigation of lepton-lepton interactions in laser fields has a long history, comprising laser-assisted e^-e^- (Møller), e^+e^- (Bhabha), and $e^-\mu^-$ scattering [Ole67, Den99, Ned07]. In contrast to the process under consideration here, these lepton-lepton scattering events can also take place without a background laser field, while the presence of the latter merely modifies the field-free cross-section.

5.1.1 Positronium decay into a muon-antimuon pair

The laser-induced process $\mathrm{Ps} \to \mu^+\mu^-$ can be calculated within the framework of laser-dressed QED employing the relativistic Volkov solutions as basis states. The Ps atom is supposed to be at rest and in its ground state initially. The $\mu^+\mu^-$ pair then is created in the laser-driven e^+e^- collisions described above. Within the SFA, the corresponding amplitude can be expressed as a superposition integral,

$$\mathcal{S}_{\mathrm{Ps}} = \int \frac{d^3p}{(2\pi\hbar)^3}\, \tilde{\Phi}(\boldsymbol{p})\, \mathcal{S}_{e^+e^-}(\boldsymbol{p}). \tag{53}$$

[6] In a background laser field the decay $\mathrm{Ps} \to \mu^+\mu^-$ is energetically possible at any laser intensity in principle, since the external field represents a practically infinite energy reservoir. However, only for laser intensities satisfying $\xi \geq \xi_{\min}$ the probability of this reaction can be significant, as it guarantees a sufficiently efficient photon absorption.

Here, $\tilde{\Phi}(\boldsymbol{p})$ is the Fourier transform of the positronium ground-state wave-function which depends on the relative momentum $\boldsymbol{p}$, and

$$\begin{aligned}\mathcal{S}_{e^+e^-}(\boldsymbol{p}) &= -\mathrm{i}\alpha \int d^4x \int d^4y \overline{\Psi}_{p_+,s_+}(x)\gamma^\mu \Psi_{p_-,s_-}(x) \\ &\quad \times D_{\mu\nu}(x-y)\overline{\Psi}_{P_-,S_-}(y)\gamma^\nu \Psi_{P_+,S_+}(y) \end{aligned} \tag{54}$$

denotes the QED amplitude for the process $e^+e^- \to \mu^+\mu^-$ in a laser wave, according to the Feynman graph in Fig. 13(b). In Eq. (54), $\Psi_{p_\pm,s_\pm}$ ($\Psi_{P_\pm,S_\pm}$) are the Volkov states of the $e^\pm$ ($\mu^\pm$), depending on the free four-momenta $p_\pm$ ($P_\pm$) and spin states $s_\pm$ ($S_\pm$) of the particles, and $D_{\mu\nu}$ is the coordinate-space representation of the free photon propagator. The free (instead of the laser-dressed) propagator may be used here since the laser field strength is far below critical and the contribution of so-called resonances (where the intermediate photon reaches the mass shell, $q^2 = 0$) is insignificant [Ole67]. In the spirit of the SFA, the Coulomb interaction between the electron and positron only determines the initial state in Eq. (53) but is ignored during their time-evolution in the laser wave. The interaction with the QED vacuum is taken into account to lowest order in the usual perturbation series expansion.

While the evaluation of $\mathcal{S}_{e^+e^-}$ is straightforward, the integration over the relative momentum in $\mathcal{S}_{\mathrm{Ps}}$ is rather involved due to the occurrence of sums of (generalized) Bessel functions of very high order $n \gtrsim 10^{10}$. By employing suitable approximations, it is still possible to obtain a compact expression for the total reaction rate R_{Ps}. In the case of linear laser polarization it reads [23, 31]

$$R_{\mathrm{Ps}} \approx \frac{2^{11}}{\pi^2}\alpha^2 \frac{(\hbar c)^2}{(mc^2\xi)^2}\sqrt{1-\frac{\xi_{\mathrm{min}}^2}{\xi^2}}\frac{c}{\xi(\alpha\xi\lambda)^3}\left(\frac{mc^2}{\hbar\omega\xi^4}\right)^{1/3}, \tag{55}$$

where λ denotes the laser wave length and the last factor has an approximately constant value of ~ 0.1 for the laser parameters of interest. The rate includes an average over the $e^\pm$ spin states and thus applies to a statistical ensemble of Ps atoms. We further note that the collision energy $\varepsilon_{\mathrm{cm}} \approx 2mc^2\xi$ appears in the denominator here. It is remarkable that Eq. (55) has a simple and intuitive explanation in terms of the cross section σ for the field-free process $e^+e^- \to \mu^+\mu^-$ on the one hand [Pes95],

$$\sigma \approx \frac{4\pi}{3}\alpha^2\frac{(\hbar c)^2}{\varepsilon_{\mathrm{cm}}^2}\sqrt{1-\frac{4m_\mu^2c^4}{\varepsilon_{\mathrm{cm}}^2}}, \tag{56}$$

and the spreading of the rapidly evolving electron and positron wave packets on the other hand. Due to quantum mechanical dispersion, the wave-packet size is growing during the evolution in the field, as schematically indicated in Fig. 13(a). Based on the initial wave-packet momentum width and the recollision time one can estimate that, starting from the atomic volume $V_i \sim a_0^3$, with the Bohr radius a_0, the electron and positron wave packets have spread to a largely enhanced size of $V_f \sim (\alpha\xi\lambda)^3 \gg V_i$ at the moment of their collision. The wave-packet size determines the particle current density (i.e., the luminosity) which relates the cross section to the reaction rate. This leads us to the expression

$$R_{\mathrm{Ps}} \sim \frac{\sigma c}{\xi(\alpha\xi\lambda)^3} \tag{57}$$

which agrees remarkably well with Eq. (55). Note that in Eq. (57) an additional factor of ξ in the denominator results from relativistic time dilation between the electron-positron center-of-mass frame and the laboratory frame. From a mathematical point of view, the origin of the wave-packet spreading can be attributed to the integration over the Ps ground-state distribution in Eq. (53). In this superposition integral each value of $\mathbf{p}$ corresponds to a certain partial wave (Fourier component) of the ground-state wave-function, which are coherently summed up. The resulting interference of the partial waves is highly destructive, leading to the observed wave-packet dispersion and rate suppression. The maximum muon production rate from a single Ps atom is on the order of $10^{-10}\,\mathrm{s}^{-1}$, as shown in Fig. 14. The corresponding process probability in a short laser pulse with a typical duration τ in the fs–ps domain is very small: $R_{\mathrm{Ps}}\tau \lesssim 10^{-20}$.

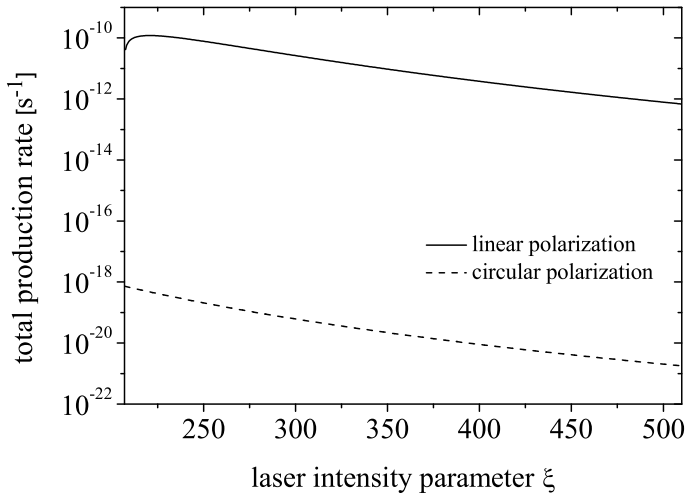

Figure 14: Total rates for laser-driven positronium decay into a muon-antimuon pair, as a function of the laser intensity parameter [see Eq. (55)]. The laser photon energy is $\hbar\omega = 1\,\mathrm{eV}$. (from [31])

In a circularly polarized laser field [17], the average over the Ps ground state leads to an even heavier suppression of the process probability (see Fig. 14). The physical reason is that the e^+e^- recollison occurs at macroscopically large impact parameters here. They are determined mainly by the classical motion of the electron and positron which co-rotate in the polarization plane at a distance $\varrho_{\mathrm{circ}} \sim \lambda\xi$. Contrary to that, in linearly polarized laser fields the classical electron-positron trajectories periodically meet and the rate damping results from quantum mechanical dispersion which leads to $\varrho_{\mathrm{lin}} \sim \alpha\lambda\xi \ll \varrho_{\mathrm{circ}}$. The phenomenon, that in a circularly polarized light wave a recollision process is suppressed due to the classical electron motion, is also known from high-harmonic generation by atoms or molecules [Bec02].

Since the probability of the coherent process scales linearly with the number of Ps atoms involved, high Ps densities are desirable. In recent years, a noticeable progress has been made in the efficient production, accumulation, and trapping of Ps atoms. The highest Ps density achieved so far is of the order of $n_{\mathrm{Ps}} = 10^{15}\,\mathrm{cm}^{-3}$ and has been produced in porous silica [Cas05]. Assuming a free gaseous Ps target

of this density, a typical laser focal volume of $V = (10\lambda)^3 \approx 10^{-9}\,\mathrm{cm}^3$ contains a million atoms. The total coherent reaction rate could accordingly be increased by this number to $R_{\mathrm{Ps}}^{(N)} \sim 10^{-4}\,\mathrm{s}^{-1}$ in a linearly polarized laser field, which, however, still seems too small to be measured. The process efficiency is mainly limited by the quantum mechanical wave-packet spreading which dilutes the particle density at the collision. Feasible ways to overcome this obstacle will be discussed in Section 5.1.2.

For comparison, we note that the rate for muon creation in a hypothetical large-scale e^+e^- collider experiment, which employs a single electron and a single positron only, would be of the order of $10^{-20}\,\mathrm{s}^{-1}$ [Pov06]. The rate resulting from the e^+e^- micro-collider based on Ps is orders of magnitude larger, due to the small impact parameters and the correspondingly large luminosities. A real collider experiment, however, employs beams of $\sim 10^{10}$ particles, corresponding to luminosities $\mathcal{L} \sim 10^{30}$–$10^{34}\,\mathrm{cm}^{-2}\mathrm{s}^{-1}$. At typical reaction cross sections $\sigma \sim 10^{-33}$–$10^{-30}\,\mathrm{cm}^2$, event rates $R = \sigma\mathcal{L}$ of about $1\,\mathrm{s}^{-1}$ are obtained this way. This number, in turn, is orders of magnitude larger than the coherent rate from a single Ps atom.

It is also instructive to compare the process $\mathrm{Ps} \to \mu^+\mu^-$ with muon pair creation from an initially nonrelativistic e^+e^- plasma which is strongly driven by a laser field. The latter process can be calculated directly via the amplitude (54), refraining from the coherent average over the relative momentum. For the corresponding *incoherent* production rate we obtain the approximate expression [31]

$$R_{e^+e^-} \approx \frac{c}{2^3\pi^2}\frac{\alpha^2\hbar^2}{m^2c^2\xi^4}\sqrt{1-\frac{\xi_{\mathrm{min}}^2}{\xi^2}}\;\frac{N_+N_-}{V}, \tag{58}$$

with N_- (N_+) the number of electrons (positrons), and V the interaction volume which is determined by the laser focal spot size. Formula (58) has been derived assuming a linearly polarized laser wave, but since quantum wave-packet spreading and classical motion are not crucial here, the incoherent rate is of the same order of magnitude for circular laser polarization. Similar as with Eq. (55) above, Eq. (58) can be equipped with an intuitive meaning. In fact, since the quantity $R_{e^+e^-}/V$ is Lorentz invariant, Eq. (58) implies that in the (primed) electron-positron center-of-mass frame the number of events per volume and time is related to the corresponding cross section (56) in the usual way: $R'_{e^+e^-}/V' \sim \sigma n'_+ n'_-/V'$, with the particle number densities $n'_\pm = N_\pm/V'$ and $V' \sim \xi V$. We point out that the coherent channel of muon production from Ps atoms evolves into the incoherent channel in the limit of large wave packet size. Namely, with increasing wave packet size the coherent rate is more and more suppressed and, moreover, electrons (positrons) stemming from different Ps atoms start to overlap so that the gas of Ps atoms transforms into an e^+e^- plasma. Therefore, the incoherent reaction rate (58) will eventually dominate the muon production process.

The muons produced in laser-driven Ps annihilation exhibit peculiar kinematic features. From the conservation law for the effective momenta one finds that, close to threshold, the muons have typical free momenta of

$$P_x \approx m_\mu c\,, \quad P_y \approx 0\,, \quad P_z \approx m_\mu c\xi_{\mathrm{min}} \tag{59}$$

in the laboratory frame. The laser wave is polarized along the x axis and propagates in z direction. Even at threshold, the muons are highly relativistic and move within a narrow cone along the laser propagation direction. Hence, similarly as

in Section 4.1.3, the muon kinematics may be called "photon-like", which results from the fact that the particles are effectively produced by a huge number of laser photons whose total energy exceeds the initial nonrelativistic energy of the electron and positron by orders of magnitude. The muon life time in the lab frame is accordingly increased from $2.2\,\mu$s to $\sim 0.2\,$ms due to time dilation. The typical number of laser photons absorbed during the process amounts to $n \sim m_\mu c^2 \xi/\hbar\omega$ which is on the order of 10^{10} at $\hbar\omega = 1\,$eV. In the electron-positron center-of-mass frame, these photons provide a total energy of $n\hbar\omega' \sim m_\mu c^2$, with the red-shifted photon frequency $\omega' \sim \omega/\xi$. This additional energy is required because the muons have to be produced with their effective mass $m_{\mu,*} = m_\mu\sqrt{1+\frac{1}{2}(\xi/\xi_{\min})^2}$ in the laser field.

The typical muon momenta in Eq. (59) can also be deduced from a classical simple-man's model [31]. To this end we assume that, at the reaction threshold ($\xi = \xi_{\min}$), the muons are created with zero momentum in the electron-positron center-of-mass frame: $\mathbf{P}'(\eta_0) = 0$, where η_0 denotes the laser phase when the muons are being born. The solution of the classical equations of motion with this initial condition reads [see Eq. (11)]

$$P'_x(\eta) = \frac{e}{c}[A(\eta) - A(\eta_0)]\,, \quad P'_y(\eta) = 0\,, \quad P'_z(\eta) = \frac{e^2}{2m_\mu c^3}[A(\eta) - A(\eta_0)]^2. \tag{60}$$

After having left the laser field, these become $P'_x = m_\mu c$, $P'_y = 0$, $P'_z = m_\mu c/2$. Note here that the vector potential at the moment of creation attains its maximum value $A(\eta_0) = A_0$, since the laser's electric field is zero at the recollision time. The Lorentz transformation to the lab frame [with the reduced velocity $\beta_{\rm cm} = \xi^2/(2+\xi^2)$ and the Lorentz factor $\gamma_{\rm cm} = \xi/2$] then yields the momentum components of Eq. (59). The assumptions that our simple-man's model is based upon can be proven by considering the saddle points of the oscillating integrand in Eq. (54). From the positions of the saddle points one can infer that, at the threshold intensity $\xi = \xi_{\min}$, the muons are preferably created at rest in the center-of-mass frame whenever the laser vector potential attains a maximum. A similar procedure is known from the famous simple-man's model of HHG and ATI, which can also be derived within a saddle-point approach by relating the saddle points with the most relevant classical electron trajectories [Bec02].

5.1.2 Laser-driven electron-positron colliders

In the previous section we have seen that particle reactions by a positronium atom exposed to a *single* laser wave are possible but not very efficient. The large spreading of the electron and positron wave packets before their recollision substantially decreases the reaction rate. We show below that the spreading can be reduced and even controlled by virtue of more complex field geometries. A suitable configuration is formed by two counterpropagating laser waves, for instance, as is realized by the Astra Gemini system at the Rutherford Appleton Laboratory [RAL] or the JETI "photon collider" at the University of Jena [Sch06b]. In this situation no analytical solutions of the Dirac equation like the Volkov states are at hand, though, which excludes an analytical SFA treatment (see also Section 4.2). We have learned, however, that the reaction rate can reliably be estimated by means of the field-free cross section and the size of the colliding wave packets [see

Eq. (57)]. The latter can be determined via a classical Monte-Carlo calculation which accounts for the spreading phenomenon.

The setup consists of a gas of positronium atoms subject to two counterpropagating laser beams of the same intensity and frequency, that are equal-handed circularly polarized. The corresponding classical equations of motion for the electron (or positron) momentum $\mathbf{p}(t)$ and position $\mathbf{r}(t)$ are given by

$$\begin{aligned}
\frac{dp_x(t)}{dt} &= eE_0 f(\eta_-)\sin(\eta_-)\left[1-\frac{cp_z(t)}{\varepsilon(t)}\right] + eE_0 f(\eta_+)\sin(\eta_+)\left[1+\frac{cp_z(t)}{\varepsilon(t)}\right], \\
\frac{dp_y(t)}{dt} &= -eE_0 f(\eta_-)\cos(\eta_-)\left[1-\frac{cp_z(t)}{\varepsilon(t)}\right] + eE_0 f(\eta_+)\cos(\eta_+)\left[1+\frac{cp_z(t)}{\varepsilon(t)}\right], \\
\frac{dp_z(t)}{dt} &= eE_0\frac{cp_x(t)}{\varepsilon(t)}\left[f(\eta_-)\sin(\eta_-) - f(\eta_+)\sin(\eta_+)\right] \\
&\quad -eE_0\frac{cp_y(t)}{\varepsilon(t)}\left[f(\eta_-)\cos(\eta_-) + f(\eta_+)\cos(\eta_+)\right], \qquad (61)
\end{aligned}$$

and $d\mathbf{r}(t)/dt = c^2\mathbf{p}(t)/\varepsilon(t)$. Here, E_0 is the peak electric field strength, $\eta_\pm = \omega t \pm kz$ are the respective laser phases, and $\varepsilon(t) = c\sqrt{\mathbf{p}(t)^2 + m^2c^2}$ is the electron energy. Furthermore, the pulses are $\cos^2$-shaped which is described by the envelope function $f(\eta_\pm)$, and propagate along the z axis. The circular polarization of the superimposed lasers generates a magnetic field which is directed along the electric field, so that a focussing force results [Mil04]. A three-dimensional treatment of the electron dynamics is required here, which renders a fully quantum mechanical simulation by numerical solution of the Dirac equation exceedingly challenging [Moc08].

We have solved the Eqs. (61) for a large microcanonical ensemble of test particles with an initial phase-space distribution corresponding to the Ps ground state. The laser fields have a photon energy of $\hbar\omega = 1.5\,\mathrm{eV}$ and an intensity of $I = 2\times10^{24}\,\mathrm{W/cm^2}$ each ($\xi = 10^3$). The contour plots in Fig. 15 display snapshots of the resulting distributions in coordinate and momentum space, taken at the moment when the electron and positron wave-packets recollide for the first time. Apparently, the spreading in the counterpropagating laser pulses is under control. In the xy-plane there is practically no spreading as the wave-packet extent of about 8 a.u. coincides with its initial value (see Figs. 15a, d). In z-direction the magnetic field leads to a compression of the wave packet (see Figs. 15b, e). The momentum distributions show that the particles have a quite well-defined collision momentum that is almost parallel to the x-axis (see Figs. 15c, f), corresponding to a collision energy of 3 GeV.

As a result, the counterpropagating-beam geometry allows for coherent e^+e^- collisions at impact parameters $\varrho_{\mathrm{coh}} \approx 10^{-7}\,\mathrm{cm}$ which is smaller by three orders of magnitude than in the case of a single driving wave and enhances the reaction rates by almost 10 orders of magnitude [see Eq. (57)]. The reason for the reduced dispersion is that the recollisions occur on a much shorter time scale, given by the laser period $T \sim 1\,\mathrm{fs}$. For a single laser wave, the recollision time was determined instead by the laser period $T' \sim T\xi \gg T$ in the electron-positron center-of-mass frame, which was moving at high velocity. In contrast to that, the laboratory and center-of-mass frames coincide in the present symmetric setup. This implies moreover that the time dilation factor $1/\xi$ of Eq. (57) is absent here, which further enhances the rate by 2-3 orders of magnitude. A total coherent rate for muon

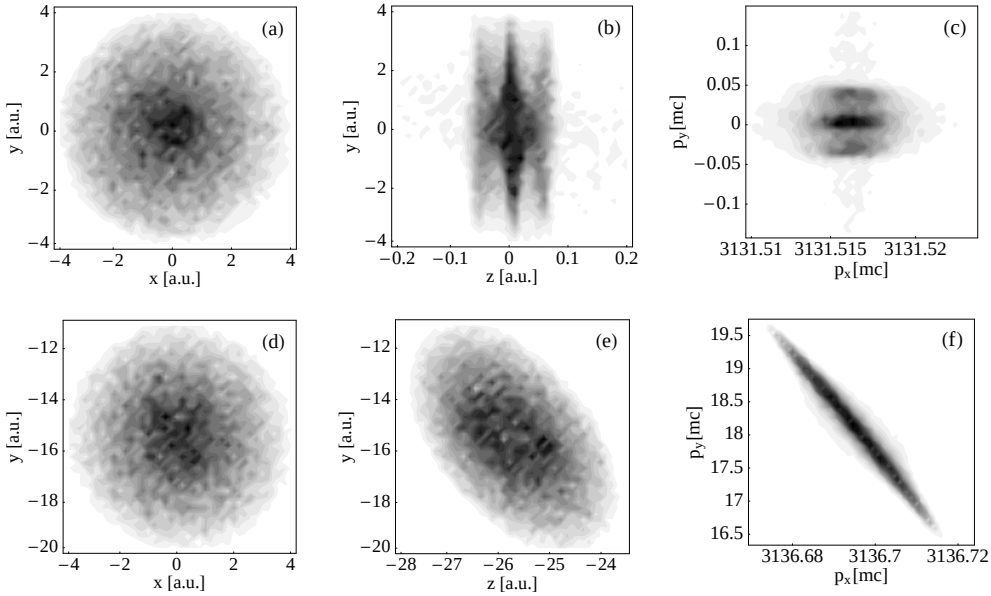

Figure 15: Monte-Carlo simulation of the e^+e^- wave-packet dynamics in counter-propagating laser pulses, based on 30,000 classical trajectories. The equal-handed, circularly polarized laser beams have an intensity of $I = 2 \times 10^{24}\,\mathrm{W/cm^2}$ and a wavelength of $\lambda = 800\,\mathrm{nm}$. (a)-(c): Coordinate- and momentum-space distributions of one of the particles at the moment of recollision for a positronium atom initially located at the origin: $x_0 = y_0 = z_0 = 0$. The wave-packet spreading is narrowly confined; the average impact parameter is $\varrho \approx a_0 = 2\,\mathrm{a.u.}$ (d)-(f): Same as (a)-(c) but for an initial offset along the beam axis of $kz_0 = 0.05$. (from [18])

pair production of $R_{\mathrm{Ps}}^{(N)} \sim 10^8\,\mathrm{s}^{-1}$ could thus be achieved, rendering the process observable at the high Ps densities [Cas05] and laser repetition rates ∼kHz [ELI] envisaged. The resulting number of events may approach $1\,\mathrm{s}^{-1}$ (assuming laser pulses of $\sim 100\,\mathrm{fs}$ duration) which, in fact, is comparable to the event rates at large-scale accelerators. The coherent luminosity of the e^+e^- micro-collider might reach $\mathcal{L} \sim 10^{28}\,\mathrm{cm^{-2}s^{-1}}$ [18]. This value is significantly higher than the luminosity of the most advanced wake-field laser accelerators [Lee06], which can be estimated as $\sim 10^{23}\,\mathrm{cm^{-2}s^{-1}}$ at the same laser repetition rate.[7]

Higher collision energies than in the counterpropagating-beam setup can be reached when a single laser wave is combined with a static magnetic field, directed along the laser magnetic field. At an intensity of $10^{25}\,\mathrm{W/cm^2}$ and a high magnetic field strength of $10^4\,\mathrm{T}$, a collision energy of 100 GeV would be achieved [18]. The high collision energies in this scheme are attained, though, at the expense of larger wave-packet spreading which diminishes the advantage of coherent collisions. The

[7] In order to relate the coherent rate $R_{\mathrm{Ps}}^{(N)} \sim N\sigma c/\varrho_{\mathrm{coh}}^3$ with the coherent component of the luminosity in Eq. (51), one has to note that the wave-packet extent along the particle collision axis is immaterial for the total reaction yield. Rather it determines the time duration $\tau_{\mathrm{coh}} \sim \varrho_{\mathrm{coh}}/c$ of the microscopic e^+e^- collision during which the wave packets penetrate each other, leading to a production probability of $R_{\mathrm{Ps}}\tau_{\mathrm{coh}} \sim \sigma/\varrho_{\mathrm{coh}}^2$ per single collision. The repetition rate f_{rep} of these collisions is given by the number of half-cycles in the laser pulse and the pulse repetition rate, $f_{\mathrm{rep}} = 2N_{\mathrm{cycle}}f_{\mathrm{pulse}}$. For the parameters assumed, one obtains $\mathcal{L}_{\mathrm{coh}} = (N_{\mathrm{Ps}}/\varrho_{\mathrm{coh}}^2)f_{\mathrm{rep}} \sim 10^{28}\,\mathrm{cm^{-2}s^{-1}}$.

use of incoherent collisions in a laser-driven e^+e^- plasma instead of Ps atoms might be more appropriate here. It should be noted that the forefront of particle physics today is aiming at e^+e^- collision energies of about 1 TeV [Mur96].

We conclude that the combination of positronium atoms with superintense laser fields in suitable configuration may establish a laser-driven high-energy e^+e^- collider with competitive performance parameters. The field-induced process $\mathrm{Ps} \to \mu^+\mu^-$ offers the challenging prospect for a proof-of-principle experiment by employing anticipated high-density Ps targets and counterpropagating laser beams from the next-generation of powerful laser devices.

5.2 Muon pair creation in XFEL-ion collisions

In this section we pursue another mechanism of muon pair creation by laser fields. It is based on the collision of an X-ray laser beam ($\hbar\omega_L = 12\,\mathrm{keV}$) with an ultrarelativistic ion beam ($\gamma = 7000$). The setup is similar to the one of Section 4.1. This parameter combination would be achieved in a supposed combination of the upcoming XFEL sources with the nuclear beam from the recently commissioned CERN-LHC. In the ion frame the photon energy amounts to $\hbar\omega \approx 2\gamma\hbar\omega_L = 168\,\mathrm{MeV}$. The energy gap of $2m_\mu c^2$ for muon pair production can thus be overcome by two-photon absorption. We note that because of pronounced recoil effects, the γ-factor which would be required for two-photon $\mu^+\mu^-$ production by a projectile electron is much larger: $\gamma \gtrsim 10^6$, corresponding to a yet unavailable electron energy in the TeV range.

At first sight, e^+e^- and $\mu^+\mu^-$ pair production in combined laser and Coulomb fields seem to be very similar processes since the electron and muon only differ by their mass (and lifetime). In this picture, the corresponding production probabilities would coincide when the laser field strength and frequency are scaled in accordance with the mass ratio $\rho = m_e/m_\mu$, i.e., $W_{\mu^+\mu^-}(E^{(\mu)}, \omega^{(\mu)}) = W_{e^+e^-}(E^{(e)}, \omega^{(e)})$ for $E^{(\mu)} = E^{(e)}/\rho^2$ and $\omega^{(\mu)} = \omega^{(e)}/\rho$ (see Section 3.1). This simple scaling argument does not apply, however, as the large muon mass is connected with a correspondingly small Compton wavelength $\lambda\!\!\!^{-(\mu)}_C = \rho\lambda\!\!\!^{-(e)}_C \approx 1.86\,\mathrm{fm}$, which is smaller than the radius of most nuclei. As a result, the nucleus does not look pointlike to the muon and its finite extension must be taken into account. Pronounced nuclear size effects have also been found for $\mu^+\mu^-$ production by single γ-photon impact on nuclei [Tsa74] and in relativistic heavy-ion collisions [Bau07].

Muon pair creation in XFEL-ion collisions can be calculated via the amplitude in Eq. (31), with the nuclear field $V_{\mathrm{ion}}(r)$ arising from an extended nucleus. We assume a spherically symmetric nucleus with a Gaussian charge distribution

$$\varrho(r) = \frac{Ze}{(\sqrt{\pi}a)^3}\,\mathrm{e}^{-r^2/a^2}, \tag{62}$$

where Z is the atomic number and the parameter a is related to the nuclear root-mean-square charge radius by $r_{\mathrm{rms}} = \sqrt{3/2}a$. This leads in Eq. (31) to the appearance of the corresponding elastic nuclear form factor

$$F(q^2) = \mathrm{e}^{-(qa/2\hbar)^2}, \tag{63}$$

with the momentum transfer to the nucleus $\mathbf{q} = \mathbf{q}_+ + \mathbf{q}_- - 2\hbar\mathbf{k}$. The form factor $F(q^2)$ leads to substantial reduction of the production rate when the recoil

$q \sim m_\mu c$ exceeds $\hbar/a$. The fully differential elastic rate for two-photon muon pair creation is obtained by summing the square of the amplitude (31) over the muon spin states:

$$dR_{\rm el} = \sum_{\rm spins} |S_{\rm ff}^{\rm SFA}|^2 \frac{d^3p_+}{(2\pi\hbar)^3} \frac{d^3p_-}{(2\pi\hbar)^3} = dR_0 Z^2 F^2(q^2)\,, \tag{64}$$

where dR_0 denotes the differential production rate for a pointlike proton. Equation (64) is called the elastic production rate since the nucleus is assumed to remain in its ground state. An additional contribution $dR_{\rm inel} \approx dR_0 Z[1 - F^2(q^2)]$ to the process stems from the inelastic channel [Tsa74], where the recoil leads to nuclear excitation. The total rate is $R_{\rm tot} = R_{\rm el} + R_{\rm inel}$. Below we show angular muon spectra as well as elastic and total production rates; all results refer to the rest frame of the projectile. The specific choice of the nuclear model has only minor influence on the results [35]. For e^+e^- creation, the nuclear size does not play a role since the electron Compton wavelength $\lambda\!\!\!^{-(e)}_C$ is larger by two orders of magnitude than the nuclear radius. The inelastic channel is thus negligible in this case since $q \sim m_e c \ll \hbar/r_{\rm rms}$, so that $F^2 \approx 1$ and $R_{\rm tot} \approx R_0 Z^2$.

Figure 16 demonstrates the influence of the nuclear extension by showing the angular distribution of the muons in the elastic production channel. Various nuclei are considered; in each case the isotope of largest abundance has been chosen. The respective root-mean-square charge radii amount to 0.875 fm (proton), 2.470 fm (^{12}C), 4.188 fm (^{84}Kr), and 5.851 fm (^{238}U). The result for a pointlike nucleus is also shown for comparison. The rates are strongly reduced with increasing nuclear size because the muons are created typically at distances $r \sim \lambda\!\!\!^{-(\mu)}_C$ inside the nucleus where they experience a reduced nuclear field. Moreover, the maximum of the angular distributions is shifted towards smaller angles because the nuclear form factor cuts the contributions from large momentum transfers, which otherwise would give rise to large emission angles.

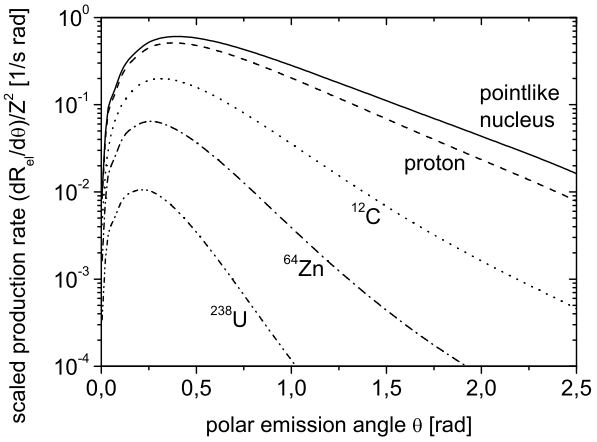

Figure 16: Angular spectra of one of the muons produced by two-photon absorption from an intense XFEL beam ($\hbar\omega_L = 12\,\text{keV}$, $I_L = 2.5 \times 10^{22}\,\text{W/cm}^2$) colliding with various ultrarelativistic nuclei ($\gamma = 7000$). The angle is measured with respect to the laser beam axis and the rates are scaled by the nuclear charge. (from [30])

Figure 17 shows integrated rates of $\mu^+\mu^-$ production for several projectiles. For a pointlike proton, the total rate coincides with the elastic rate in our approximation and amounts to $R_0 \approx 0.58\,\mathrm{s}^{-1}$ [see Eq. (35)]. For an extended projectile, the elastic rate increases with its charge as Z^2 but decreases with its size. This interplay leads to the emergence of maximum elastic rates for medium-heavy ions ($Z \approx 60$). We note that a maximum also arises for elastic muon production by a single photon of twice the energy. The total rate R_{tot} does not exhibit a maximum but saturates at high Z values since the inelastic contribution increases with nuclear charge. The total rates are still considerably smaller than the point-nucleus results. For heavy ions the main contribution stems from the inelastic channel where the protons inside the nucleus act incoherently ($R_{\mathrm{inel}} \propto Z$). This implies that despite the high charges, Coulomb corrections to the SFA treatment are of minor importance.

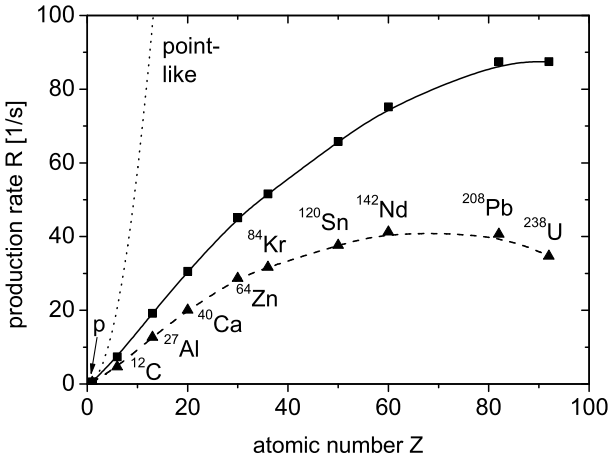

Figure 17: Integrated rates for muon pair creation in XFEL-ion collisions as in Fig. 16. The triangles show elastic rates, whereas the squares indicate total ('elastic + inelastic') rates. The numerical data are connected by fit curves. The dotted line holds for a pointlike nucleus. (from [30])

According to our results, muon pair creation in XFEL-nucleus collisions will be experimentally feasible by merging near-future technologies. In the laboratory frame, the production rates of Fig. 17 are reduced by a factor γ^{-1} due to relativistic time dilation and, accordingly, reach values of about $R_{\mathrm{lab}} \approx 10^{-2}\,\mathrm{s}^{-1}$. In the collision of an ion beam containing $N = 10^{11}$ particles [Yao06] with an XFEL pulse of $\tau = 100\,\mathrm{fs}$ duration [Alt06], the probability for production of one muon pair is $W_{\mu^+\mu^-} \approx R_{\mathrm{lab}}\tau N/2 \approx 10^{-4}$. At the envisaged average XFEL repetition rate of 40 kHz, one muon production event per second would be obtained. The typical lab-frame energy of the muons $\sim 500\,\mathrm{GeV}$ is highly relativistic; the muonic lifetime is accordingly increased to $\sim 10\,\mathrm{ms}$. As a background process, also e^+e^- pairs are produced by single-photon absorption in the nuclear field. The rate is given by Eq. (38) and amounts to $\sim Z^2 \times 10^{11}\,\mathrm{s}^{-1}$ in the lab frame. We emphasize that this rather strong background process does not deplete the X-ray beam: assuming a pulse duration of 100 fs and a focal radius of 100 nm, the latter contains about 10^{15} photons, whereas only $\sim Z^2 \times 10^{-2}$ e^+e^- pairs are generated per ion.

6 Conclusion and Outlook

With the recent availability of superintense laser sources and the ongoing technological advances in this field, during the next decade yet another chapter is likely to be added to the 50-years success story of laser-matter interactions. Substantially increased laser field strengths and frequencies will allow for experimental studies on the coupling of coherent electromagnetic radiation with an enhanced variety of targets, involving highly charged ions (see [Epp07]) and exotic atoms, bare atomic nuclei, and even the quantum vacuum. In this thesis we have presented several theoretical proposals along these envisaged lines for laser-induced highly energetic reactions in atomic, nuclear, and particle physics. While some of them can be tested in the laboratory with current devices already today (such as the APT-assisted production of hard X-ray harmonics), most processes under consideration have assumed laser parameters of near-future facilities which are currently in the design or development phase. For certain applications the combination of advanced laser sources with other cutting-edge technologies, like dense positron target generation or powerful ion acceleration, appears promising. This way, further research fields can be opened up to laser science and to the concepts developed in intense laser-atom physics during the last decades.

The multiphoton, above-threshold, and tunneling regimes of interaction, familiar from strong-field atomic ionization, exist as well for e^+e^- pair production in ultrastrong laser fields. Laser-induced pair creation processes enable investigations of the QED vacuum structure, which can supplement corresponding studies in heavy-ion collisions as the external fields exhibit a very different space-time dependence. The first observation of nonlinear Bethe-Heitler pair creation in combined laser and nuclear fields is in principle coming into reach when an (attosecond) XUV laser source is operated in conjunction with CERN-LHC. This experimental prospect calls for refined theoretical treatments which, for example, involve the polarization properties of the leptons and nuclear recoil effects. Corresponding calculations are on the way [39]. Signatures of the nuclear size and shape arise in the muon pair production through the multiphoton Bethe-Heitler process in X-ray laser fields.

Interesting quantum optical features are apparent in the spectra of electrons and positrons generated in two counterpropagating high-frequency laser pulses, such as Rabi oscillations and Autler-Townes splitting. Methods from the quantum optics of coherently driven bound atomic states may also be applied fruitfully to free single-electron wave-packets interacting with a relativistically strong laser wave. The wave-packet structure is implicitly imprinted on the Thomson photoemission via the electron Wigner function, which might be revealed via higher-order photon correlation functions. Similar efforts are currently undertaken with respect to tomographic imaging of molecular orbitals based on HHG by several research groups [Lei07].

Exotic systems such as muonic atoms or positronium possess favorable dynamical properties in the presence of ultrastrong laser fields, allowing for a natural extension of the ionization-recollision scheme towards nuclear and particle physics. Laser-driven muons can dynamically probe nuclear structure features via the harmonic radiation they emit. Corresponding studies on hadronic (e.g., pionic) atoms are also conceivable but rendered more difficult by the very short lifetimes of these systems [37]. Electrons and positrons from a bound positronium state can be

laser-guided into microscopic high-energy collisions producing, for instance, pairs of muons. An obstacle, which needs to be overcome in view of the small focal spot sizes of intense laser pulses, is formed by the low densities of exotic-atom samples available, so that future experimental studies require improved preparation and accumulation methods. It is encouraging that corresponding efforts are already being made with respect to other scientific cases, ranging from muon-spectroscopy on unstable nuclear isotopes [Nil04] to Bose-Einstein condensation of Ps atoms [Cas05] and laboratory astrophysics of hot positron plasmas [Che09].

Most probably, the future of high-power laser science will witness even further fruitful mergings with other novel techniques, which are unexpected as yet. We may be curious to see which range of new research areas the strongly amplified stimulated emission of electromagnetic radiation will lead physicists eventually to.

A Complete list of publications

Refereed journals and conference proceedings

[1] A. B. Voitkiv, C. Müller, and N. Grün, *Nonperturbative and relativistic effects in projectile-electron loss in relativistic collisions with atomic targets*, Phys. Rev. A **62**, 062701 (2000).

[2] C. Müller, A. B. Voitkiv, and N. Grün, *Der Projektilelektronverlust in relativistischen Stößen mit neutralen Targets*, in "Arbeitsbericht der 22. Tagung über Energiereiche Atomare Stöße (Riezlern, Austria, 21.01.-27.01.01)", EAS Report **22**, 29 (2001) [available online via http://www.mpipks-dresden.mpg.de/∼eas/].

[3] C. Müller, A. B. Voitkiv, and N. Grün, *Die Ionisation schwerer, heliumähnlicher Projektile in ultrarelativistischen Stößen mit schweren Targetatomen*, in "Arbeitsbericht der 23. Tagung über Energiereiche Atomare Stöße (Riezlern, Austria, 17.02.-22.02.02)", EAS Report **23**, 111 (2002) [available online via http://www.mpipks-dresden.mpg.de/∼eas/].

[4] C. Müller, A. B. Voitkiv, and N. Grün, *Electron loss from heavy helium-like projectiles in ultrarelativistic collisions with many-electron atomic targets*, Phys. Rev. A **66**, 012716 (2002).

[5] C. Müller, *On the Steinberg presentation for Lie-type groups of type C_2*, J. Algebra **252**, 150 (2002).

[6] C. Müller, A. B. Voitkiv, and N. Grün, *Paarerzeugung in Stößen relativistischer Ionen mit intensiven Laserfeldern*, in "Arbeitsbericht der 24. Tagung über Energiereiche Atomare Stöße (Riezlern, Austria, 16.02.-21.02.03)", EAS Report **24**, 58 (2003) [available online via http://www.mpipks-dresden.mpg.de/∼eas/].

[7] C. Müller, A. B. Voitkiv, and N. Grün, *Multiphoton pair production by a highly-charged ion in an intense laser field*, Nucl. Instr. Meth. Phys. Res. B **205**, 306 (2003).

[8] A. B. Voitkiv, C. Müller, and N. Grün, *On the high-energy limits for the double-to-single ionization ratio of helium and heliumlike ions in collisions with charged and neutral particles*, Nucl. Instr. Meth. Phys. Res. B **205**, 504 (2003).

[9] C. Müller, A. B. Voitkiv, and N. Grün, *Differential rates for multiphoton pair production by an ultrarelativistic nucleus colliding with an intense laser beam*, Phys. Rev. A **67**, 063407 (2003) [and July 2003 issue of Virtual J. Ultrafast Science].

[10] C. Müller, A. B. Voitkiv, and N. Grün, *Nonlinear bound-free pair creation in the strong electromagnetic fields of a heavy nucleus and an intense X-ray laser*, Phys. Rev. Lett. **91**, 223601 (2003) [and December 2003 issue of Virtual J. Ultrafast Science].

[11] C. Müller, A. B. Voitkiv, and N. Grün, *Nichtlineare Paarerzeugung mit Einfang in hochenergetischen Kern-Laser-Stößen*, in "Arbeitsbericht der 25. Tagung über Energiereiche Atomare Stöße (Riezlern, Austria, 08.02.-13.02.04)", EAS Report **25** (2004) [available online via http://www.mpipks-dresden.mpg.de/∼eas/].

[12] C. Müller, A. B. Voitkiv, and N. Grün, *Few-photon electron-positron pair creation in the collision of a relativistic nucleus and an intense X-ray laser beam*, Phys. Rev. A **70**, 023412 (2004) [and September 2004 issue of Virtual J. Ultrafast Science].

[13] C. Müller, A. B. Voitkiv, and N. Grün, *Electron-positron pair creation on highly charged ions with intense laser fields*, in "ILIAS Ion and Laser beam Interaction and Application Studies: A scientific portrait of the PHELIX theory group", GSI Report 2005-04, June 2005, 26 (GSI, Darmstadt, Germany, 2005).

[14] C. Müller, *Groups with root systems of type G_2*, J. Algebra **294**, 552 (2005).

[15] K. Z. Hatsagortsyan, C. Müller, and C. H. Keitel, *Nonperturbative multiphoton processes and electron-positron pair production*, AIP Conf. Proc. **827**, 442 (2005).

[16] A. I. Milstein, C. Müller, K. Z. Hatsagortsyan, U. D. Jentschura, and C. H. Keitel, *Polarization-operator approach to electron-positron pair production in combined laser and Coulomb fields*, Phys. Rev. A **73**, 062106 (2006).

[17] C. Müller, K. Z. Hatsagortsyan, and C. H. Keitel, *Muon pair creation from positronium in a circularly polarized laser field*, Phys. Rev. D **74**, 074017 (2006) [and November 2006 issue of Virtual J. Ultrafast Science].

[18] K. Z. Hatsagortsyan, C. Müller, and C. H. Keitel, *Microscopic laser-driven high-energy colliders*, Europhys. Lett. **76**, 29 (2006) [selected as an "EPL Highlight of 2006"].

[19] A. Di Piazza, C. Müller, J. Evers, K. Z. Hatsagortsyan, and C. H. Keitel, *QED, nuclear and high-energy processes in extremely strong laser pulses*, in "ILIAS Ion and Laser beam Interaction and Application Studies", Progress Report No. 2 of the PHELIX theory group, ed. P. Mulser, T. Schlegel, GSI Report 2007-03, February 2007, 19-25 (GSI, Darmstadt, Germany, 2007).

[20] J. Peatross, C. Müller, and C. H. Keitel, *Electron wave-packet dynamics in a relativistic electromagnetic field: 3-D analytical approximation*, Opt. Express **15**, 6053 (2007).

[21] A. Shahbaz, C. Müller, A. Staudt, T. J. Bürvenich, and C. H. Keitel, *Nuclear signatures in high-order harmonic generation from laser-driven muonic atoms*, Phys. Rev. Lett. **98**, 263901 (2007) [and July 2007 issue of Virtual J. Ultrafast Science].

[22] C. Müller, G. R. Mocken, K. Z. Hatsagortsyan, and C. H. Keitel, *High-energy Quantum Dynamics in Ultra-Intense Laser Pulses*, AIP Conf. Proc. **963**, 552 (2007).

[23] C. Müller, K. Z. Hatsagortsyan, and C. H. Keitel, *Particle physics with a laser-driven positronium atom*, Phys. Lett. B **659**, 209 (2008).

[24] M. Klaiber, K. Z. Hatsagortsyan, C. Müller, and C. H. Keitel, *Coherent hard X-rays from attosecond pulse train-assisted harmonic generation*, Opt. Lett. **33**, 411 (2008) [and April 2008 issue of Virtual J. Ultrafast Science].

[25] C. Müller, A. Palffy, A. Ipp, A. Shabaz, A. Di Piazza, T. J. Bürvenich, J. Evers, and C. H. Keitel, *Coupling of nuclear matter to intense photon fields*, in "ILIAS Ion and Laser beam Interaction and Application Studies", Progress Report No. 3 of the PHELIX theory group, ed. P. Mulser, GSI Report 2008-05, April 2008, 26-32 (GSI, Darmstadt, Germany, 2008).

[26] C. Müller, A. Di Piazza, A. Shahbaz, T. J. Bürvenich, J. Evers, K. Z. Hatsagortsyan, and C. H. Keitel, *High-energy, nuclear and QED processes in strong laser fields*, Laser Phys. **18**, 175 (2008).

[27] J. Peatross, C. Müller, K. Z. Hatsagortsyan, and C. H. Keitel, *Photoemission of a Single-Electron Wave Packet in a Strong Laser Field*, Phys. Rev. Lett. **100**, 153601 (2008).

[28] K. Z. Hatsagortsyan, M. Klaiber, C. Müller, M. C. Kohler, and C. H. Keitel, *Laser-driven relativistic recollisions*, J. Opt. Soc. Am. B **25**, B92 (2008).

[29] M. Verschl and C. Müller, *Laser-driven collisions of electron bunches*, Opt. Comm. **281**, 4352 (2008).

[30] C. Müller, C. Deneke, and C. H. Keitel, *Muon pair creation by two X-ray laser photons in the field of an atomic nucleus*, Phys. Rev. Lett. **101**, 060402 (2008).

[31] C. Müller, K. Z. Hatsagortsyan, and C. H. Keitel, *Muon pair creation from positronium in a linearly polarized laser field*, Phys. Rev. A **78**, 033408 (2008) [and October 2008 issue of Virtual J. Ultrafast Science].

[32] C. Deneke and C. Müller, *Bound-free e^+e^- pair creation with a linearly polarized laser field and a nuclear field*, Phys. Rev. A **78**, 033431 (2008) [and October 2008 issue of Virtual J. Ultrafast Science].

[33] C. Müller, *Nonlinear Bethe-Heitler pair creation with attosecond laser pulses at the LHC*, Phys. Lett. B **672**, 56 (2009).

[34] M. Ruf, G. R. Mocken, C. Müller, K. Z. Hatsagortsyan, and C. H. Keitel, *Pair production in laser fields oscillating in space and time*, Phys. Rev. Lett. **102**, 080402 (2009).

[35] C. Müller, C. Deneke, M. Ruf, G. R. Mocken, K. Z. Hatsagortsyan, and C. H. Keitel, *Lepton Pair Production in High-Frequency Laser Fields*, Laser Phys. **19**, 791 (2009).

[36] A. Shahbaz, C. Müller, T. J. Bürvenich, and C. H. Keitel, *Laser-induced nonresonant nuclear excitation in muonic atoms*, Nucl. Phys. A **821**, 106 (2009).

[37] C. Müller, A. Shahbaz, T. J. Bürvenich, K. Z. Hatsagortsyan, and C. H. Keitel, *Exotic Atoms in Superintense Laser Fields*, Eur. Phys. J. Spec. Top., in press.

[38] A. Shahbaz, T. J. Bürvenich, and C. Müller, *Isotope effects in the harmonic response from hydrogenlike muonic atoms in strong laser fields*, to be submitted.

[39] S. Müller and C. Müller, *Multiphoton pair creation by relativistic muon impact on an intense laser beam*, in preparation.

Invited talks

[T1] C. Müller, A. B. Voitkiv, and N. Grün, Atomphysik-Seminar der Gesellschaft für Schwerionenforschung (GSI), Darmstadt, April 2003
Pair production by a relativistic nucleus colliding with an intense laser beam

[T2] C. Müller, A. B. Voitkiv, and N. Grün, Atomphysik-Seminar der Gesellschaft für Schwerionenforschung (GSI), Darmstadt, November 2004
Few-photon electron-positron pair creation in the collision of a relativistic nucleus and an intense X-ray laser beam

[T3] C. Müller, A. B. Voitkiv, and N. Grün, Atomphysik-Seminar des Instituts für Theoretische Physik der Justus-Liebig-Universität Gießen, 11.05.2006
Muon pair creation from a laser-driven positronium atom

[T4] C. Müller, A. B. Voitkiv, N. Grün, K. Z. Hatsagortsyan, and C. H. Keitel, Seminar der AG Quantenoptik, Universität Kaiserslautern, 19.05.2006
Intense laser-matter interactions: from photoionization to particle production

[T5] C. Müller, K. Z. Hatsagortsyan, and C. H. Keitel, ILIAS-Seminar der Gesellschaft für Schwerionenforschung (GSI), Darmstadt, 21.11.2006
Lepton Pair Creation in Strong Laser Fields

[T6] C. Müller, K. Z. Hatsagortsyan, and C. H. Keitel, International Workshop on Atomic Physics, Max-Planck-Institut für Physik komplexer Systeme, Dresden, 27.11.-01.12.2006
Lepton Pair Creation in Strong Laser Fields

[T7] C. Müller, "PIzzA Night", Ruprecht-Karls-Universität Heidelberg, 14.06.2007
Theoretische Quantendynamik in intensiven Laserfeldern

[T8] C. Müller, SPARC Workshop, Gesellschaft für Schwerionenforschung (GSI), Darmstadt, 17.07.2007
Relativistic quantum dynamics in strong laser fields

[T9] C. Müller, A. Di Piazza, J. Evers, K. Z. Hatsagortsyan, and C. H. Keitel, 16th International Laser Physics Workshop (LPHYS'07), Leon, Mexiko, 20.08.-24.08.2007
High-energy, nuclear and QED processes in strong laser fields

[T10] C. Müller, FIAS Seminar, Frankfurt Institute for Advanced Studies, Frankfurt, 15.11.2007
Photon physics then and today: From Einstein's photoelectric effect to modern laser applications in physics and medicine

[T11] C. Müller, A. Shahbaz, G. R. Mocken, K. Z. Hatsagortsyan, and C. H. Keitel, Spring Meeting of the DPG, Darmstadt, 10.03.-14.03.2008 (Hauptvortrag)
Laser-driven recollisions: From atomic to nuclear physics and beyond

[T12] C. Müller, "PIzzA Night", Ruprecht-Karls-Universität Heidelberg, 29.05.2008
Theoretische Quantendynamik in intensiven Laserfeldern

[T13] C. Müller, C. Deneke, M. Ruf, K. Z. Hatsagortsyan, and C. H. Keitel, 17th International Laser Physics Workshop (LPHYS'08), Trondheim, Norway, 30.06.-04.07.2008
Lepton Pair Creation in High-Frequency Laser Fields

[T14] C. Müller, A. Shahbaz, C. Deneke, K. Z. Hatsagortsyan, and C. H. Keitel, ELI-Workshop, Palaiseau, France, 07.07.-10.07.2008
Laser-induced nuclear probing and excitation via muonic atoms and lepton pair creation

[T15] C. Müller, A. Shahbaz, K. Z. Hatsagortsyan, and C. H. Keitel, Topical Problems of Nonlinear Wave Physics (NWP), Nizhny Novgorod, Russia, 20.07.-26.07.2008
Particle and Nuclear Physics with Exotic Atoms in Superintense Laser Fields

[T16] C. Müller, A. Shahbaz, K. Z. Hatsagortsyan, and C. H. Keitel, ELI Workshop on Fundamental Physics in Ultra-High Fields, Frauenwörth, 28.09.-02.10.2008
Particle and Nuclear Physics with Exotic Atoms in Superintense Laser Fields

[T17] C. Müller, IAP-Kolloquium, Technische Universität Darmstadt, 18.11.2008
Relativistic electron (re)collisions in intense laser fields

B References

[Ada48] G. P. Adams, Phys. Rev. **74**, 1707 (1948).

[Agg97] C. K. Agger and A. H. Sørensen, Phys. Rev. A **55**, 402 (1997).

[Ago04] P. Agostini and L. F. DiMauro, Rep. Prog. Phys. **67**, 813 (2004).

[Alk01] R. Alkofer *et al.*, Phys. Rev. Lett. **87**, 193902 (2001).

[Alt06] M. Altarelli *et al.*, Technical Design Report of the European XFEL, DESY 2006-097 (http://www.xfel.net).

[Amo02] M. Amoretti *et al.*, Nature **419**, 456 (2002).

[Aut55] S. H. Autler and C. H. Townes, Phys. Rev. **100**, 703 (1955).

[Bai75] V. N. Baier, A. I. Milstein, and V. M. Strakhovenko, Zh. Eksp. Teor. Fiz. **69**, 1893 (1975) [Sov. Phys. JETP **42**, 961 (1976)].

[Bak06] S. Baker *et al.*, Science **312**, 424 (2006).

[Bal60] M. Ya. Balats *et al.*, Zh. Eksp. Teor. Fiz. **38**, 1715 (1960) [Sov. Phys. JETP **11**, 1239 (1960)].

[Bal97] G. C. Baldwin and J. C. Solem, Rev. Mod. Phys. **69**, 1085 (1997).

[Bau07] G. Baur, K. Hencken, and D. Trautmann, Phys. Rep. **453**, 1 (2007).

[Bec75] W. Becker and H. Mitter, J. Phys. A **8**, 1638 (1975).

[Bec02] W. Becker *et al.*, Adv. At. Mol. Opt. Phys. **48**, 35 (2002).

[Bel08] A. R. Bell and J. G. Kirk, Phys. Rev. Lett. **101**, 200403 (2008).

[Ber71] V. B. Berestetskii, E. M. Lifshitz, and L.P. Pitaevskii, *Relativistic Quantum Theory* (Pergamon Press, Oxford, 1971).

[Ber91] J. F. Berger, D. M. Gogny, and M. S. Weiss, Phys. Rev. A **43**, 455 (1991).

[Bet34] H. A. Bethe and W. Heitler, Proc. Roy. Soc. London A **146**, 83 (1934).

[Bor82] E. Borie and G. A. Rinker, Rev. Mod. Phys. **54**, 67 (1982).

[Bou92] J. A. Bounds and P. Dyer, Phys. Rev. C **46**, 852 (1992).

[Boy85] K. Boyer and C. K. Rhodes, Phys. Rev. Lett. **54**, 1490 (1985).

[Bra08] C. Brandau *et al.*, Phys. Rev. Lett. **100**, 073201 (2008).

[Bre34] G. Breit and J. A. Wheeler, Phys. Rev. **46**, 1087 (1934).

[Bre70] E. Brezin and C. Itzykson, Phys. Rev. D **2**, 1191 (1970).

[Bre89] W. H. Breunlich and P. Kammel, Annu. Rev. Nucl. Part. Sci. **39**, 311 (1989).

[Bru07] H. Bruhns, J. Braun, K. Kubicek, J. R. Crespo Lopez-Urrutia, and J. Ullrich, Phys. Rev. Lett. **99**, 113001 (2007).

[Bul03] S. V. Bulanov, T. Esirkepov, and T. Tajima, Phys. Rev. Lett. **91**, 085001 (2003).

[Bul06] S. S. Bulanov, N. B. Narozhny, V. D. Mur, and V. S. Popov, Zh. Eksp. Teor. Fiz. **129**, 14 (2006) [J. Exp. Theor. Phys. **102**, 9 (2006)].

[Bur97] D. Burke *et al.*, Phys. Rev. Lett. **79**, 1626 (1997).

[Bür06] T. J. Bürvenich, J. Evers, and C. H. Keitel, Phys. Rev. Lett. **96**, 142501 (2006).

[Car04] J. J. Carroll, Laser Phys. Lett. **1**, 275 (2004).

[Cas02] M. Casu and C. H. Keitel, Europhys. Lett. **58**, 496 (2002).

[Cas05] D. B. Cassidy *et al.*, Phys. Rev. Lett. **95**, 195006 (2005).

[Che04] S. Chelkowski, A. D. Bandrauk, and P. B. Corkum, Phys. Rev. Lett. **93**, 083602 (2004).

[Che08] T. Cheng, N. I. Chott, Q. Su, and R. Grobe, Laser Phys. **18**, 190 (2008).

[Che09] H. Chen *et al.*, Phys. Rev. Lett. **102**, 105001 (2009).

[Chi02] C. C. Chirilă, N. J. Kylstra, R. M. Potvliege, and C. J. Joachain, Phys. Rev. A **66**, 063411 (2002).

[Chi04] C. C. Chirilă, C. J. Joachain, N. J. Kylstra, and R. M. Potvliege, Phys. Rev. Lett. **93**, 243603 (2004).

[Cho05] E. A. Chowdhury, I. Ghebregziabiher, and B. C. Walker, J. Phys. B **38**, 517 (2005).

[Cla04] G. Claverie *et al.*, Phys. Rev. C **70**, 044303 (2004).

[Cor93] P. B. Corkum, Phys. Rev. Lett. **71**, 1994 (1993).

[Den99] O. I. Denisenko and S. P. Roshchupkin, Laser Phys. **9**, 1108 (1999).

[DiM07] L. F. DiMauro *et al.*, J. Phys. Conf. Ser. **88**, 012058 (2007).

[DiP08a] A. Di Piazza, K. Z. Hatsagortsyan, and C. H. Keitel, Phys. Rev. Lett. **100**, 010403 (2008).

[DiP08b] A. Di Piazza and K. Z. Hatsagortsyan, Eur. Phys. J. Spec. Top. **160**, 147 (2008).

[Dre05] M. Drescher and F. Krausz, J. Phys. B **38**, S727 (2005).

[Dro09] B. Dromey *et al.*, Nature Phys. **5**, 146 (2009).

[Eis76] J. M. Eisenberg and W. Greiner, *Nuclear Theory, Vol. 2: Excitation Mechanisms of the Nucleus* (North-Holland, Amsterdam, 1976).

[ELI] See the proposal on the Extreme Light Infrastructure (ELI) available on http://www.eli-laser.eu .

[Epp07] S. W. Epp *et al.*, Phys. Rev. Lett. **98**, 183001 (2007).

[Erg06] Th. Ergler *et al.*, Phys. Rev. Lett. **97**, 193001 (2006).

[Esa95] E. Esarey, P. Sprangle, and J. Krall, Phys. Rev. E **52**, 5443 (1995).

[Esi04] T. Esirkepov *et al.*, Phys. Rev. Lett. **92**, 175003 (2004).

[Fed97] M. V. Fedorov, *Atomic and Free Electrons in a Strong Light Field* (World Scientific, Singapore, 1997).

[Fed06] M. V. Fedorov, M. A. Efremov, and P. A. Volkov, Opt. Comm. **264**, 413 (2006).

[Fis06] R. Fischer, M. Lein, and C. H. Keitel, Phys. Rev. Lett. **97**, 143901 (2006).

[Fit53] V. L. Fitch and J. Rainwater, Phys. Rev. **92**, 789 (1953).

[Fra91] E. S. Fradkin, D. M. Gitman, and Sh. M. Shvartsman, *Quantum Electrodynamics with unstable vacuum* (Springer, Berlin, 1991).

[Gah00] C. Gahn *et al.*, Appl. Phys. Lett. **77**, 2662 (2000).

[Gie05] H. Gies and K. Klingmüller, Phys. Rev. D **72**, 065001 (2005).

[Gie08] H. Gies, J. Phys. A **41**, 164039 (2008).

[Goe31] M. Goeppert-Mayer, Ann. Phys. **9**, 273 (1931).

[Gol76] V. Gol'danskii and V. A. Namiot, Phys. Lett. B **62**, 393 (1976).

[Grü07] F. Grüner *et al.*, Appl. Phys. B **86**, 431 (2007).

[Heg06] B. M. Hegelich *et al.*, Nature (London) **439**, 441 (2006).

[Hen04] B. Henrich, K. Z. Hatsagortsyan, and C. H. Keitel, Phys. Rev. Lett. **93**, 013601 (2004).

[Hof05] D. H. H. Hoffmann *et al.*, Laser Part. Beams **23**, 47 (2005); see also http://www.gsi.de/forschung/phelix/.

[Itz80] C. Itzykson and J. B. Zuber, *Quantum Field Theory* (McGraw-Hill, New York, 1980).

[Jør05] L. V. Jørgensen *et al.*, Phys. Rev. Lett. **95**, 025002 (2005).

[Kam06] J. Z. Kaminski, K. Krajewska, and F. Ehlotzky, Phys. Rev. A **74**, 033402 (2006).

[Kap07] H. Kapteyn *et al.*, Science **317**, 775 (2007).

[Kar99] S. Karsch *et al.*, Laser Part. Beams **17**, 565 (1999).

[Kei02] C. H. Keitel and S. X. Hu, Appl. Phys. Lett. **80**, 541 (2002).

[Kel64] L. V. Keldysh, Zh. Eksp. Teor. Fiz. **47**, 1945 (1964) [Sov. Phys. JETP **20**, 1307 (1965)].

[Kis00] S. Kishimoto *et al.*, Phys. Rev. Lett. **85**, 1831 (2000).

[Kla06] M. Klaiber, K. Z. Hatsagortsyan, and C. H. Keitel, Phys. Rev. A **74**, 051803(R) (2006).

[Kor07] A. S. Kornev and B. A. Zon, Laser Phys. Lett. **4**, 588 (2007).

[Kre02] P. Krekora *et al.*, Laser Phys. **12**, 455 (2002).

[Kre04] P. Krekora, Q. Su, and R. Grobe, Phys. Rev. Lett. **92**, 040406 (2004).

[Kuc87] M. Yu. Kuchiev, Pis'ma Zh. Eksp. Teor. Fiz. **45**, 319 (1987) [JETP Lett. **45**, 404 (1987)].

[Kuc07] M. Yu. Kuchiev, Phys. Rev. Lett. **99**, 130404 (2007).

[Kul93] K. C. Kulander, K. J. Schafer, and J. L. Krause, NATO Advanced Studies **316**, 95 (1993).

[Kur99] A. V. Kurilin, Nuovo Cimento Soc. Ital. Fis. A **112**, 977 (1999).

[Led03] K. W. D. Ledingham, P. McKenna, and R. P. Singhal, Science **300**, 1107 (2003).

[Lee06] W. P. Leemans *et al.*, Nature Phys. **2**, 696 (2006).

[Lei07] M. Lein, J. Phys. B **40**, R135 (2007).

[Lin06] Q. Lin, S. Li, and W. Becker, Opt. Lett. **31**, 2163 (2006).

[Mar06] M. Marklund and P. K. Shukla, Rev. Mod. Phys. **78**, 591 (2006).

[Mat98] S. Matinyan, Phys. Rep. **298**, 199 (1998).

[Mat05] V. I. Matveev, E. S. Gusarevich, and I. N. Pashev, Zh. Eksp. Teor. Fiz. **127**, 1187 (2005) [J. Exp. Theor. Phys. **100**, 1043 (2005)].

[McD99] K. T. McDonald and K. Shmakov, Phys. Rev. STAB **2**, 121301 (1999).

[Mil04] N. Milosevic, P. B. Corkum, and T. Brabec, Phys. Rev. Lett. **92**, 013002 (2004).

[Mil06] D. B. Milosević, G. G. Paulus, D. Bauer, and W. Becker, J. Phys. B **39**, R203 (2006).

[Mit75] H. Mitter, Acta Phys. Austr. Suppl. **14**, 397 (1975).

[Mit87] M. H. Mittleman, Phys. Rev. A **35**, 4624 (1987).

[Moc04] G. R Mocken and C. H. Keitel, J. Phys. B **37**, L275 (2004).

[Moc08] G. R. Mocken and C. H. Keitel, Comput. Phys. Comm. **178**, 868 (2008).

[Mor73] M. Morita, Prog. Theor. Phys. **49**, 1574 (1973).

[Mou06] G. A. Mourou, T. Tajima, and S. V. Bulanov, Rev. Mod. Phys. **78**, 309 (2006).

[MPQ] For current information, see http://www.attoworld.de/research/PFS.html .

[Mul06] F. Mulhauser *et al.*, Phys. Rev. A **73**, 034501 (2006); for current information, see http://www.triumf.info/ and http://www.psi.ch .

[Mur96] H. Murayama and M. E. Peskin, Annu. Rev. Nucl. Part. Sci. **46**, 533 (1996).

[Nak04] K. Nakajima, AIP Conf. Proc. **737**, 614 (2004).

[Ned07] V. N. Nedoreshta, A. I. Voroshilo, and S. P. Roshchupkin, Laser Phys. Lett. **4**, 872 (2007).

[Nik85] A. I. Nikishov, J. Sov. Laser Res. **6**, 619 (1985).

[Nil04] T. Nilsson *et al.*, Nucl. Phys. A **746**, 513 (2004).

[Ole67] V. P. Oleinik, Zh. Eksp. Teor. Fiz. **52**, 1049 (1967) [Sov. Phys. JETP **25**, 697 (1967)].

[Oto78] K. Otozai, R. Arakawa, and T. Saito, Nucl. Phys. A **297**, 97 (1978).

[Pal07] A. Pálffy, J. Evers, and C. H. Keitel, Phys. Rev. Lett. **99**, 172502 (2007).

[Pal08] A. Pálffy *et al.*, Phys. Lett. B **661**, 330 (2008).

[Pes95] M. E. Peskin and D. V. Schroeder, *An Introduction to Quantum Field Theory* (Addison-Wesley, Reading, 1995).

[Pop71] V. S. Popov, JETP Lett. **13**, 185 (1971).

[Pov06] B. Povh, K. Rith, C. Scholz, and F. Zetsche, *Particles and Nuclei* (Springer, Berlin, 2006).

[Puk06] A. Pukhov, Nature Phys. **2**, 439 (2006).

[RAL] For current information, see http://www.clf.rl.ac.uk .

[Rei62] H. R. Reiss, J. Math. Phys. **3**, 59 (1962).

[Rei79] H. R. Reiss, Phys. Rev. A **19**, 1140 (1979).

[Rei80] H. R. Reiss, Phys. Rev. A **22**, 1786 (1980).

[Rei92] H. R. Reiss, Prog. Quant. Electron. **16**, 1 (1992).

[Rin01] A. Ringwald, Phys. Lett. B **510**, 107 (2001).

[Rit72] V. I. Ritus, Nuclear Phys. B **44**, 236 (1972).

[Rit85] V. I. Ritus, J. Sov. Laser Res. **6**, 497 (1985).

[Rom00] J. S. Romăn, L. Roso, and H. R. Reiss, J. Phys. B **33**, 1869 (2000).

[Sal06] Y. I. Salamin, S. X. Hu, K. Z. Hatsagortsyan, and C. H. Keitel, Phys. Rep. **427**, 41 (2006).

[Sau31] F. Sauter, Z. Phys. **69**, 742 (1931).

[Sch04] K. J. Schafer *et al.*, Phys. Rev. Lett. **92**, 023003 (2004).

[Sch51] J. Schwinger, Phys. Rev. **82**, 664 (1951).

[Sch06a] H. Schwoerer, J. Magill, and B. Beleites (Eds.), *Lasers and Nuclei: Applications of ultra-high Intensity Lasers in Nuclear Science* (Springer, Heidelberg, 2006).

[Sch06b] H. Schwoerer *et al.*, Phys. Rev. Lett. **96**, 014802 (2006).

[Scr06] A. Scrinzi *et al.*, J. Phys. B **39**, R1 (2006).

[Scu97] M. O. Scully and M. S. Zubairy, *Quantum Optics* (Cambridge University Press, Cambridge, England, 1997).

[Ser05] J. Seres *et al.*, Nature **433**, 596 (2005).

[Sol88] J. C. Solem and L. C. Biedenharn, J. Quant. Spectrosc. Radiat. Transfer **40**, 707 (1988).

[Sor07] A. A. Sorokin *et al.*, Phys. Rev. Lett. **99**, 213002 (2007); for current information, see http://www-hasylab.desy.de/facility/fel .

[Str85] D. Strickland and G. Mourou, Opt. Commun. **56**, 219 (1985).

[Tar00] V. D. Taranukhin, Laser Phys. **10**, 330 (2000).

[Ton06] T. Toncian *et al.*, Science **312** 410 (2006).

[Tsa74] Y.-S. Tsai, Rev. Mod. Phys. **46**, 815 (1974).

[Tsa06] G. D. Tsakiris *et al.*, New J. Phys. **8**, 19 (2006).

[Ver07] M. Verschl and C. H. Keitel, J. Phys. B **40**, F69 (2007).

[Vol35] D. M. Volkov, Z. Phys. **94**, 250 (1935).

[VUL] See http://www.clf.rl.ac.uk/Facilities/vulcan/laser.htm for current information.

[Wal02] M. W. Walser, D. J. Urbach, K. Z. Hatsagortsyan, S. X. Hu, and C. H. Keitel, Phys. Rev. A **65**, 043410 (2002).

[Yak65] V. P. Yakovlev, Zh. Eksp. Teor. Fiz. **49**, 318 (1965) [Sov. Phys. JETP **22**, 223 (1966)].

[Yan08] V. Yanovsky *et al.*, Opt. Express **16**, 2109 (2008); for current information, see http://www.engin.umich.edu/research/cuos/.

[Yao06] W.-M. Yao *et al.*, J. Phys. G **33**, 1 (2006); for current information, see http://lhc.web.cern.ch .

C Selected publications

1) C. Müller, A. B. Voitkiv, and N. Grün
Nonlinear bound-free pair creation in the strong electromagnetic fields of a heavy nucleus and an intense X-ray laser
Phys. Rev. Lett. **91**, 223601 (2003)
(and December 2003 issue of Virtual J. Ultrafast Science)

2) K. Z. Hatsagortsyan, C. Müller, and C. H. Keitel
Microscopic laser-driven high-energy colliders
Europhys. Lett. **76**, 29 (2006)
(selected as an "EPL Highlight of 2006")

3) A. Shahbaz, C. Müller, A. Staudt, T. J. Bürvenich, and C. H. Keitel
Nuclear signatures in high-order harmonic generation from laser-driven muonic atoms
Phys. Rev. Lett. **98**, 263901 (2007)
(and July 2007 issue of Virtual J. Ultrafast Science)

4) C. Müller, K. Z. Hatsagortsyan, and C. H. Keitel
Particle physics with a laser-driven positronium atom
Phys. Lett. B **659**, 209 (2008)

5) M. Klaiber, K. Z. Hatsagortsyan, C. Müller, and C. H. Keitel
Coherent hard X-rays from attosecond pulse train-assisted harmonic generation
Opt. Lett. **33**, 411 (2008)
(and April 2008 issue of Virtual J. Ultrafast Science)

6) J. Peatross, C. Müller, K. Z. Hatsagortsyan, and C. H. Keitel
Photoemission of a Single-Electron Wave Packet in a Strong Laser Field
Phys. Rev. Lett. **100**, 153601 (2008)

7) C. Müller, C. Deneke, and C. H. Keitel
Muon pair creation by two X-ray laser photons in the field of an atomic nucleus
Phys. Rev. Lett. **101**, 060402 (2008)

8) C. Deneke and C. Müller
Bound-free e^+e^- pair creation with a linearly polarized laser field and a nuclear field
Phys. Rev. A **78**, 033431 (2008)
(and October 2008 issue of Virtual J. Ultrafast Science)

9) C. Müller
Nonlinear Bethe-Heitler pair creation with attosecond laser pulses at the LHC
Phys. Lett. B **672**, 56 (2009)

10) M. Ruf, G. R. Mocken, C. Müller, K. Z. Hatsagortsyan, and C. H. Keitel
Pair Production in Laser Fields Oscillating in Space and Time
Phys. Rev. Lett. **102**, 080402 (2009)